ACM-V

SCIENTIFIC BULLETIN

of the "POLITEHNICA" University of Timişoara

Transactions on Mechanics

XIIIth International Symposium

Young People and Multidisciplinary Research

Organizer: Association for Multidisciplinary Research in the West Zone of Romania

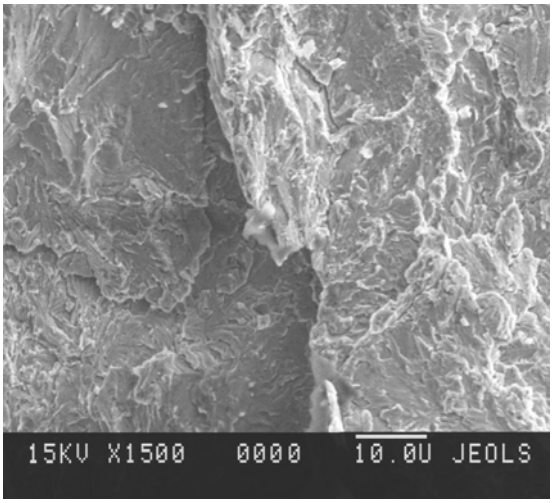

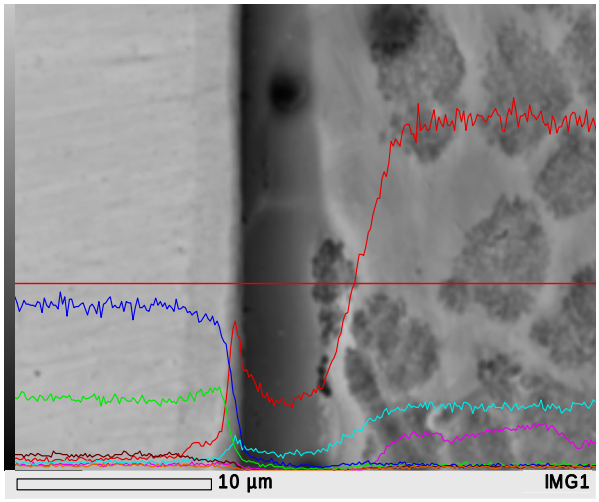

Vol 56(70), Special ISSUE S1, 2011
ISSN 1224-6077

Editura Politehnica

ACM-V

SCIENTIFIC BULLETIN

of the "POLITEHNICA" University of Timisoara

Transactions on Mechanics

XIIIth International Symposium

Young People and Multidisciplinary Research

Organizer: Association for Multidisciplinary Research in the West Zone of Romania

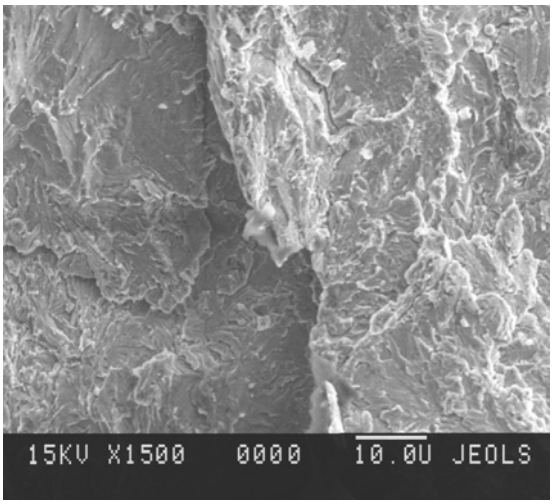

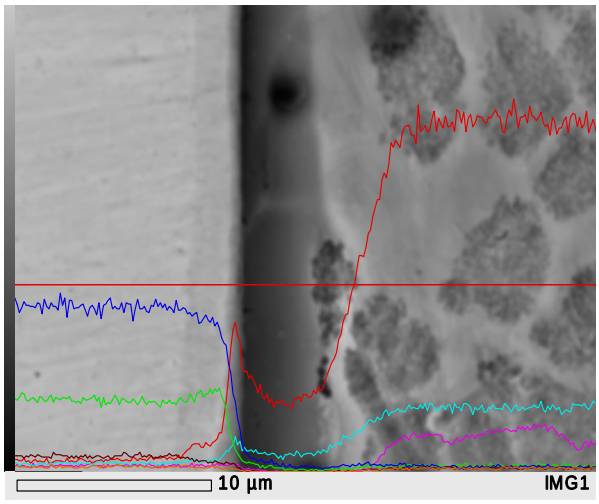

Edited by

I. Mitelea, Valeria Farbaş, R.A. Roşu

Symposium organized by Association for Multidisciplinary Research in the West Zone of Romania
- ISYPMPR 2011-

International scientific Committee

Paper realized by the Financial Support of the National Authority for Scientific Research

CONTENTS

CUPRINS

SCIENTIFIC BULLETIN OF
THE „POLITEHNICA" UNIVERSITY OF TIMISOARA, ROMANIA
TRANSACTIONS ON MECHANICS
BULETINUL ŞTIINŢIFIC AL
UNIVERSITĂŢII „POLITEHNICA" DIN TIMIŞOARA, ROMÂNIA
Tom 56 (70) ISSN 1224 - 6077 Fasc. S1, 2011

ELECTRICAL PHENOMENA ACOUSTIC INVESTIGATION

Constantin BARBULESCU, Nicolae HERISANU, Vasile BACRIA
[*] "Politehnica" University of Timisoara, Romania, Electrical and Power Engineering Faculty, constantin.barbulescu@et.upt.ro
[**] "Politehnica" University of Timisoara, Romania, Mechanical Engineering Faculty, herisanu@mec.upt.ro, bracia@mec.upt.ro

Abstract. Within the power systems field characteristic phenomena are recorded. Among them, there are highlighted: synchronous generator operation, electric transformer operation, corona effect in case of overhead power lines, etc. While these phenomena are producing acoustical energy is also generated. The paper aims to study these types of phenomena, the acoustical energy travelling way, the frequency spectrum, acoustical level statistical distribution. Based on the investigation results, noise level reduction methods are proposed for the electric phenomena studied.

Keywords: electric transformer, rotating machine, noise generated, phonic pollution decreasing methods.

1. Introduction

The noise has, for the human beings, a harmful effect. It depends on the intensity and the spectral component of the noise, the length of exposure to it during a workday and the whole length of exposure during the lifespan [1].

Human beings during their working activity are negatively affected by the noise. But, it becomes more disturbing in case of resting periods, even if the noise level is lower.

The transformers installed in the inhabited neighbourhoods or in their proximity have a large part to play in creating the background noise during the night.

On the world scale, the problem of power supply substation phonic pollution reduction has moved to the forefront during the past ten years. In our country, nowadays, there are several interests in monitoring the phonic pollution. The noise causes and sources within the power supply substations, the phonic pollution measurement and analysis process, as well as the means of decreasing the generated noise have to be studied.

Within the paper the attention is focused on power system elements: electric transformers, overhead power lines, electric rotating machines.

Electric machine (rotating machines and electric transformers) noise generated study requests a mix between the acoustic and design fields. The movement of the particles within an elastic environment among an equilibrium position represents an acoustic vibration. Sound represents the acoustic vibration able to produce an auditory sensation. Noise is defined as an annoying noise without well-defined components. The acoustic field represents the region within an elastic environment that is vibrating, housing some acoustic waves.

The operating electric machines and transformers are noise sources, because their pieces and parts are generating acoustic vibrations, subjected to different nature forces periodically variable.

2. Noise sources in case of power system elements

The electric rotating machine generated noise is due to specific constructive elements behaviour. Their mechanical and electric sizing determines its intensity. The loading level of the electric rotating machine also influences the noise intensity.

The cooling agent forced flow inside the machine represents the most significant aerodynamic noise source.

The electric machine aerodynamic noises are a direct or indirect consequence of the rotor movement.

The magnetic forces from the air gap occurring between the stator and rotor, due to the fact that they are elastic elements, mechanical oscillations are generated. The radiation of these forced oscillations together with the magnetostriction phenomenon are generated the magnetic noise.

Other noise sources in case of electric rotating machines are the following ones: bearing noise, noise brushes.

The noise generated by an electric machine cannot be completely avoided. It has an inferior natural and technical limit. It is named electric machine ideal noise. The lubricant quality and quantity also reduces or amplifies bearing noise.

The electric transformers installed in the inhabited neighbourhoods or in their proximity have a large part to play in creating the background noise during the night.

Also, for the case of the electric transformers, the magnetostriction represents the main cause of the noise generated by the electric transformers. Regarding the magnetic circuit, other sources of noise are identified: the magnetic forces that occur at the joining of the armature core discs, the constructive particularities of the fastening of the core and the mechanical reverberation of all these elements. Additionally, the influences exercised by the props and by the positioning system in the cuve, by the assembling method of the transformer and by the area where the transformer is set to work, are pointed out.

For large transformers, there have been detected other sources as well: fans and oil pumps, used to induce cooling, switches for adjusting the work of the transformers and the electrodynamic effort of the coils, as a direct result of the load and its degree of dissymmetry.

The noise generated by the transformers depends also on their electromagnetic and mechanical sizing.

Power quality has also an important influence on electric transformer generated noise. In case of harmonics the phonic pollution is amplified.

In case of the electric overhead lines the noise is generated through corona effect. A corona discharge is an electric discharge brought on by the ionization of a fluid surrounding a conductor that is carrying a current. The discharge will occur when the strength (potential gradient) of the electric field produced by the current is high enough to form a conductive region, but not high enough to cause electric breakdown or arcing to nearby objects.

Coronas can generate audible and radio-frequency noise, particularly near overhead lines. They also represent a power loss, and their action on atmospheric particulates, along with associated ozone production, can also be disadvantageous to human health where electric overhead lines run through built-up areas. Therefore, power transmission equipment is designed to minimise the formation of corona discharge.

3. Mathematical model

The vibrations are propagating in surroundings medium as spherical waves and cylindrical waves and at greater distance as plane waves.

- spherical waves:

The differential equation for an elastic homogeneous and isotropic medium with the speed potential ϕ as parameter is

$$\frac{\partial^2\phi}{\partial r^2}+\frac{2}{r}\cdot\frac{\partial\phi}{\partial r}+\frac{1}{r^2\sin\theta}\cdot\frac{\partial}{\partial\theta}\left(\sin\theta\frac{\partial\phi}{\partial\theta}\right)+\frac{1}{r^2\sin^2\theta}\cdot\frac{\partial^2\phi}{\partial\varphi^2}=\frac{1}{c^2}\cdot\frac{\partial^2\phi}{\partial t^2} \quad (1)$$

where r, ϕ, θ – the spherical coordinates which are positioning the volume element; c – the travel speed of the wave.

In case of the movement along the radius vector the acoustical pressure has the following expression

$$p=\rho_0\omega\frac{A}{r}\sin(\omega t-kr+\alpha) \quad (2)$$

allowing the acoustical pressure in any point of the acoustical field to be established.

- cylindrical waves, having the equation

$$\frac{\partial^2\phi}{\partial r^2}+\frac{1}{r}\cdot\frac{\partial\phi}{\partial r}+\frac{1}{r^2}\cdot\frac{\partial^2\phi}{\partial\varphi^2}=\frac{1}{c^2}\cdot\frac{\partial^2\phi}{\partial t^2} \quad (3)$$

where ϕ has the known signification; r and φ are the cylindrical coordinates of the volume element.

One solution for this differential equation can be obtained by using the variable separation method. It has the following form

$$\phi=\left[AJ_m(kr)+jBY_m(kr)\right]e^{-jm\varphi}e^{-j\omega t} \quad (4)$$

where A and B are constants, J_m is the Bessel function of the first degree and m range, and Y_m is the Bessel-Neumann function of the second degree and m range.

In case of waves that travels uniform ($m = 0$), the acoustical pressure becomes

$$p = A\left[J_0(z) + jY_0(z)\right]e^{-j\omega t} \quad (5)$$

where $z = kr = \frac{\omega}{c}r = \frac{2\pi}{\lambda}r$.

For small values of the variable, the expression (5) becomes

$$p = j\left(\frac{2A}{\pi}\right)\ln(kr)e^{-j\omega t} \quad (6)$$

and considering a great distance from the source

$$p = A\sqrt{\frac{2}{\pi kr}}e^{j\cdot\left[k(r-ct)-\frac{\pi}{4}\right]} \quad (7)$$

- plane waves having the equation

$$p = \rho_0\omega A\sin(\omega t - kx + \varphi) \quad (8)$$

If we consider the pressure at a moment of the wave propagation is p, then the level of the acoustical pressure is

$$L = 20\lg\frac{p}{p_0} \quad (9)$$

where $p_0 = 2\cdot10^{-5}[N/m^2]$ – the reference acoustical pressure.

For the regular constructed transformers, after identifying the sources and causes of the noise, there has been established an empiric equation to determine the acoustical level L_1 of the first harmonic of the noise [4].

$$L_1 = 73 + 20\lg\frac{2f}{100} + 20\lg H + 20\lg\varepsilon\cdot10^6\ [dB] \quad (10)$$

where f – network frequency [Hz], H – height of the column [m], ε – relative lengthening of the armature core disc used.

4. Case study

Two case studies the authors have been focused on.

The measurements have been performed for an electric transformer installed inside a close space at a production factory in Timisoara. The values have been recorded on 26th September 2011, 19:20 hour, for a 5 minutes time period.

The electrical transformer has the following characteristics:

$S_n = 1000\ kVA$, $U_n = 20\ kV / 0.4\ kV$.

The noise level measurements have been carried out using a 2250 Hand-Held Analyzer, according to STAS 6161/1-08 "Noise level measurement in the civil constructions" and STAS 7150-77 "Means to measure the level of noise in the industry".

In Figure 1 the noise level time variation is presented.

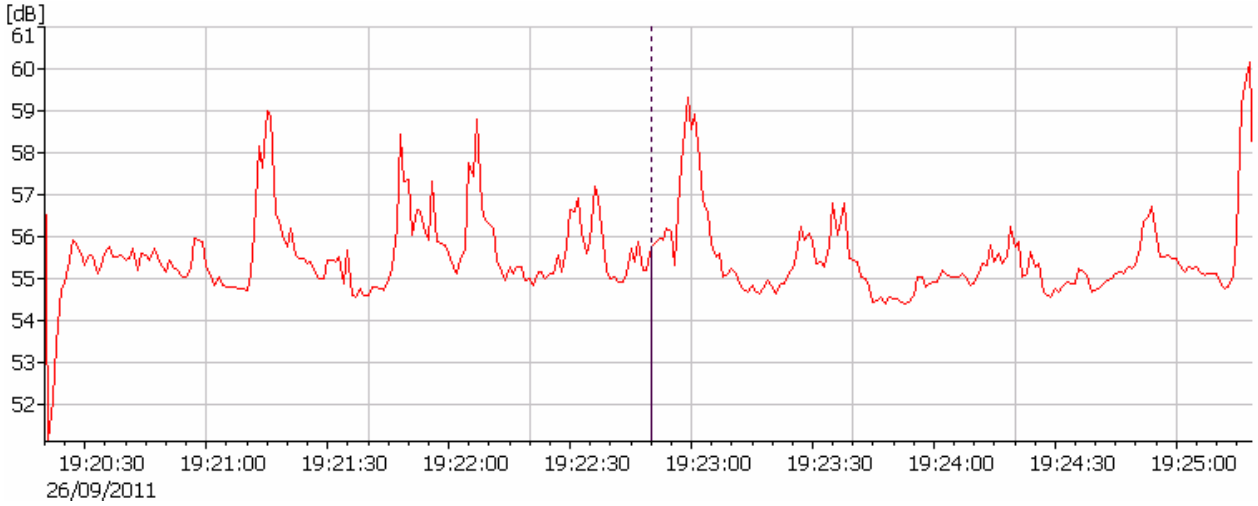

Figure 1 Noise level time variation

The greatest values are ranging between 56 dB – 60 dB. The measurements have been carried-out during the evening. This noise amplifies the background noise during the night. It also has negative effects on working staff inside the offices nearby the transformer.

In Figure 2 the noise level spectral distribution is presented. *LAeq* represents the equivalent noise level. It corresponds to an equivalent intensity that could be constant during the whole considered time. It is defined as

$$LA_{eq} = 10 \cdot \lg\left[\frac{1}{T} \cdot \int_{o}^{T} (10^{0,1 \cdot L(t)})dt\right] \qquad (11)$$

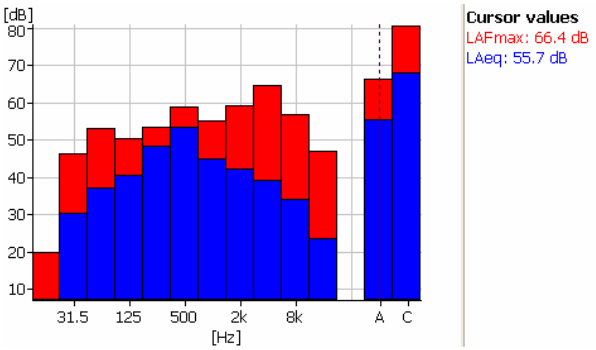

Figure 2 Noise level spectral distribution

The frequency domain is situated between 31.5 Hz and 9 kHz; the study was effectuated on A and C curves. It can be observed that the characteristic spectrum for the transformers case is defined by lower frequencies.

In Figure 3 the noise level percentage variation is presented.

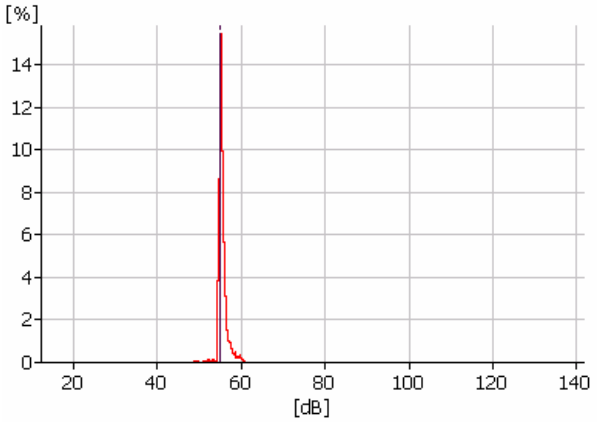

Figure 3 Noise level percentage variation

This figure validates the conclusions and the measurements presented in Figure 1. The values ranging between 56 dB and 59 dB have the greatest percentage density.

According to STAS 6156-86, the tolerable limit of the noise level in an occupied room is 35 dB. It is stipulated that, in an occupied room, the level of noise overnight, to guarantee the optimum state of tranquillity, must not rise above 25 dB (A), although it is advisable to drop to 20 dB [4].

Another set of measurements have been performed in case of a power supply substation, also in Timisoara city.

Figure 4 illustrates the measurement points positioning in case of a single transformer, while Figure 5 illustrates it for two transformers.

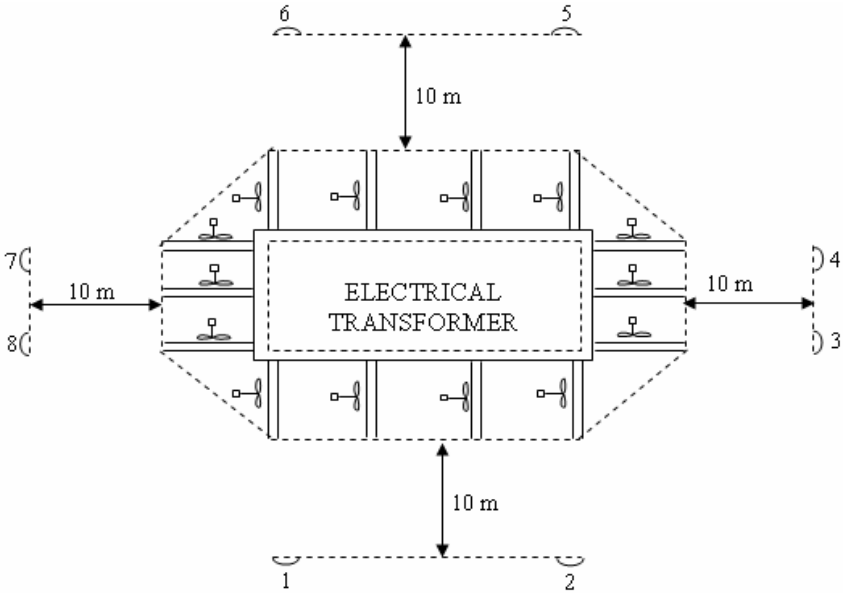

Figure 4 Measurement points positioning system

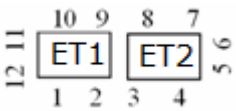

Figure 5 Measurement points positioning system

The two electrical transformers have the following characteristics:

- ET 1: $S_n = 40\ MVA$, $U_n = 110\ kV / 10\ kV$;
- ET 2: $S_n = 25\ MVA$, $U_n = 110\ kV / 22\ kV$.

Measurements were taken in open space conditions, during the day, in two different conditions: when the fans were working and when the fans were stopped.

The equivalent noise level has been measured.

For the first transformer the noise values are situated between 79.5 dB and 82.4 dB with working fans and between 61.3 dB and 68.2 dB with stopped fans.

In the case of the second transformer the noise values are situated between 74.9 dB and 90.4 dB, with working fans and between 59.1 dB and 68.2 dB, with stopped fans.

When the two transformers are working in parallel, we measured for the first case, when the fans are working, values between 77.5 dB and 90.3 dB. For the second case, when the fans are stopped, the measured values are ranging between 58.8 dB and 64.7 dB.

At a distance of 2 m from the objective, the results are situated between 47.4 dB and 59.6 dB.

Using Type 2250 Hand-Held Analyzer the frequency analysis has been performed (Figure 6).

Figure 6 Frequency analysis

The frequency domain is situated between 12.5 Hz and 20 kHz; the study has been conducted on *A* and *C* curves. It can be observed that the transformer characteristic spectrum is defined by lower frequencies.

5. Noise attenuation methods

In case on electric machines it is recommended to use impurities free lubricant. Otherwise, the bearing noise is amplified and the impurities could damage the bearing.

Special metals must be used for reducing the noise generated by the electrical machines, which lead to the adequate choice of the noise suppressors.

The electric transformer is installed in the proximity of the inhabited centres. It is recommended to be a tolerable noise source. According to the measurements the noise level value that travels inside the inhabited rooms exceeds the acceptable one. So, noise decreasing methods are necessary to be taken.

It has been highlighted that magnetostriction is the main noise source, in case of the electric transformer. To decrease the noise it is crucial to reduce the induction in columns and yokes.

The magnetic forces generated noise may me avoided by using exclusively homogenous armature core discs, having identical magnetic and mechanic properties. The iron plate must have an uniform thickness on its entire surface.

The positioning the decuvable part on elastic sets will not allow the vibrations to travel from the core to the cuve. Phono-absorbent barriers introduced inside the cuve is another means of decreasing the noise level.

Currently, oil is used as cooling agent. For reducing the noise generated through the cuve it is recommended to replace the oil with SF_6. It has phono-absorbent properties.

The noise decreasing methods previously presented are very efficient, but their major drawback refers to the fact that they are extremely expensive.

Considering these facts, the attention is focused on noise decreasing methods by the means of external measures. The use of acoustical screens or phono-absorbent rooms is a case in point. The most efficient means to reduce the noise of the transformers is attained through the use of completely sealed rooms, with massive walls. Such rooms are able to decrease the noise by 30-40 dB.

References

1. Grumazescu, M., Stan, A., Wegener N.: Marinescu, V., *Combaterea zgomotului si vibratiilor*, Editura Tehnica Publishing House, Bucharest, 1964 (in Romanian)
2. Darabont, A., Vaiteanu, D. : *Combaterea poluarii sonore si a vibratiillor*, Editura Tehnica Publishing House, Bucharest, 1975 (in Romanian)
3. Enescu, N., Magheti, I., Sarbu, M.A.: *Acustica tehnica,* I.C.P.E. Publishing House, Bucharest, 1998 (in Romanian)
4. Lazaroiu, F.D., Bichir, N.I.: *Zgomotul masinilor si transformatoarelor electrice*, Editura Tehnica Publishing House, Bucharest, 1968 (in Romanian)
5. Barbulescu, C., Herisanu, N., Bacria, V.: *Modelling system to mitigate noise generated by electrical transformers*, "Politehnica" University of Timisoara Scientific Bulletin, Transaction on Mechanics, Vol. 55 (69), Special Issue S1, 2010, p. 1-4, ISSN 1224-6077, Timisoara, Romania
6. Barbulescu, C., Bacria V.: *Examining and reducing the noise generated by some power equipment*, Proceedings of the International Conference Research People an Actual Tasks on Multidisciplinary Sciences, Editor Name Atanas Atanasov, p. 6-8, ISBN 978-954-91147-3-7,

Lozenec, Bulgaria, 6-8 June, 2007, Publisher Angel Kunchev

7. ***: Ständtebauliche Lärmfibel. Hinweise für die Bauleitplanung,Baden-Würtemberg Innenministerium, 1991

Investigarea acustică a fenomenelor electrice

Rezumat

În industria electroenergetică se produc fenomene caracteristice. Dintre acestea enumerăm: funcționarea generatoarelor sincrone, funcționarea transformatoarelor electrice, efectul corona în cazul liniilor electrice aeriene etc. În timpul desfășurării acestor fenomene se generează şi energie acustică. În lucrare se studiază aceste tipuri de fenomene precizându-se modul de propagare al energiei acustice, spectrele de frecvență şi distribuția statistică a nivelelor acustice. Pe baza rezultatelor investigațiilor se propun metode de reducere a nivelului de zgomot generat de aceste fenomene.

Scientific reviewers: **Prof.dr.ing. Ion Dumitru, "Politehnica" University of Timisoara**
Ş.l.dr.ing. Flaviu Mihai Frigura-Iliasa, "Politehnica" University of Timisoara

SCIENTIFIC BULLETIN OF
THE „POLITEHNICA" UNIVERSITY OF TIMISOARA, ROMANIA
TRANSACTIONS ON MECHANICS
BULETINUL ŞTIINŢIFIC AL
UNIVERSITĂŢII „POLITEHNICA" DIN TIMIŞOARA, ROMÂNIA
SERIA MECANICĂ
Tom 56 (70) **ISSN 1224 - 6077** **Fasc. S1, 2011**

ELEMENTARY MATHEMATICAL ANALYSIS OF AN UNCONVENTIONAL POWER TRANSMISSION SYSTEM

Liviu BĂRNUŢIU[*], Ioan POP[**]
[*]Takata-Petri RO, Zona Industriala Vest Arad, Str. III, Nr. 9, 310375 Arad, e-mail: Liviu:Barnutiu@eu.takata.com
[**] Catedra de Maşini unelte şi Roboţi Industriali, Universitatea Tehnică Cluj, B-dul Muncii nr. 103-105, Cluj-Napoca, e-mail: ioanpop@yahoo.com

Abstract. The transmission problem, broadly speaking, is to calculate and design a mechanism to carry out transmission and mechanical energy conversion, from an engine called primary with continuous action on the input axle (primary) of the system, to the output axle (secondary) of the mechanism. In this paper a calculation of the analytical output angle based on the input angle for an own building mechanism with a simple structure, different from the classics was performed. Analytical form of dependence between the two angles can be used for a complete dynamic study of the mechanism.

Keywords: transmission, input angle, output angle

1. Introduction

Starting with the very beginning of the computers, there was a major interest in their application for the understanding of complex processes in different activity fields. As a result, tools like MatLab, Mathcad or the much known Excel – were tailored to answer to the increase demand for processes visualization. In the mechanical domain, combined with superior mathematics, these tools can be used from vibrational studies to the active control of the fluids transport devices or for the integrals equations methods much used in mechanics and acoustics [1-5].

The purpose of this study was the use of mathematics and computers for the calculation/visualization of the analytical output angle based on the input angle for an own built mechanism with application in power transmission.

2. Procedure

The main cinematic elements comprising the constructive variant described in figure 1 are mostly simple.

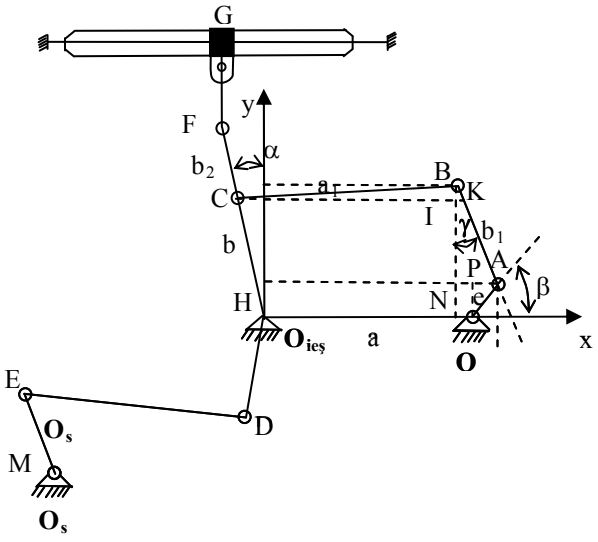

Figure 1 Schematic representation of the mechanism: Oin – input tree, Oies – output tree, Os – synchronization tree

All cinematic couplings connecting the mechanism elements are flat and provide a permanent contact, being closed from the construction point of view.

Couplings are generally reversible in cinematic terms; the relative movements are the same regardless which element is considered fixed.

The study started from the cartesian coordinates equations of the cinematic couplings denoted by A, B and C:

$$\begin{cases} x_A = a + e \cdot \cos\beta \\ y_A = e \cdot \sin\beta \end{cases} \quad (1)$$

$$\begin{cases} x_B = a \pm e \cdot \cos\beta \\ y_B = e \cdot \sin\beta + b_1 \cdot \cos\gamma \end{cases} \quad (2)$$

$$\begin{cases} x_C = b \cdot \sin\alpha \\ y_C = b \cdot \cos\alpha \end{cases} \quad (3)$$

For the mathematical modeling, the following relations were considered:

$$BC^2 = BI^2 + CI^2 \quad (4)$$

$$BI = y_B - y_C; \quad BI = e\sin\beta + b_1\cos\gamma - b\cos\alpha \quad (5)$$

$$CI = x_B - x_C; \quad CI = a \pm e\cos\beta - b\sin\alpha \quad (6)$$

It was noted:

$$k_1 = a \pm e\cos\beta \quad (7)$$

$$k_2 = e\sin\beta + b_1\cos\gamma \quad (8)$$

By replacing BC, BI and CI with their values, relation (4) became:

$$a_1^2 = (k_2 - b\cos\alpha)^2 + (k_1 - b\sin\alpha)^2 \quad (9)$$

$$a_1^2 = k_2^2 - 2k_2 b\cos\alpha + b^2\cos^2\alpha + k_1^2 - 2k_1 b\sin\alpha + b^2\sin^2\alpha \quad (10)$$

$$2k_2 b\cos\alpha = k_1^2 + k_2^2 + b^2 - a_1^2 - 2k_1 b\sin\alpha \quad (11)$$

Knowing that:

$$\cos\alpha = \sqrt{1 - \sin^2\alpha} \quad (12)$$

equation (11) became:

$$2k_2 b\sqrt{1 - \sin^2\alpha} = k_1^2 + k_2^2 + b^2 - a_1^2 - 2k_1 b\sin\alpha \quad (13)$$

3. Results

The solutions of the equation (13) were found to be:

$$\sin\alpha = \frac{k_1\left(k_1^2 + k_2^2 + b^2 - a_1^2\right)}{2b\left(k_1^2 + k_2^2\right)} \pm \frac{k_2\left(k_1^2 + k_2^2 - b^2 - a_1^2\right)}{2b\left(k_1^2 + k_2^2\right)} \quad (14)$$

Equation (14) can be used for the representation of the relationship between the input (β) and the output (α) angle, considering two alternatives:

First alternative (figure 2)

$$\alpha = \arcsin\left[\frac{k_1\left(k_1^2 + k_2^2 + b^2 - a_1^2\right)}{2b\left(k_1^2 + k_2^2\right)} + \frac{k_2\left(k_1^2 + k_2^2 - b^2 - a_1^2\right)}{2b\left(k_1^2 + k_2^2\right)}\right] \quad (12)$$

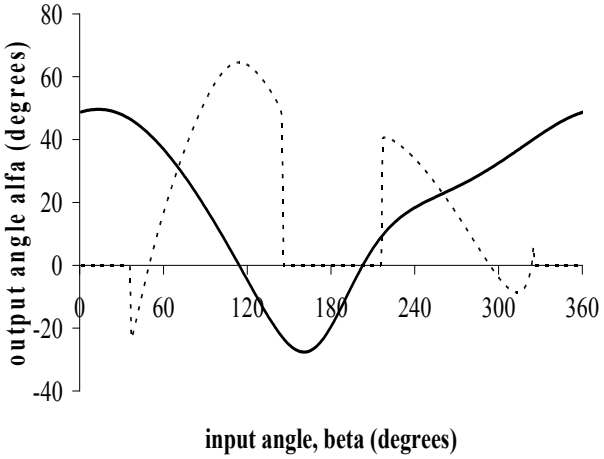

Figure 2 Representation of the output angle as a function of the input angle for 1a (full) and 1b (dashed) alternatives

Second alternative (figure 3)

$$\alpha = \arcsin\left[\frac{k_1\left(k_1^2+k_2^2+b^2-a_1^2\right)}{2b\left(k_1^2+k_2^2\right)} - \frac{k_2\left(k_1^2+k_2^2-b^2-a_1^2\right)}{2b\left(k_1^2+k_2^2\right)}\right] \quad (13)$$

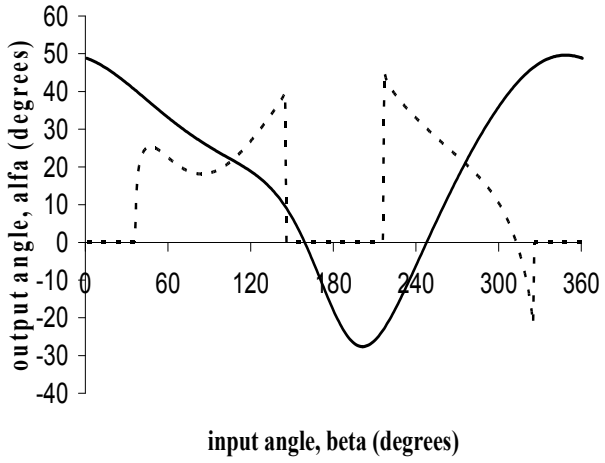

Figure 3 Representation of the output angle as a function of the input angle
for 2a (full) and 2b (dashed) alternatives

For both alternatives, two situations were considered:

$$\text{Situation a: } \begin{cases} k_1 = a + e\cos\beta \\ k_2 = e\sin\beta \end{cases} \quad (13)$$

$$\text{Situation b: } \begin{cases} k_1 = a - e\cos\beta \\ k_2 = e\sin\beta + b_1\cos\gamma \end{cases} \quad (14)$$

In order to obtain practical values, the following extremes were analyzed:

$$\text{Case 1: } \begin{cases} k_1 = a + e\cos\beta \\ k_2 = e\sin\beta \end{cases} \quad (15)$$

In this case BA (from figure 1) is perpendicular on OX, $\gamma = 0$.

$$\text{Case 2: } \begin{cases} k_1 = a - e\cos\beta \\ k_2 = e\sin\beta + b_1\cos\gamma \end{cases} \quad (16)$$

Since:

$$x_B = a - e\cos\beta \quad (17)$$

From ANB triungle:

$$AN = b_1\sin\gamma \quad (18)$$

But:

$$AP = e\cos\beta \quad (19)$$

And:

$$PN = e\cos\beta \quad (20)$$

$$AN = AP + PN \quad (21)$$

After replacing AN, PN and AP, the following relationship between angles β and γ is obtained:

$$2e\cos\beta = b_1\sin\gamma \quad (22)$$

Using the results obtained for $\sin\alpha$, the coordinates of F point (related to piston displacement – figure 1) can be determined.

$$x_F = x_C \pm b_2\cdot\sin\alpha \quad (23)$$

$$x_F = b\cdot\sin\alpha \pm b_2\cdot\sin\alpha \quad (24)$$

$$x_F = \left(b \pm b_2\right)\cdot\sin\alpha \quad (25)$$

$$x_F = \left(b \pm b_2\right)\cdot\left[\frac{k_1\left(k_1^2+k_2^2+b^2-a_1^2\right)}{2b\left(k_1^2+k_2^2\right)} \pm \frac{k_2\left(k_1^2+k_2^2-b^2-a_1^2\right)}{2b\left(k_1^2+k_2^2\right)}\right] \quad (26)$$

The results are shown in figure 4:

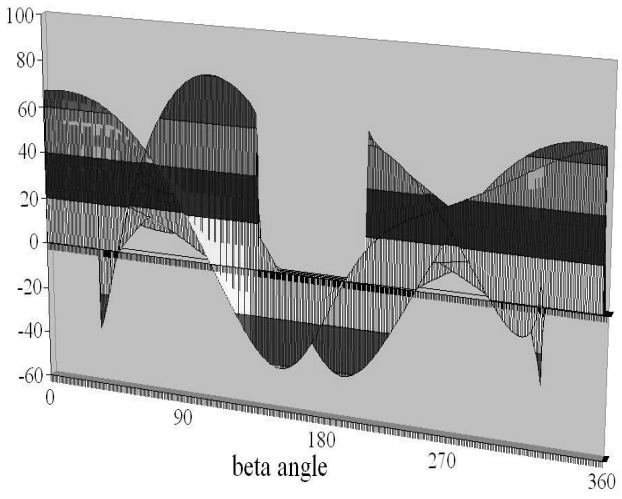

Figure 4 Successive representation of the mechanism for a variation of β ∈ [0-360]

4. Conclusion

The mathematical modeling has an important role for the visualization of the complex mechanical structures otherwise inaccessible. The research activity conducted this way led to the integration

of the dynamical behavior of the studied systems thus helping the development of the knowledge about the power transmission systems.

5. References

1. Buzdugan, G., Fetcu, L., Radeş, M.: *Vibrations of mechanical systems*, RSR Academy Publishing, Bucharest, 1975 (RO: Vibraţiile sistemelor mecanice)

2. Marin, C.: *Vibrations of mechanical structures,* Impuls Publishing, Bucharest, 2003 (RO: Vibraţiile structurilor mecanice)

3. Hristev, A.: *Mechanics and acoustics*, Didactic and Pedagogic Publishing, Bucharest, 1984 (RO: Mecanică şi acustică)

4. Constantinescu, G.: *Sonic Theory,* RSR Academy Publishing, Bucharest, 1985 (RO: Teoria sonicităţii)

5. Bratu, P.: *Theoretical Mechanics,* Impuls Publishing, Bucharest, 2004 (RO: Mecanică teoretic

Analiza matematică a unui sistem neconvenţional de transmisie a puterii

Rezumat

Problema transmisiei, in sensul larg al cuvântului, constă în calcularea şi proiectarea unui mecanism care să realizeze transmiterea şi conversia energiei mecanice, provenite de la un motor numit primar cu acţiune continuă asupra arborelui de intrare (primar) al sistemului, la axul de ieşire (secundar) al mecanismului.

În această lucrare s-a realizat un calcul analitic al unghiului de ieşire în funcţie de cel de intrare pentru un mecanism de construcţie proprie, cu o structură simplă, diferită de cele clasice. Forma analitică a dependenţei dintre cele două unghiuri poate fi folosită pentru un studiu dinamic complet al mecanismului.

Scientific reviewers: **Mihaela POPESCU, Politehnica University of Timisoara**
Ion MITELEA, Politehnica University of Timisoara

SCIENTIFIC BULLETIN OF
THE „POLITEHNICA" UNIVERSITY OF TIMISOARA, ROMANIA
TRANSACTIONS ON MECHANICS
BULETINUL ŞTIINŢIFIC AL
UNIVERSITĂŢII „POLITEHNICA" DIN TIMIŞOARA, ROMÂNIA
SERIA MECANICĂ
Tom 56 (70) ISSN 1224 - 6077 Fasc. S1, 2011

ALTERNATIVE CONSTRUCTION PROPOSAL FOR AN UNCONVENTIONAL POWER TRANSMISSION SYSTEM

Liviu BĂRNUŢIU*, Ioan I. POP**
*Takata-Petri RO, Zona Industriala Vest Arad, Str. III, Nr. 9, 310375 Arad, e-mail: Liviu:Barnutiu@eu.takata.com
**Catedra de Maşini unelte şi Roboţi Industriali, Universitatea Tehnică Cluj, B-dul Muncii nr. 103-105, Cluj-Napoca, e-mail: ioanpop@yahoo.com

Abstract.
In the proposed cinematic scheme, the rotation movement derived from the primary generator (internal combustion engine of a car, an electric motor or other source) is taken from the input axle on which are two eccentrics. By the two eccentric positioned in 180 º, the rotation movement is transformed in translation movement. Hence the translational movement is transmitted through the arms of two rods mounted on the output axle with the transmission ratio 1:1

Keywords: transmission, cinematic scheme, primary generator, eccentrics, flywheel

1. Introduction

The transmission problem, broadly defined, is that from a primary axle which rotates continuously, driven by a prime motor, to transmit power to another axle called secondary, so that regardless torque and speed fluctuations of the secondary axle, the primary engine naturally develops the power with maximum efficiency.

Starting from the block diagram of signal transmission mode shown in figure 1 and from the principle of inertia gearbox, respectively from examples of unconventional mechanisms of power transmission - without going into details of their construction – the goal of the present research was to obtain an inertial automatic gearbox.

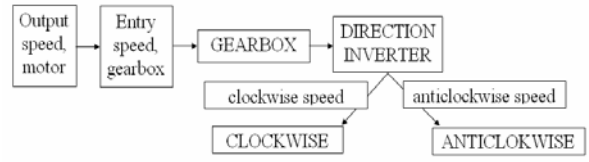

Figure 1 The block diagram

2. Problem description

There are several alternatives for the unconventional power transmission systems [1-5].

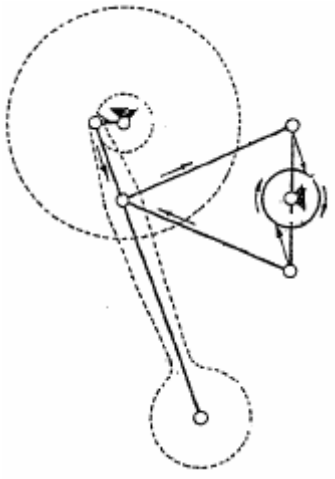

Figure 2 First constructive alternative of the inertial gearbox

One of the alternatives (figure 2) involves the crank of the motor axle to be connected directly to an oscillating member, bearing a heavy weight. An intermediate point of the free member is bound by rods to the coupling valve that set in motion the rotor.

In this case, in addition to the horizontal oscillation movement of the inertial mass, there is a vertical one too, but it is negligible if the amplitude of oscillation has no considerable value relative to the length of the crank.

If the balancing of the inertial forces is desired, two or more such systems can be installed on the same shaft, providing that the phase angles between the cranks are appropriately selected.

Another alternative (figure 3) involves the crank being connected to an intermediate point and the connecting rods at the top of the free member.

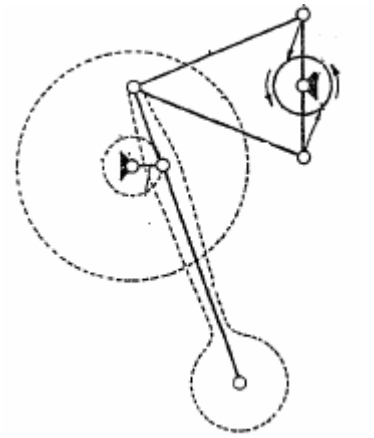

Figure 3 Second constructive alternative of the inertial gearbox

3. Procedure

The proposed cinematic scheme is shown in figure 4.

The rotation movement derived from the primary generator (internal combustion engine of a car, an electric engine or any other source) is taken from the input whereon two eccentrics are. Thro the two eccentrics displaced at 180 degrees, the rotation motion turns to translation movement of the flywheel mounted on them through two bearings. Hence the translational movement is transmitted by means of two rods to the arms, mounted on the output shaft, with the transmission ratio 1:1.

By the coupling valve mounted on the output shaft, the translational movement of the arm is transformed into a rotating movement of the output shaft. On a complete rotation of the input shaft, the flywheel runs a full oscillation, as well as the arm - so that half of its movement becomes motor movement. For this reason, in order to have a permanent rotating movement at the output, the two eccentrics are displaced at 180 degrees, each contributing with to half of the complete rotation of the output shaft.

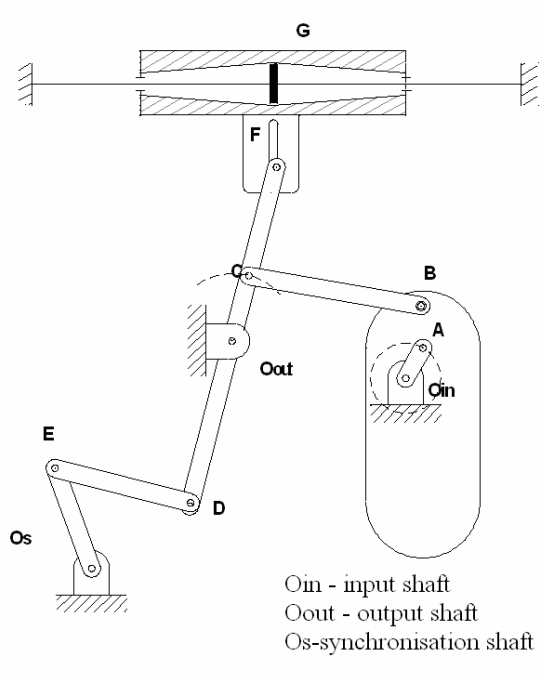

Figure 4 The cinematic scheme

To better understand how this mechanism works, suppose (purely theoretical) that the point of articulation between the rod and flywheel is not moving either left or right, only up and down (+/ - 10mm from the average position). In this case the flywheel will perform an oscillation around the articulation, the arm having a barely perceptible oscillation. This oscillation of the flywheel is produced by rotating the input shaft - so it is driven with a force dependent on its mass, eccentricity and frequency.

At this driving force in the joint the reaction force appears. The oscillation amplitude of the arm depends on the output shaft load, the higher the load is is, the speed is lower.

To ensure a permanent 180 degrees displacement between the arms movements, a synchronization shaft was introduced, rigid tied on them.

When the load is very low or the speed is high compared the required values, appears the possibility of large swings, uncontrollable, elements can hit each other. To avoid it, this movement is limited; that limitation has a secondary effect: limits the maximum ratio between output and input speed.

To remove the shocks when the travel is limited, a buffer cylinder was created, formed

from a body and a plunger. With this cylinder is realised, in case of maximum oscillations, a speed brake on the last quarter of the oscillation motion. Thus all oscillations with amplitude greater than 0.75 of the maximum amplitude will have a brake on this portion. Braking is done by means of two chokes, one fixed and one adjustable. To remove the appearance of the shoks and the starting of the movement in the opposite direction after being slowed down, a check valve was made.

4. Results

All rotation movements are transmitted through the bearings and translational movements by bolts – thus reducing friction to the maximum and also the overheating risk.

The gearbox housing is a welded construction consisting of a number of four plates welded together in a rectangular shape and provided with four feet, which are designed to support the mechanism and the screw it on the tests table, in order to obtain the effect of reducing vibration and noise during operation. The housing is provided with a two bays on the side of it, with the purpose of mounting the three shafts and a top cover for the buffer cylinder.

The flywheel is mounted on input shaft in the eccentricities area, the counterweights are attached on it. These may have a number four mounting positions: and can thus the effect of their positioning on the output shaft speed can be followed. Through the flywheel, the rotation input movement shaft turns in translational movement and it is transmitted through a valve coupling to the shaft output.

The main components are detailed in figure 5.

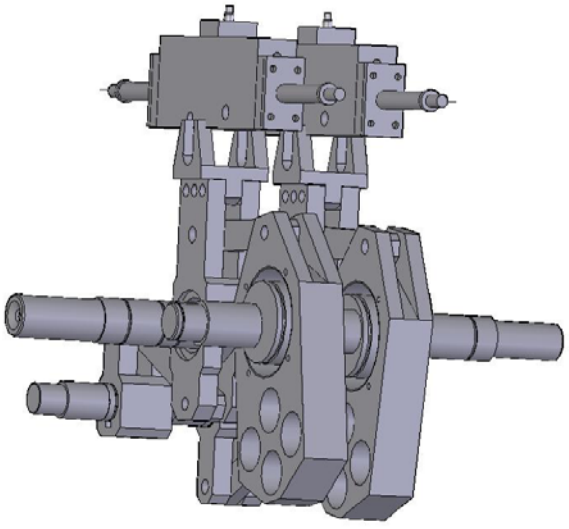

Figure 5a General view

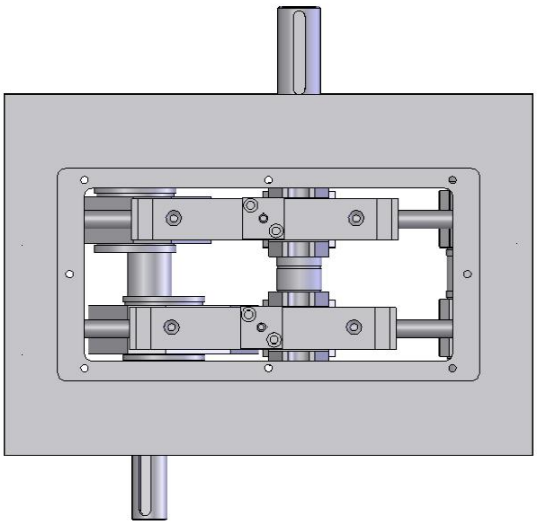

Figure 5b View from upside

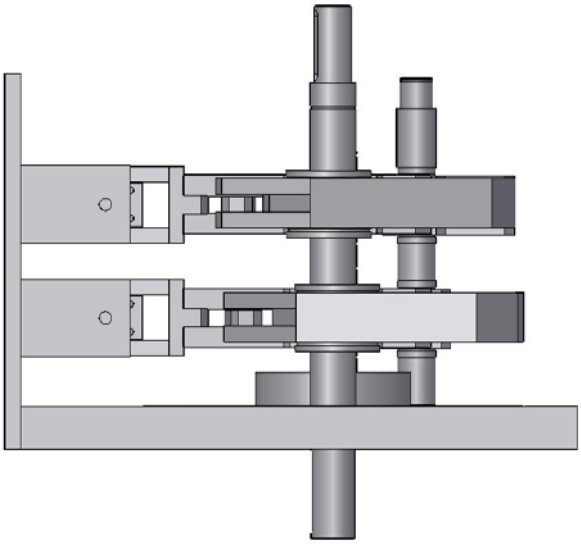

Figure 5c View from downside

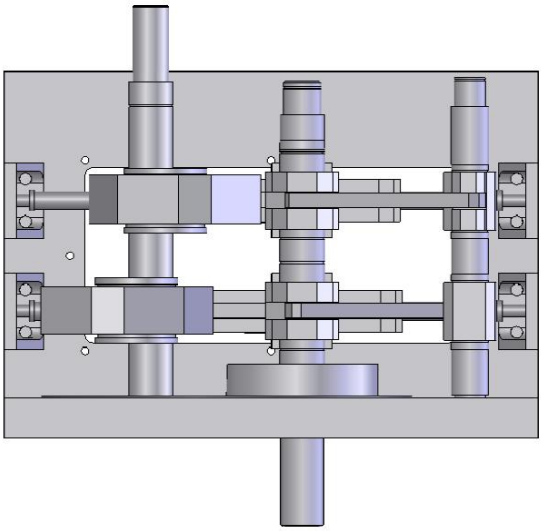

Figure 5d Lateral view

5. Conclusion

By this work it was designed and implemented a mechanism of power transmission and conversion, inspired from a model invented by the Romanian inventor Gogu Constantinescu. The innovation consisted in designing and implementing of a system with two oscillating input shaft eccentricities. They are mounted on two flywheels with counterweights attachable in four positions, allowing thus the effective monitoring of changes in output shaft speed depending on their positioning. In order to avoid shocks when arms travel is limited and to maintain movement of oscillation around the mean value, a buffer cylinder was used.

6. References

1. Pop, I.I., *Treaty of sonic theory*, Performantica Publisher, Iaşi, 2006 (RO: *Tratat de teoria sonicităţii*)
2. Negrea, C., Pavelescu, T., *Clutch and gearbox*, Technical Publisher, Bucureşti, 1980 (RO: *Ambreiajul şi cutia de viteze*)
3. Pop, I.I., et all., *Inventions integral*, vol. 1, Performantica Publisher, Iaşi, 2006 (RO: *Integrala invenţiilor*)
4. Ciolan Gh., Preda, I., Pereş Gh., Automotive gearboxes, E.D.P. Publisher, Bucureşti, 1998 (RO: *Cutii de viteze pentru automobile*)
5. Tabacu I., *Mechanical transmisions for cars*, Technical Publisher, Bucureşti, 1999 (RO: *Transmisii mecanice pentru autoturisme*)

Propunere de variantă constructivă pentru un sistem neconvenţional de transmisie a puterii

Rezumat

În schema cinematică propusa, mişcarea de rotaţie provenită de la generatorul primar (motorul cu ardere internă al unei maşini, un motor electric de curent alternativ sau altă sursă) este preluată de arborele de intrare pe care se găsesc două excentrice. Prin intermediul celor două excentrice decalate la 180º mişcarea de rotaţie se transformă în mişcare de translaţie a volanţilor montaţi pe ele prin intermediul a doi rulmenţi. De aici mişcarea de translaţie se transmite prin intermediul a două tije la braţele montate pe arborele de ieşire cu raportul de transmitere *1:1*.

Scientific reviewers: **Mihaela POPESCU, Politehnica University of Timisoara**
Ion MITELEA, Politehnica University of Timisoara

SCIENTIFIC BULLETIN OF
THE „POLITEHNICA" UNIVERSITY OF TIMISOARA, ROMANIA
TRANSACTIONS ON MECHANICS
BULETINUL ŞTIINŢIFIC AL
UNIVERSITĂŢII „POLITEHNICA" DIN TIMIŞOARA, ROMÂNIA
SERIA MECANICĂ
Tom 56 (70) ISSN 1224 - 6077 Fasc. S1, 2011

THE BENEFIT OF DUPLEX SURFACE TREATMENTS ON THE MECHANICAL PARTS WEAR

Ramona Monica DOBRA*, Ion MITELEA*
* University "Politehnica" Timişoara, Faculty of Mechanical Engineering Bd.Mihai Viteazul Nr.1, 300222 Timisoara;
Email: rmdobra@gmail.com, imitelea@mec.upt.ro

Abstract. The increase of the performance of machinery and mechanical parts involves a judicious selection of the steel, heat and surface treatments in order to obtain the desired properties. Besides the main problem which is a compromise between hardness and toughness, other problems that needs to be solved is related to abrasive and adhesive wear, gripping, dry and lubricated friction, fatigue and corrosion. These requirements can be satisfied exploring the potential of Duplex Treatments technologies. This paper presents the benefic effect of these treatments on the wear reduction of mechanical parts.

Keywords: duplex treatments, wear, friction coefficient.

1. Introduction

In modern industrialized societies there is a growing need to reduce or control friction and wear for several reasons, for example to extend the lifetime of machinery and bio-systems, to make engines and devices more efficient, to develop new advanced products, to conserve scarce material resources, to save energy, and to improve safety.

Historically, these aims were achieved by design changes, selecting improved bulk materials or by utilizing lubrication techniques. The lubrication techniques would include the use of liquid lubricants such as mineral or synthetic oils or solid lubricants such as molybdenum disulphide.

Recently, the tribologists have made increasing use of another approach to friction and wear control – that is to utilize surface treatments and coatings. This has led to, and to some extent been fuelled by, the growth of a new discipline called surface engineering.

This growth has been encouraged by two main factors. The first has been the development of new coating and treatment methods, which provide coating characteristics and tribo-chemical properties that were previously unachievable. The second reason for the growth in this subject area has been the recognition by engineers and materials scientists that the surface is the most important part in many engineering components. It is at the surface that most failures originate, by wear, fatigue or corrosion [1].

Incorrect materials selection as well as unsuitable or missing protective layers leads to manifold damages and are presented in Figs. 1 and 2 [2].

The surface may also have other functionally important attributes, not confined to mechanical or chemical properties, such as thermal, electronic, magnetic and optical characteristics that influence the choice of surface material [1].

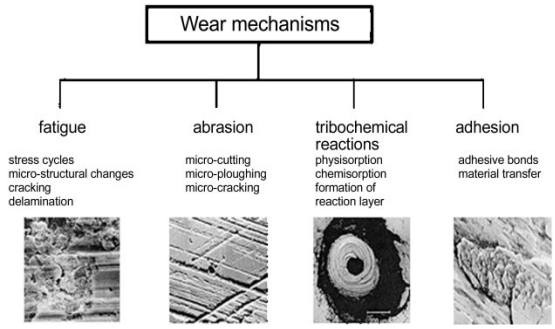

Figure 1 Wear mechanism

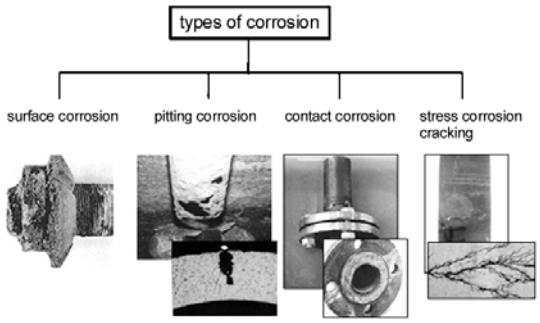

Figure 2 Corrosion types

2. Duplex surface treatments

A high resistance of metals against wear, fatigue and corrosion can be achieved by several different treatments, like thermal, mechanical, thermochemical and coating processes, but in an increasing number of cases, the resistance of metals against complex loads is no longer high enough. Combining successful single processes into one treatment can result in an even higher resistance of metals against complex loads, e.g. superimposed wear, fatigue and corrosion, because of the addition of the single process advantages.[3]

Duplex surface treatment term has been used for the first time in 1990, but Brainard and Weeler introduced the concept in 1979. [4]

The basic principle of combined processes is illustrated in figure 3. Two single processes A and B with their advantages and disadvantages are combined into one treatment AB, so that their advantages are added and their disadvantages preferably annihilated.[3]

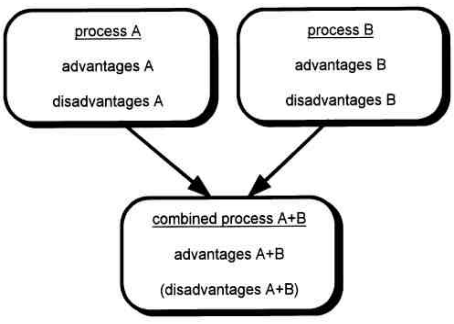

Figure 3 Duplex treatment principle [3]

3. Wear reduction by Duplex treatments

Wear reduction can be achieved by Duplex treatments consisting of a carburizing thermochemical treatment followed by a surface induction hardening.

The first step in realizing the Duplex treatment was gas carburizing the steel samples, but without make a further quenching martensite. The used gas for the treatment comes from the industrial network. The carburizing temperature was 920 ± 10 ° C. After the process, that lasted 8 hours, the samples were air cooled, or in the oven treatment. After the carburizing, the layer's thickness obtained is about 0.6 mm. In the second step, the thermochemically treated specimens were surface induction hardened, obtaining a layer thickness of 0.8 - 1 mm. The parameters of the second process are: the specific power, ΔP=0, 9 kW/cm^2, the heating time t = 4s, the frequency f = 32 kHz. The cooling was water realized.

To reduce the internal stress, appeared as the result of the surface induction hardening, the samples were tempering treatment subjected, at 180°C for 90 minutes.

The sliding wear rates were determined with the pin-on-disc test. The sliding wear rates were determined with the TRIBOX software, by introducing the measured area of the wear tracks and the diagonals of the testing's balls worn cape.

The samples were tested for a 500 m distance, with a 10 m/s velocity under a 5 N load against a WC ball of 6 mm diameter. The relative humidity was 65%. In table 1,the wear measurements of the samples are presented.[5]

Table 1 Wear measurements of the samples

The sample	**h [µm]**	**s [µm]**	**Ball wear diagonals [µm]**	**Wear rate [10^{-5} mm^3/Nm]**
Tempered state	18.2	341.3	354x353	3.66
Carburized state	9.4	387.7	368x397	2.14
Duplex treated	8.3	388.2	381x381	1.89

The friction coefficients were recorded by measuring the deflection of the tribometers elastic arm. In table 2, are presented their values.

Table 2 Wear measurements of the samples

The sample	μ_{min}	μ_{max}	μ_{mediu}
Tempered state	0.113	0.429	0.271
Carburized state	0.094	0.743	0.418
Duplex treated state	0.119	0.400	0.259

In figure 4, is presented the histogram of the wear rates for the structural states. The beneficial effect of the Duplex treatment on reducing the wear could be clearly observed.

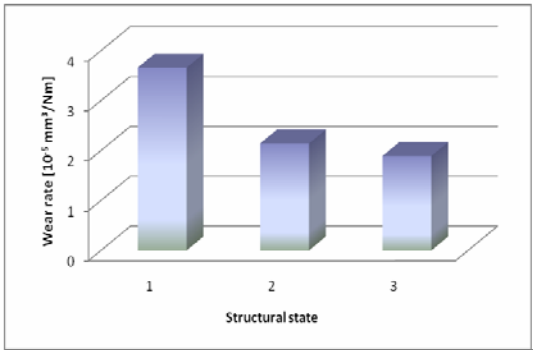

Figure 4 Wear rate: 1- tempering sample; 2 – carburized sample; 3 – Duplex treated sample

Therefore, the Duplex surface treatment consisting in carburizing followed by surface induction hardening with high frequency and low tempering reduce the wear rate by 51% compared with the tempered condition and by 12% compared with the carburized state.

Another Duplex surface treatment presented in literature that reduces the wear consists of plasma nitriding + PAPVD coating. Non-duplex and duplex (Ti,Al)N, TiN and Cr-N coatings (plasma nitriding + PAPVD coating) were deposited onto hardened AISI H13 steel substrates by ion plating using electron beam evaporation. The duplex specimens were plasma nitrided and PVD coated in a continuous process.

The micro-abrasive and impact wear responses of these coatings were evaluated and the values are shown in table 3. [6]

Table 3 Micro-abrasive wear test results: coating and substrate wear coefficients (k_C and k_S) [6]

Specimen	**k_c si C. I. (95 %) (x $10^{-3}m^3N^{-1}m^{-1}$)**		**K_s si C. I. (95 %) (x $10^{-3}m^3N^{-1}m^{-1}$)**	
Non-duplex (Ti,Al)N	2,36	2,20 – 2,55	9,62	8,22 – 11,61
Duplex (Ti,Al)N	1,44	1,34 – 1,54	8,84	8,63 – 9,07
Non-duplex TiN	7,27	7,15 – 7,39	9,65	9,54 – 9,76
Duplex TiN	3,86	3,81 – 3,90	8,75	8,46 – 9,05
Non-duplex Cr-N	27,79	22,13 – 38,09	9,84	9,58 – 10,12
Duplex Cr-N	18,11	16,63 – 19,86	9,53	9,39 – 9,68
Substrat neacoperit	-------	----------	9,40	9,00 – 9,82

In terms of micro-abrasive wear resistance, all coating systems, except for both duplex and non-duplex Cr-N coatings, exhibited higher micro-abrasive wear resistance than the uncoated substrate.

The duplex (Ti,Al)N showed the highest micro-abrasive resistance (lowest *kc* wear coefficient), followed by the nonduplex (Ti,Al)N, duplex TiN, non-duplex TiN, duplex Cr-N and non-duplex Cr-N. Although the duplex treatment provides an improvement in terms of abrasive wear (the duplex-treated samples showed higher micro-abrasive wear resistance in comparison to their non-duplex counterparts), the choice of the PAPVD coating still plays an important role in terms of improving the micro-abrasive wear resistance. For instance, a non-duplex (Ti,Al)N coating exhibited a higher micro-abrasive wear resistance than a duplex TiN coating. Both duplex and non-duplex Cr-N displayed the lowest wear resistances to abrasion.

According to Sukru Taktak and his coworkers another treatments combination that reduces the wear consists of thermo-reactive deposition/diffusion (TRD) chromizing and plasma nitriding.

AISI 52100 and 8620 bearing steels were used as the substrate material for duplex treatment. TRD carbide coatings were prepared by a pack method at 1000 °C for 5 h. Having completed the TRD heat treatment, test materials were removed from the box and air- quenched.

The TRD chromium carbide-coated steels were washed in water distilled, ultrasonically cleaned in acetone and rinsed in alcohol. The nitriding treatment was carried out in a dc-pulsed plasma system, with power supply frequency of 5 kHz and duty cycle of 75%. The specimens were placed into the plasma chamber. The chamber was evacuated to 8.2×10−4 mbar.

Prior to plasma nitriding, the chromized steels were subjected to cleaning by hydrogen sputtering for 30 min and the specimens were then plasma nitrided at 500 °C under a constant pressure of 10 mbar for 5 h at various gas mixtures of nitrogen-hydrogen atmospheres (100%N2, 25%N2+75%H2, 50% N2+50%H2 and 75%N2+25%H2).

Wear tests of the duplex treated bearing steels were performed using a ball-on-disc test device. The bottom movable flat surface was the treated steel and the upper fixed surface was the WC–Co ball, with a diameter of 8mm. The ball was fixed and the disk sample was rotated at the speed of 300 rpm (0.3 m/s). The applied loads on the ball were 5 and 20 N and the sliding time was 60 min for each test.

Wear tests were carried out in the unlubricated condition at room temperature in air.

The friction force was detected by a load cell through a friction force measurement arm. The friction coefficient was recorded continuously during the tests.

Steady state friction coefficient values for loads of 5 and 20 N are illustrated for the steels chromized (TRD) and duplex treated (TRD+PN) at various gas compositions in figure 5.

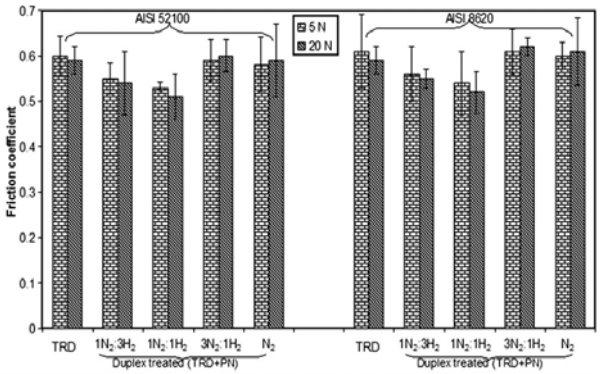

Figure 5 Steady state friction coefficient values for AISI 52100 and 8620 steels only TRD chromized and duplex treated at various gas mixtures under loads of 5 and 20 N.

Friction results indicated that, for both steels, the lowest steady state friction coefficient was observed for the samples duplex treated in a gas mixture of 50%N2+50%H2 followed by the samples duplex treated in the gas mixture of 25%N2+75%H2. This might be attributed to the lower friction coefficient of chromium nitride. However, contrary to expectations, the samples treated in a 75%N2+25%H2 plasma exhibited a similar friction coefficient to that seen for the samples TRD chromized and treated in a 100% N2 plasma.

Figure 6 shows wear rate values of AISI 52100 and 8620 steels TRD chromized and duplex treated (TRD+PN) in various gas compositions for loads of 5 and 20 N.

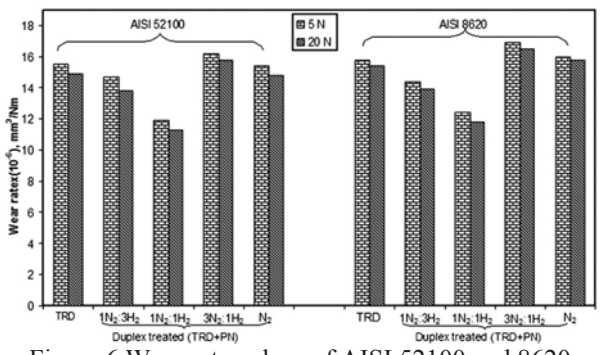

Figure 6 Wear rate values of AISI 52100 and 8620 steels only TRD chromized and duplex treated at various gas mixtures for loads of 5 and 20 N.

The wear rates of samples worn with a 5 N load are only slightly higher than those with a load of 20N. This is because the rate of increase in the wear amount of volume is less than the increase of applied load. Duplex treated samples in the gas mixture of 50%N2+50%H2 give the best wear resistance values followed by steels treated by plasma nitriding in 25%N2+75%H2. It was noted that there was only a small difference between the wear rates of steels only chromized and duplex treated steels in a 100%N2 plasma. This might be due to the absence of chromium nitride phase. The wear rate values of the samples duplex treated in the 50%N2+50%H2 plasma were about 30% and 36% lower, respectively, compared to only TRD chromized ones and samples duplex treated in a 75%N2+25%H2 gas mixture. [7]

The literature presents the uses of salt bath nitrocarburizing–quenching duplex treatments as surface modification processes to increase the sliding wear performance of 1045 steel. In order to compare the results, non-Duplex treatments of quenching, tempering and nitrocarburizing were made. Nitrocarburizing was performed in a 3 kW salt bath furnace. The treatment parameters and detailed processing sequences for several treatments are indicated in table 4 and figure 7, respectively. [8]

Table 4 Treatment techniques

Specimen no.	Treatment parameters
N1	850°C (0.5 h) quenched (water cooled) + 200°C (2.0 h) tempered
N2	570°C (1.5 h) nitrocarburized + air cooled
N3	570°C (1.5 h) nitrocarburized + air cooled → 840°C (0.5 h) quenched (water cooled) + 200°C (2.0 h) tempered

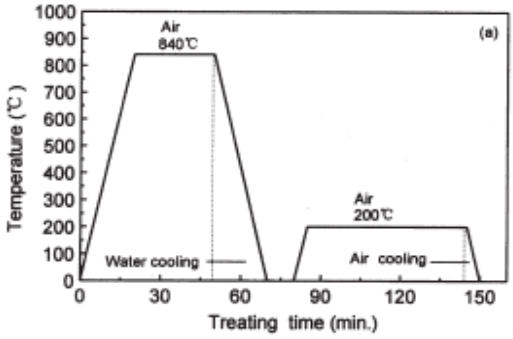

(a) Quenching+tempering

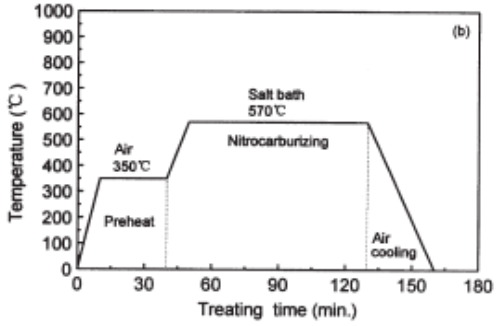

（b）Nitrocarburizing

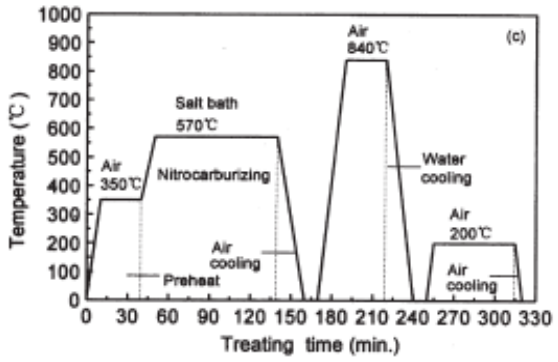

（c）Nitrocarburizing＋quenching and tempering

Figure 7 Processing sequences of three treatments

Friction tests on a series of blocks subject to several treatments were carried out under lubricated and unlubricated conditions. The test results are presented in figure 8.

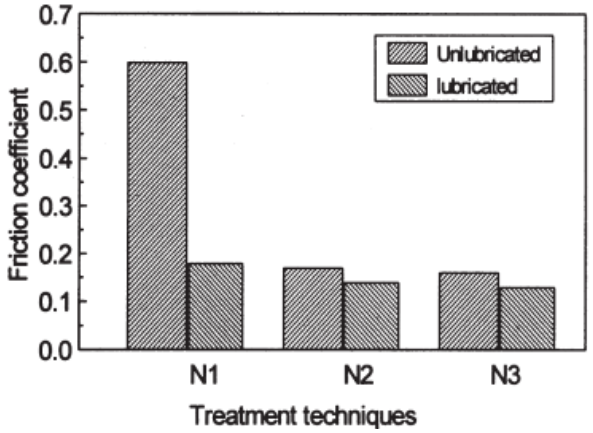

Figure 8 Friction coefficient after various treatments.

It can be seen that under both conditions, blocks nitrocarburized and nitrocarburized–quenched were found to have lower friction coefficient compared with quenched–tempered specimens. This indicates that the e-phase produced on the specimen has a significant effect on reducing friction.

In addition, it is found that under lubricated and unlubricated conditions, the friction coefficients of nitrocarburized and nitrocarburized–quenched specimens have no apparent difference. This means that lubrication has no significant effect on reducing the friction coefficients of nitrocarburized and nitrocarburized–quenched specimens.

The sliding wear test was conducted on a MRH-3 ring-on-block apparatus under both lubricated and unlubricated conditions. The ring was made of 52100 bearing steel with a diameter of 49.3 mm and a hardness about 59–63 HRC. Under lubricated condition, the testing load was 600 N, the speed 500 rpm and the time 30 minutes. The wear volume was measured every 5 minutes and the specimen was continuously lubricated by liquid paraffin at a constant drip rate of 20–25 drops per minute. Under unlubricated condition, the testing load was 100 N, the speed 200 rpm and the time 10 minutes. The experimental results for lubricated and unlubricated wear tests are indicated in figures 9 and 10.

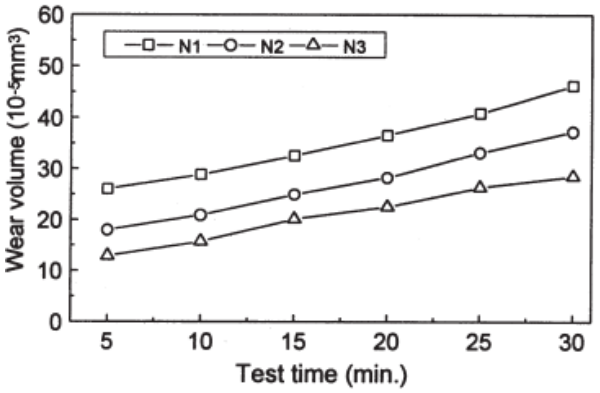

Figure 9 Wear volumes of various treatments under lubrication

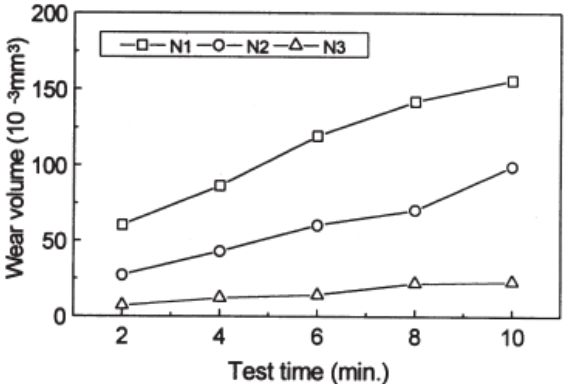

Figure 10 Wear volumes of various treatments under unlubrication

It is found that nitrocarburizing can improve the wear-resistance significantly under lubricated and unlubricated conditions due to the

intermetallic structure, higher hardness and the lower friction coefficient of the compound layer.

Excellent sliding and running properties are well-established advantages of nitrocarburized components. After nitrocarburized–quenched treatment, the wear resistance is improved even further because of the duplex strengthening of nitrocarburizing and quenching.

A striking feature of nitrocarburized–quenched specimens is the higher sub-surface hardness and hardness profile of the diffusion zone. This is a major factor to promote wear resistance.

5. Conclusions

Duplex surface treatments confirm the benefic effect of these treatments on the wear reduction and friction coefficient of mechanical parts.

The Duplex surface treatment consisting in carburizing followed by surface induction hardening with high frequency and low tempering reduce the wear rate by 51% compared with the tempered condition and by 12% compared with the carburized state.

References

1. H. Kenneth, A. Matthews: *Coatings Tribolgy Properties, Mechanisms, Techniques and Applications in Surface Engineering*, Tribology and Interface Engineering Series, no 56, ISBN 978-0-444-52750-9, Oxford, 2009, pp. 311-316.

2. W. Tillmann, E. Vogli : *Modern Surface Technologies*, ISBN 3-527-31532-2, 2006, pp.1-10.

3. O.H. Kessler, F.T. Hofmann, P.Mayer, *Combination of coating and heat treating processes: establishing a system for combined processes and examples*, Surface and coatings technologies, 1998, pp.211-216.

4. T. Bell: *Towards Designer Surfaces*, Metals and Materials, ISBN 0873392256, August, 1991.

5. R.M. Dobra, I. Mitelea, C. Locovei: *Improvement of wear resistance of mechanical parts using a Duplex Treatment*, The 15th International Conference Modern Technologies, Quality and Innovation, 2011, ISSN 2069-6736, pp.329-333.

6. J. C. Avelar-Batista, C.Godoy, R. D. Mancosu, J. Morais, A.Matthews, *Plasma Nitriding and PAPVD Hard Coating: A Critical Overview of Duplex Coating Processing*, Jornadas SAM/ CONAMET/ SIMPOSIO MATERIA, 2003, pp. 600-603.

7. S. Taktak, I. Gunes, S.Ulker, Y.Yalcin, Materials Characterization, 2008, pp.1784-1791.

8. Y.H. Qiang, S.R. Ge, Q.J. Xue, *Microstructure and tribological behavior of nitrocarburizing-quenching duplex treated steel*, Tribology International, 1999, pp. 131-136.

Efectul tratamentelor de suprafata Duplex asupra uzurii pieselor

Rezumat

Cresterea performantelor utilajelor si pieselor mecanice implica atat o selectie judicioasa a otelului, cat si alegerea corespunzatoare a tratamentelor aplicate suprafetei otelului in vederea obtinerii propietatilor dorite. Alaturi de problema de baza, care vizeaza un compromis intre duritate si tenacitate, trebuie sa se rezolve probleme legate de uzarea abraziva sau adeziva, gripare, frecare uscata sau lubrefiata, oboseala si coroziune. Aceste cerinte pot fi indeplinite numai prin exploatarea potentialului tehnologiilor de suprafata Duplex. Lucrarea de fata prezinta efectul benefic al acestor tratamente asupra reducerii semnificative a uzarii si coeficientului de frecare al pieselor mecanice.

Acknowledgement

This work was partially supported by the strategic grant POSDRU/88/1.5/S/50783, Project ID50783 (2009), co-financed by the European Social Fund – Investing in People, within the Sectoral Operational Programme Human Resources Development 2007-2013.

Scientific reviewers: **Victor BUDĂU, Politehnica University of Timisoara**
Livius UDRESCU, Politehnica University of Timisoara

SCIENTIFIC BULLETIN OF
THE „POLITEHNICA" UNIVERSITY OF TIMISOARA, ROMANIA
TRANSACTIONS ON MECHANICS
BULETINUL ŞTIINŢIFIC AL
UNIVERSITĂŢII „POLITEHNICA" DIN TIMIŞOARA, ROMÂNIA
SERIA MECANICĂ
Tom 56 (70) ISSN 1224 - 6077 Fasc. S1, 2011

STUDIES REGARDING THE ACQUIREMENT OF HARDNESS STANDARD BLOCKS FOR TRANSMITTING THE BRINELL 10/3000 HBW HARDNESS SCALES

Iuliana DUMA[*], Sebastian Titus DUMA[**], Cosmin LOCOVEI[**]
[*] National Institute of Research and Development in Welding and Material Testing, ISIM Timişoara
[**] Politehnica University of Timişoara, Faculty of Mechanical Engineering, Bd. Mihai Viteazu Nr.1, 300222 Timişoara
e-mail: iuliana.duma@yahoo.com

Abstract. The revision of ASTME 10, the standard method of testing the hardness of metallic materials was founded by E28.06 with regard to testing penetration resistance. The actual version of the E 10 requires metallic carbide spheres only when testing materials with the hardness higher than 400-450HBW. Steel sphere penetrators are used for softer materaials. Using this method, an increase in the precision of Brinell testing will be expected by reducing measuring errors caused by flattened steel spheres and thus prolonging the life of the penetrator. Moreover, this change will bring ASTM E 10 to ISO 6506 metallic materials- brinell hardness testing standards. Considering these aspects the work mainly presents the requirements that the hardness gauge blocks have to meet in order to produce Brinell HBW scales. Starting from these conditions, the accent is set on choosing the proper material, the primary and secondary thermical treatment applied, and also on complying with the metrological conditions imposed to these hardness gauges.

Keywords: Brinell, HBW scales, hardness standard blocks, testing

1. Introduction

The hardness standard blocks are measures with unique value. These are materializations of standardized hardness points. They are used to verify periodically the hardness determining devices, being a very important constituent of a high quality product. The calibre plates for marks are used at verifying the instalations that measure the specific size of the mark and for instructions.
The hardness standard blocks of calibre for indents are those plates at which the initial indents are marked by encircling and their specific sizes are noted in the calibration certificate.

2. Conditions imposed by the Brinell hardness standard blocks

In the Brinell hardness test [1] a ball indenter of diameter D (mm) is pressed against the surface of the test piece using a prescribed force F (N), and the diameter of the indentation d (mm) is measured after the force has been removed. (figure 1). The time for the initial application of the force is 2 s to 8 s, and the test force is maintained for 10 s to 15 s.

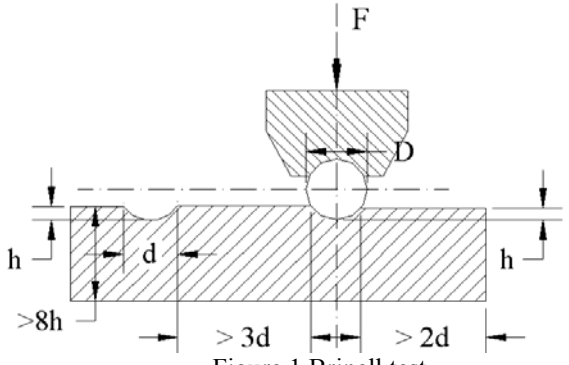

Figure 1 Brinell test

The Brinell hardness value is proportional to the test force divided by the surface area of the indentation:

HBW = Constant × Test force / Surface area of indentation

$$HBW = 0.102 \times \frac{2F}{\pi D\left(D - \sqrt{D^2 - d^2}\right)} \quad (1)$$

Consultation of the standard provides the complete list of the Brinell hardness scales, as shown in Table 1.

Table 1 Brinell hardness scales and test forces

Hardness scale	Ball diameter, D [mm]	Nominal value of test force, F [N]
HBW 10/3 000	10	29 420
HBW 10/1 500	10	14 710
HBW 10/1 000	10	9 807
HBW 10/500	10	4 903
HBW 10/250	10	2 452
HBW 10/100	10	980,7
HBW 5/750	5	7 355
HBW 5/250	5	2 452
HBW 5/125	5	1 226
HBW 5/62,5	5	612,9
HBW 5/25	5	245,2
HBW 2,5/187,5	2,5	1 839
HBW 2,5/62,5	2,5	612,9
HBW 2,5/31,25	2,5	306,5
HBW 2,5/15,625	2,5	153,2
HBW 2,5/6,25	2,5	61,29
HBW 1/30	1	294,2
HBW 1/10	1	98,07
HBW 1/5	1	49,03
HBW 1/2,5	1	24,52
HBW 1/1	1	9,807

The hardness standard blocks are made out of steel or metals and non-ferrous alloys with a homogenous and stable structure, as to ensure the uniformity and stability in time of the hardness. Irregularities such as cracks, pores or non-metalic inclusions are not accepted. Grain size has to be fine and uniform.

The base surfaces of the hardness standard blocks must be:

- flat and parallel
- finely rectified
- without corosion spots, scratches or other imperfections that might influence the hardness tests.

The hardness standard blocks must have a high uniformity of the hardness on the testing surface. The uniformity of the hardness is given by the fidelity error that must not cross a specified value. The maximum value accepted for the fidelity error depends on the method of hardness testing, the hardness scale, the hardness interval and the precision class. For the scales analyzed in the present work the uniformity of the hardness must be high, $e_f \leq 1\%$.

For the Brinell method the error is calculated as following:

$$e_f = \frac{R}{\overline{d}} \cdot 100 \quad [\%],$$

where:

amplitude $R = d_{\max} - d_{\min}$

$d_{\max}$ – the maximum average diameter obtained at the measuring of every indent made at calibration;

$d_{\min}$ – the minimum average diameter obtained at the measuring of every indent made at calibration.

$\overline{d} = \frac{1}{n}\sum_{i=1}^{n} d_i$ - the average of the n indents from where the periodical hardness is calculated;

$d = \frac{d_I + d_-}{2}$ - average indent diameter;

d_I, d_- - the measured diameters on two perpendicular directions.

3. Experimental results

The material chosen for experimentations is 100Cr6 steel (RUL 1). From previous experiments [2], [3], results that the analyzed material may have a homogenous structure that ensures the uniformity and stability in time of the hardness. One of the primary conditions is the suplementary refinement of the steel by remelting with a void spring (RAV) and electrical remelting under cinder (REZ) and primary thermic treatment (annealing of globulization).

The chemical composition of the samples, after elaboration, is presented in table 2.

Table 2 Chemical composition of the samples

C [%]	Mn [%]	Si [%]	Cr [%]	P [%]	S [%]	Ni [%]
1.00	0.33	0.29	1.6	0.01	0.006	0.12

The whole experimental lot was quenched at 840°C, temperature obtained as optimum after previous experiments [3]. After this, the subzero treatment is applied (-183°). After the treatment each sample is metallographically prepared and structurally analysed, using electron microscopy and X-rays diffraction. The structure is homogenous in section and formed out of fine martensite, remnant carbides from initial status – globulisation, small carbides and uniformity spread and small quantities of residue austenite (figure 2). The tempering temperatures experimented were 200 and 450 °C. After tempering, the Brinell HBW 10/3000 hardness has been determined for all tempered. The sclerometrical determing was made by the calibration device for Brinell hardness determing currently in the endovment of the National Institute of Metrology.

In order, to confer the nominal hardness and to have the possibility to calculate the fidelity error, an each sample the hardness was measured in five points. In the following tables the experimental results are presented for the samples that led to acquiring a hardness of approx. 410, 570 HBW 10/3000.

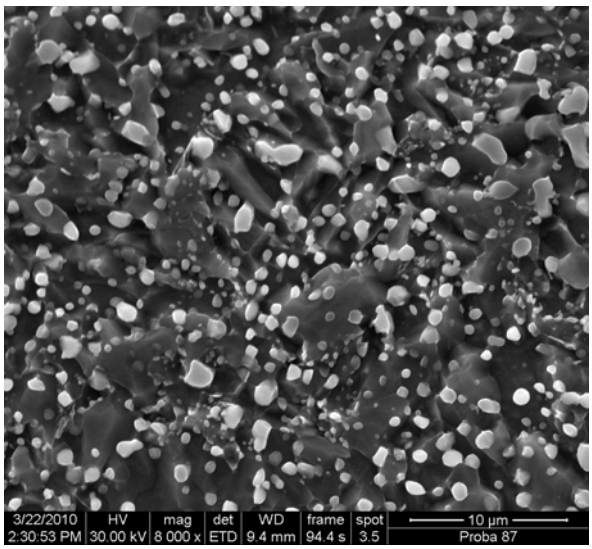

Figure 2 Globulizated samples

In table 3 the results of the measuring are presented for five plates of about 410 HBW 10/3000 and in table 4 the results of the measuring are presented for five plates of about 570 HBW 10/3000.

Table 3 Results of the measuring

No. crt.	**Material; Thermic treatment**	**The average diameters of the prints (mm)**					$\overline{d} = \frac{\sum_{i=1}^{5} d}{5}$	**Hardness HBW 10/3000**	**Fidelity error**
		d_1	**d_2**	**d_3**	**d_4**	**d_5**			**ef, %**
1	100Cr6 Q+T la 450 ºC	3,019	3,020	3,015	3,021	3,025	3,020	409	0,33
2		3,020	3,036	3,028	3,026	3,030	3,028	407	0,52
3		3,024	3,022	3,026	3,028	3,030	3,026	407	0,26
4		3,032	3,020	3,026	3,025	3,027	3,026	407	0,40
5		3,017	3,022	3,017	3,017	3,012	3,017	410	0,33

Table 4 Results of the measuring

No.crt.	Material; Thermic treatment	The average diameters of the prints (mm)					$\overline{d} = \frac{\sum_{i=1}^{5} d}{5}$	Hardness HBW 10/3000	Fidelity error
		d_1	d_2	d_3	d_4	d_5			ef, %
1	100Cr6 Q+T la 200 °C	2,562	2,560	2,558	2,566	2,564	2,562	572	0,31
2		2,568	2,564	2,560	2,556	2,552	2,560	573	0,62
3		2,570	2,580	2,577	2,575	2,573	2,575	566	0,38
4		2,566	2,568	2,566	2,564	2,566	2,566	570	0,15
5		2,555	2,569	2,549	2,559	2,563	2,559	569	0,78

It is observed that all the samples are proper for the hardness gauge performing. (hardness uniformity is between the specified limits).

In figure 3 a part (for 2θ = 31…39) of the diffraction spectrum is presented for the sample tempered at 200 and 450°C.

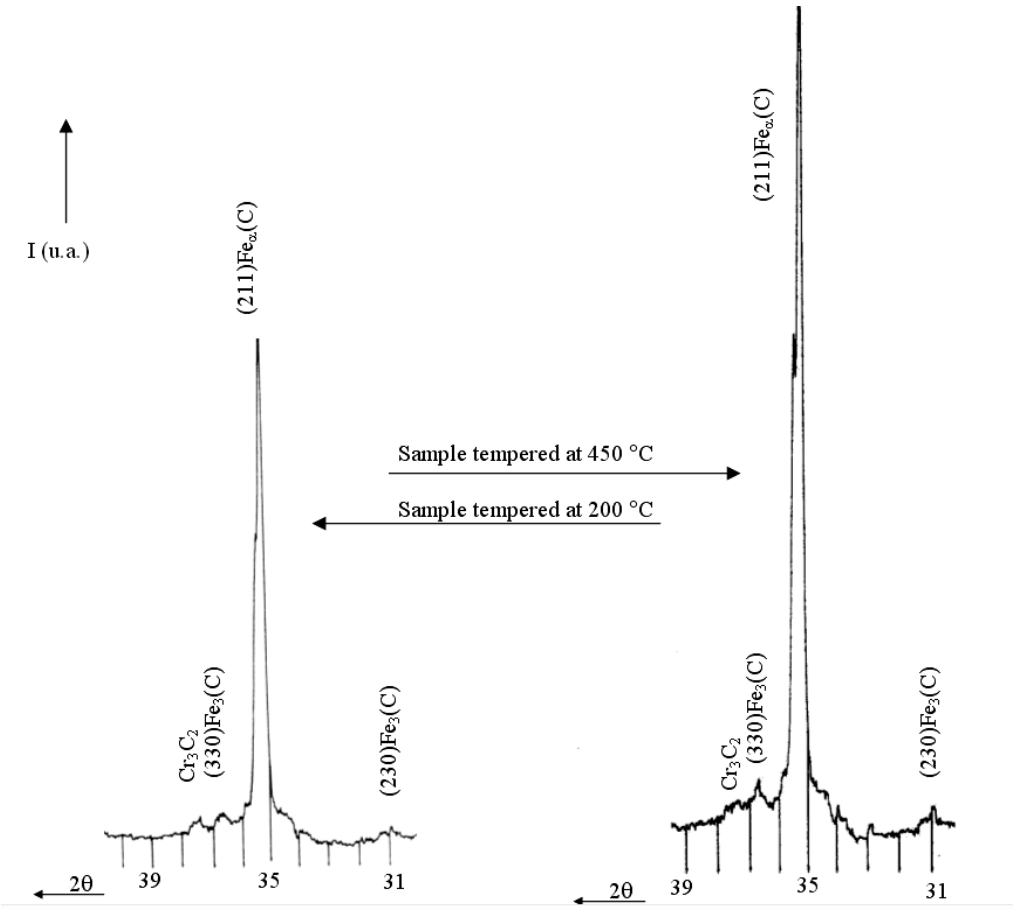

Figure 3 Diffraction spectrum

Each sample was analysed using X-rays diffraction. The structures observed with the aid of electron microscopy show a part of the effects previously mentioned. Figure 4 presents structural aspect of the material after the tempering at 200 °C, (a) and 450 ºC, (b).

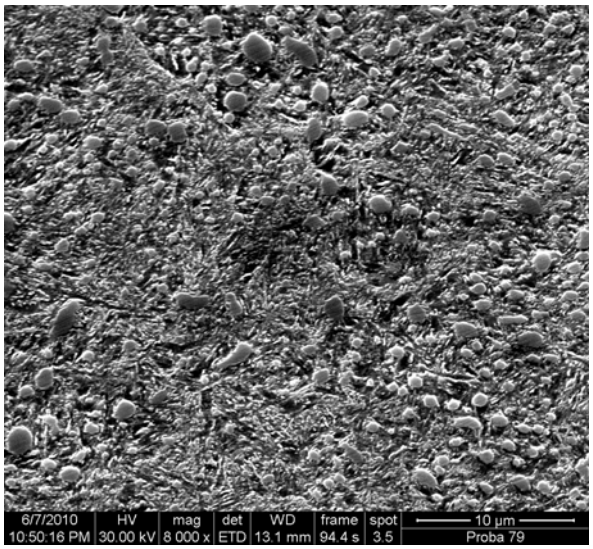

(a)

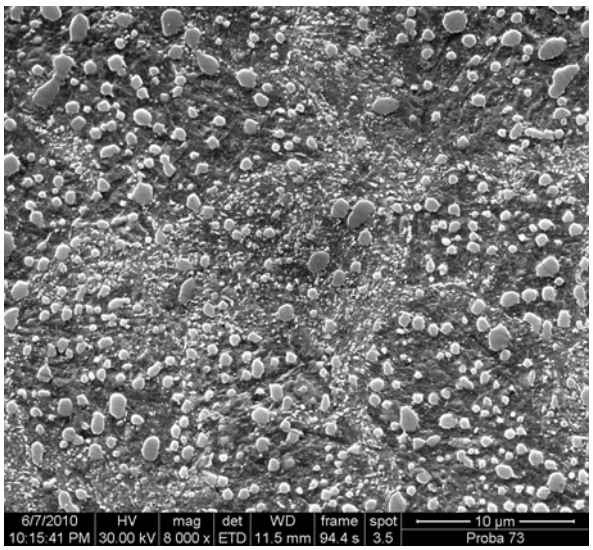

(b)

Figure 4 Structural aspect of the material after the tempering at 200 °C, (a) and 450 ºC, (b)

Analysing the resulting hardness values, X-rays diffractions and microstructures it can be observed that the growth of the tempering temperature is the bigger the carbide particles are and the lower internal tensions which leads to a decreasement of the hardness.

4. Conclusions

To comply with the requirements of uniformity and stability in time imposed to the hardness standard blocks, some conditions must be respected. The most important are:

- using a premium quality steel, suplementary refined and received with high strictness bar by bar;
- the correct appliance of the primary and secondary thermic treatment (in this case: globulisations + quenching + subzero treating + tempering).

The apropriate elaboration of the 105Cr6 and the primary treatment following by quenching and subzero treating give an uniformity and stability in time of the properties (especiallly hardness). The value of the hardness is established with the tempering treatment.

Studiu privind obținerea placutelor etalon pentru transmiterea scarilor de duritate Brinell HBW

Rezumat: Revizuirea ASTME 10, metoda standard de testare a durității Brinell a materialeor metalice, a fost initiata de E28.06 în baza testărilor durității la penetrare. Actuala versiune a E 10 necesita sfere din carburi metalice numai in cazul testarii materialelor cu duritatea mai mare de 400-450 HBW. Penetratoarele cu sfere din oțel sunt folosite la materiale mai moi. Este de asteptat ca aceasta schimbare sa imbunatateasca precizia testării Brinell prin reducerea erorilor de măsurare cauzate de sfere din oțel aplatizate si, in consecință, ar trebui sa creasca durata de viata a penetratorului. În plus, schimbarea va ridica ASTM E 10 la standerdele ISO 6506, materiale metalice – testarea durității Brinell. Având în vedere aceste aspecte lucrarea prezinta centralizat conditiile pe care trebuie sa le indeplineasca placutele etalon de duritate pentru materializarea scărilor Brinell HBW. Plecand de la aceste condiții se pune accent pe alegerea materialului, tratamentul termic primar si secundar aplicat precum si pe satisfacerea condițiilor metrologice impuse acestor etaloane de duritate.

References

1. xxx http://www.npl.co.uk
2. S. Duma, I. Cartis, L. Dobosan *Influenta tratamentului termic asupra caracteristicilor metrologice ale masurilor de duritate,* Conf. internationala de metrologie, Buc., sept. 2001
4. I. Cartis, S. Duma, *Importanța tratamentului termic de revenire în asigurarea uniformității şi stabilității în*

timp a durității pentru etaloanele de duritate, Zilele Academice Timişene, U.P.T, Editia a VIII-a, mai 2003

5. Duma. S.: *Studies regarding the acquirement of hardness standard blocks for transmitting the Knoop hardness scale 275…577 $HK_{0.2}$ and Brinell 416…589HBW 5/750* – Scientific Bulletin of the " POLITEHNICA" University of Timisoara, 2009, Tom 54(68) Fasc. 3, ISSN :1224-6077;

6. Hazotte. A. (ed.): - *Solid State Transformation and Heat Treatment*. Wiley-VCH, Weinheim 2004, ISBN-10: 352731007X, ISBN-13: 9783527310074;

7. Popescu, M., Duma, S., Locovei, C.: *Experimental research concerning structural and hardness stability of 100Cr6 steel machine parts,* 10th International Conference ″Research and Development in Mechanical Industry″ RaDMI 2010, 16 - 19. September 2010, Donji Milanovac, Serbia, ISBN 978-86-6075-018-3;

8. Serban, V.A., Răduță, A.: *Ştiinţa şi Ingineria Materialelor*, Editura Politehnica, Timişoara, 2010, ISBN: 978-606-554-044-6.

Scientific reviewers: **Roland CUCURUZ, Politehnica University of Timisoara**
Victor Budău, Politehnica University of Timisoara

SCIENTIFIC BULLETIN OF
THE „POLITEHNICA" UNIVERSITY OF TIMISOARA, ROMANIA
TRANSACTIONS ON MECHANICS
BULETINUL ŞTIINŢIFIC AL
UNIVERSITĂŢII „POLITEHNICA" DIN TIMIŞOARA, ROMÂNIA
SERIA MECANICĂ
Tom 56 (70) ISSN 1224 - 6077 Fasc. S1, 2011

INCOMPATIBILITY PROBLEMS IN OBTAINING Ti-6Al-4V + X10CrNiTi18-10 WELDS

Cosmin GROZA [*], Ion MITELEA [**],
[*]University "Politehnica" of Timişoara, Mihai Viteazul, nr.1 Timişoara, Romania, E-mail: cosmin81_ro@yahoo.com
[**] University "Politehnica" of Timişoara, Mihai Viteazul, nr.1 Timişoara, Romania, E-mail:ion.mitelea@mec.upt.ro

Abstract. This study has analyzed the main problems that appear when welding dissimilar materials, with a special focus on the combination α + β titanium alloy and an austenitic stainless steel. The phase equilibrium diagrams of binary alloys represent a useful tool in assessing the microstructure of the weld; they also identify the types of chemical combinations that can be obtained at the contact point of the two materials.

Keywords: dissimilar materials, welding, incompatibility

1. Introduction

Joining dissimilar materials through techniques that assure a metallic continuity is based on making the most of a favourable combination of properties, such as:

- The favourable mechanical properties of one material and the reduced specific weight of the other;
- The favourable mechanical properties of one material and a good corrosion stability of the other;
- The favourable mechanical properties of one material and the good electrical properties of the other.

One of the main reasons of employing dissimilar metallic structure is the reduction in their total weight. A lot of structures in the industries of aeronautical, terrestrial, and space vehicle design are manufactured from dissimilar materials.

2. The bases of dissimilar materials weldability

The problems related to the weldability of this type of materials are mainly due to the differences that may appear among their mechanical, physical and chemical properties:

- The type and parameter of the crystalline lattice;
- The melting temperature;
- The specific weight;
- The linear expansivity;
- The heat conductivity;
- The type of phase equilibrium diagram of the two base metals;

Moreover, their ability to be joined by brazing and soldering also has a significant impact. Table 1 displays all properties taken into account when analysing the weldability of some dissimilar metals.

In order to assess the structural changes that occur when welding various combinations of materials, phase equilibrium diagrams can be used, providing information related to:

- The solubility of a component into another;

- The tendency towards chemical or intermetallic compound formation;
- The sensitivity to welding cracks.

Figure 1 displays the possible types of phase equilibrium diagrams as well as the simplified microstructure of the welds obtained from dissimilar metals.

Table 1 The properties of some metals used in obtaining dissimilar joints

Property	**Metal**						
	Ti	**Fe**	**Cu**	**Ni**	**Al**	**Mo**	**Zn**
The type of phase equilibrium diagram at 20˚C	HCP	bcc	fcc	fcc	fcc	bcc	HCP
The parameter of the crystalline lattice, Å	a=2,95 c=4,86	a=2,86	a=3,607	a=3,517	a=4,04	a=3,14	a=2,67 c=4,94
The linear expansivity, 1/K	$8,3x10^{-6}$	$11,7\text{-}12,3 x10^{-6}$	$16,5x10^{-6}$	$13,3x10^{-6}$	$23,5x10^{-6}$	$5,1x10^{-6}$	$33x10^{-6}$
The specific heat, J/gK	0,54	0,46	0,37	0,46	0,91	0,27	0,37
The heat conductivity, W/cm K	0,15	0,92	3,97	0,92	2,3	1,42	1,13
The melting temperature, ˚C	1725	1538	1083	1455	658	2622	419
Density kg/m³	4505	7870	8940	8907	2720	10200	7430
Hardness HB, daN/mm²	140-200	50-80	32-37	65-70	20-25	200	30
Tensile strength, N/mm²	230-550	180-320	160-235	280-300	50-100	500-550	150
Yield strength, N/mm²	150-480	90-250	35-75	140-200	15-30	350	40
Modulus of elasticity, N/mm²	116000	196000	115000	214000	69000	300000	130000
Elongation, %	15-70	30-50	25-60	35-40	35-50	40-50	20-25

No.	Phase equilibrium diagram	The simplified microstructure of the weld	Predictable properties of the weld
1.	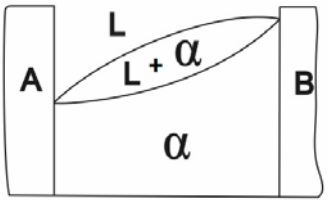	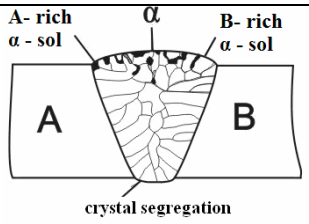	- The weld is formed from a solid solution with a low sensitivity to welding cracks - The weld has favourable mechanical properties - The weld exhibits heat-affected segregations and cracks
2.	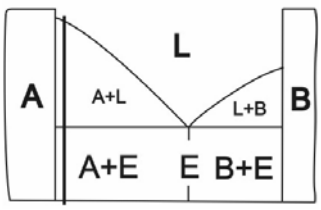	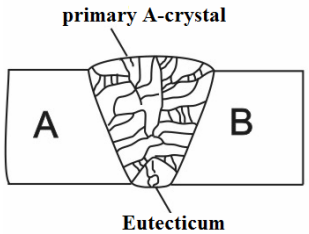	- The properties of the weld depend on those of the eutectic - The values of the properties are inferior to those of the primary solid solution - The low melting temperature of the eutectics can produce heat-affected crack
3.1	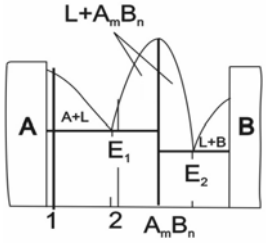	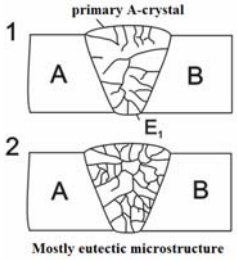	- Additional measures may influence: o The decrease in the proportion of intermetallic compounds o The increase in the quantity of A and B crystals

3.2	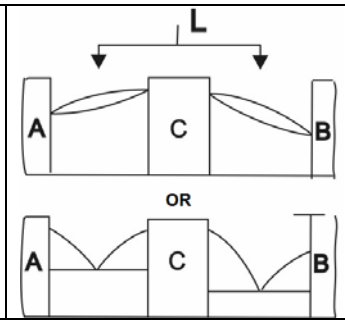	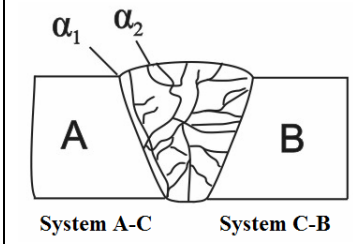	The selection of metal C and metal coating A secures the formation of systems A-C and C-B, presenting intermetallic compounds.

Figure 1 The connection between the phase equilibrium diagrams and the microstructure of dissimilar metals

The following situations are characteristic to the process of welding dissimilar materials:

- Both materials melt during the welding process
- Only one material melts during the welding process
- Neither of the materials melts during the welding process

Regardless of the changes in state that may have occurred, the welding process can be divided into two phases:

a) The 'close-in' phase, when the atoms of the two metals get so close that the distance between them is smaller than the parameter of the crystalline structure; this phase facilitates the processes of diffusion and plastic deformation

b) The phase of the interactive reaction between the contact surfaces, leading to the formation of metallic and/or covalent bonds.

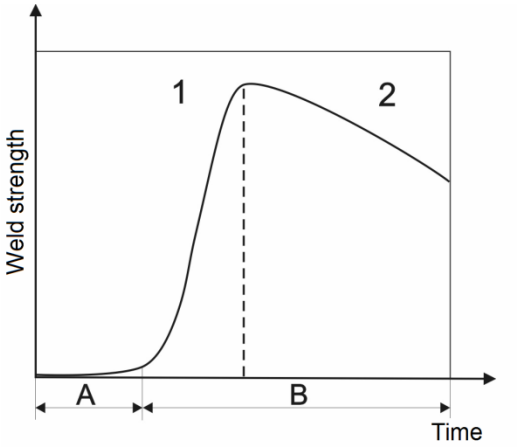

Figure 2 The formation of a weld from dissimilar materials: A - physical activity, B -chemical activity of the contact surfaces; 1 - formation of the solid solution; 2 - formation and growth of intermetallic compounds

Figure 2 presents the main phases in the process of forming a weld from dissimilar materials as well as the ways to change the mechanical strength. The following are the most important cautions that have to be taken into account for a reliable process:

- To minimize the contact time in the liquid state;
- To avoid allowing air in the molten metal bath;
- To prevent the formation and growth of intermetallic compounds;

These can be accomplished by taking any of the measures below:

- Welding with linear energy in the smallest possible doses;
- Gas-shielded arc welding (Ar, He, vid) and using protective coats on the material part which does not melt during the welding process (Ni, Cu, Al), because they lead to a better wettability of the material part that melts during the welding process. The most dangerous aspect of the quality and security of a welded bond is represented by the chemical combinations that appear at the surface of contact between the two materials. They can be formed both in the molten metal bath and the solid phase, depending on the thermal cycle of each welding point. The maximum temperature that can be reached when welding and the duration of keeping it above the superior critical transformation point have the biggest influence on developing and growing some chemical combinations. The nature and quantity of chemical and intermetallic compounds may depend on:
  - A thorough selection of the welding additive material;
  - The use of buffer layers between the two base materials with a good welding compatibility;
  - The use of specialised welding equipment, having a controlled thermal cycle.

Table 2 offers a synthetic presentation of the main combination of dissimilar materials used for welding, of the problems that may appear and the recommended welding processes.

Table 2 Dissimilar materials welding-specific problems

Combinations of materials	Processes of fusion welding	Processes of pressure welding	Specific phenomena	
			Solubility	Types of compounds
Steel and Ti alloys	WIG, MIG, laser	Friction, diffusion	Up to 0,5% Fe in Ti_α	FeTi; Fe_2Ti
Steel and Al alloys	WIG, MIG, laser, electron beam	Friction, diffusion, resistance, explosion	Up to 33% Al in Fe_α	$FeAl_3$, Fe_2Al_5
Steel and Cu alloys	WIG, MIG, electron beam, laser	Friction, explosion	Up to 8% Cu in Feγ; up to 1,4% Cu in Fe_α	-
Al – Cu	WIG, MIG	Explosion	Up to 9,8% Al in Cu	Al_2Cu
Al – Ti	WIG, MIG	Friction, diffusion, explosion	Up to 6% Al in Ti_α	TiAl, Al_3Ti
Cu -Ti	WIG, MIG	Diffusion, explosion	Up to 2,1% Cu in Ti_α; up to 17%Cu in Ti_β	TiCu, Ti_2Cu, Ti_2Cu_3

3. Opportunities in obtaining dissimilar titanium alloys – austenitic steels bonds

Taking into account the extremely favourable properties of titanium and its alloys, their applicability in the chemical, aerospace and nuclear energy industry has been continuously extending. Its main disadvantage, however, is its significantly high price. Technically pure titanium is approximately 10 times more expensive than stainless steel and 100 times more expensive than carbon steel. Due to this, many car parts and waggons are not manufactured from titanium but from cheaper materials, only coated with a titanium layer. For instance, bins for chlorine-rich city waste are produced this way. However, many times there has been a practical need for combining titanium-based materials with steel elements. One such example would be the vessel bond between titanium exhaust pipes and steel shielding mesh.

The positioning of fitting layers between the two materials and the use of special welding methods are the main solutions to resolve welding problems.

We will further briefly present the main advantages and disadvantages of some of the most popular welding methods (Figure 3).

3.1 WIG Welding

Electric arc welding of titanium to steel produces welding cracks which can be due to the brittleness of the intermetallic phases followed by the incomplete solubility of the titanium into iron. The phase equilibrium diagram of Fe-Ti presented in Figure 3 shows that Fe concentration of more than 0,1% in the solid solution of titanium in iron are associated with the intermetallic phases FeTi or Fe_2Ti with embrittling effect.

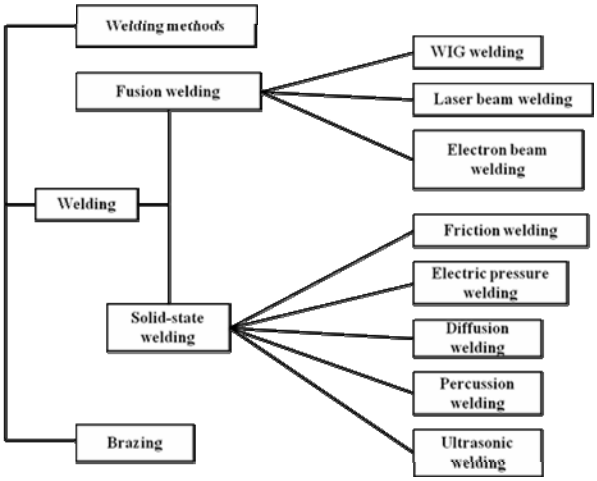

Figure 3 Welding methods

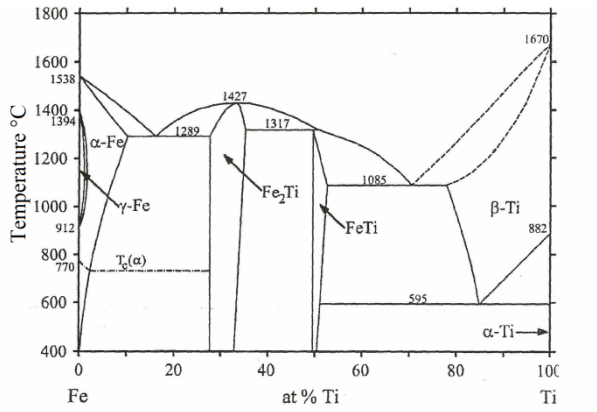

Figure 4 Fe-Ti phase equilibrium diagram

There have been global attempts to use the WIG welding method to weld titanium OT4 alloys to austenitic stainless steel 1X18H9T by introducing a layer of technical tantalum on the side of the titanium and a bronze foil on the side of the steel. The results obtained are irrelevant,

namely the mechanical properties of the welded bond were only satisfying and the risk for defects was still present. Other attempts focused on the foil welding of tantalum and vanadium.

Another disadvantage of WIG welding these dissimilar materials is represented by the need to use very expensive tantalum or vanadium foils and to run a multiple-phase process.

3.2 Explosion welding

Explosion welding is the method of obtaining joints as a result of the explosive-generated dynamic pressure on the welded surface (Figure 5). It can be employed to produce wrought disks and titanium coated foils. While using this method to weld titanium and steel, a layer of intermetallic phases is formed on the contact surface. However, their thickness is significantly smaller than the one specific to other welding methods. Moreover, the cavities that appear on the welding edges affect the continuity and adherence of this layer.

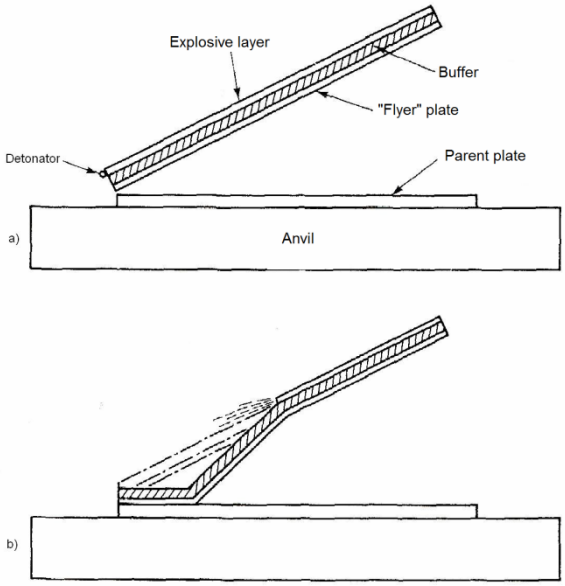

Figure 5 Explosion welding

Previous researches have proved that this welding method has the advantage of guaranteeing increased mechanical strength for the obtained bonds. For example, when welding 6000 mm long and 1250 mm wide plates, the obtained shear stress values were over 1250 mm.

The advantages of employing this method to weld titanium and steel are:

- the possibility of welding building materials of variable width;
- satisfying mechanical and technological properties of the joint;
- cheap price.

The main disadvantage, however, is the need for a special place to conduct the welding process.

3.3 Brazing titanium to stainless steel

The attempts to employ this method by using an eutectic compound $Ag_{72}Cu_{28}$ with a melting temperature of 779°C as a welding additive material did not generate satisfying results due to the formation of a brittle intermetallic phase with Cu and Ti and phases with Ag and Ti characterised by high plasticity. To enhance the mechanical strength characteristics of the joint, a new welding additive material $AgCu_{24}In_{14}Ti$ was selected but, although the number of brittle phases decreased, the wettability of the stainless steel was reduced and the brazing temperature exceeded 900°C.

Other researches focused on selecting welding additive materials of the Ti-Zr-Be, Ti-Ni-Cu, Ni-Cr-Fe-Si-B, Au-Ni and Pd-Ag-Si types. But they do not sustain quality results. Moreover, beryllium is toxic, nickel causes brittleness and gold and palladium are expensive.

To prevent the development of brittle intermetallic phases, the surface of the titanium should be covered with a metal coating or an alloy to act as a protective barrier against the diffusion of elements in the addition material. The PVD method of placing a 3-layered coating of Cr-Ni-Cu makes this process much more different and the associate costs much higher.

3.4 Friction welding

Attempts to weld titanium to ARMCO iron through direct friction proved that the intermetallic phases in the bond are inevitable. They form at 2/3 of the radius distance, starting from the centre of the sample. For this reason, there have been attempts to position vanadium and copper layers between the two materials, titanium – steel. To obtain such a bond, the steps below should be followed:

- welding steel and copper;
- welding titanium and vanadium;
- welding the titanium-vanadium component to the copper-steel component.

The results obtained proved that the mechanical strength of the joints is quite small, the breakage always occurring in the copper layer area.

Another disadvantage of the conventional friction welding of titanium to steel is the need to

use buffer layers, a fact that prolongs the welding preparation time.

4. Conclusions

Welding different materials is still a matter of concern as it cannot be fully accomplished with the help of common techniques, such as manual electric arc welding, MIG welding , WIG welding etc.

Laser beam welding or solid state welding (through friction, diffusion or explosion) may solve the incompatibility problems between titanium alloys and stainless steels.

Modifying the chemical composition of the welding pool is an attempt to avoid the formation of brittle intermetallic phases between iron and titanium, and the working environment of the welding process will prevent the rapid oxidation of titanium.

Friction welding of the two materials is estimated to result in welds with enhanced mechanical properties and presenting no flaws or cracks.

References

1. Blazczyk W., Melechow R., Tubielewicz K: *Tytan I jego stopy.* Wydawnictwo Politechniki Czestochowskiej, Czestochowa, 2004.
2. Walczak W.: *Zgrzewanie wybuchowe metali i jego zastosowanie.* WNT, Warszawa, 1989.
3. Welding Titanium a Designers and Users Handbook. Guide to Best Practice ,1999.
4. Lison R., Metzger G., *Electron Beam Welding of Dissimilar Metals,* pp.230-s-240s, Welding Journal (1976),
5. Poradnik Inzyniera. Spawalnictwo. Pod dedakcja Jana Pilarczya. Wydawinctwo Naukowo-Techniczne, 2005.

Probleme de incompatibilitate la realizarea îmbinărilor sudate Ti-6Al-4V+X10CrNiTi18-10

Rezumat

În lucrare se analizează principalele probleme care apar la sudarea materialelor disimilare, cu accent pe combinaţia dintre un aliaj de titan cu structură bifazică α + β şi un oţel inoxidabil austenitic. Diagramele de echilibru ale aliajelor binare constituie un instrument util pentru evaluarea microstructurii sudurii cu identificarea tipurilor de combinaţii chimice care se pot forma în zona de contact a celor două materiale.

Scientific reviewers: **Victor Budău*, University Politehnica of Timisoara**
Mihaela Popescu, University Politehnica of Timisoara**

SCIENTIFIC BULLETIN OF
THE „POLITEHNICA" UNIVERSITY OF TIMISOARA, ROMANIA
TRANSACTIONS ON MECHANICS
BULETINUL ŞTIINŢIFIC AL
UNIVERSITĂŢII „POLITEHNICA" DIN TIMIŞOARA, ROMÂNIA
SERIA MECANICĂ
Tom 56 (70) ISSN 1224 - 6077 Fasc. S1, 2011

RESEARCH ON CRITICAL PLANE POSITIONS AND STRESSES IN MATERIALS SUBJECTED TO CYCLIC TENSION-TORSION LOADING

Lorand KUN*, Ion DUMITRU*

* "Politehnica" University of Timisoara, Mechanical Engineering Faculty, Strength of Materials Department, Mihai Viteazul Blvd no.1, 300222 Timisoara, Romania

Abstract. Durability evaluation of materials subjected to multiaxial fatigue represents today a very important stage of mechanical design. In this context, in recent years extensive multiaxial fatigue studies have been carried out in laboratories and on equipment capable of generating tension-torsion loading. Correct selection of the load path in order to plot the fatigue limit curve of a material imposes a careful analysis of critical planes and normal and/or shear stresses acting on them. This is necessary since critical plane positions are unknown under such complex load paths. In the first part of the paper an analysis is carried out on the influence of normal/shear stress amplitude ratio and of the phase angle on critical plane positions – critical planes being the material planes on which the normal or shear stresses reach extreme values. The second part of the paper presents a critical plane analysis based on three different multiaxial fatigue models: Yokobori, Matake and McDiarmid. Finally a comparison between these models is presented based on their corresponding equivalent stresses, since these equivalent stresses are used in plotting fatigue limit curves for tension-torsion loading.

Keywords: multiaxial fatigue, tension-torsion, critical plane, phase shift, stress ratio

1. Introduction

Multiaxial stresses and strains are present in case of almost every component of equipment designed in the machine building industry. This is why even today much research is done regarding the fatigue evaluation of materials [1, 2]. In this context, various new studies have been carried out regarding durability analysis of materials subjected to tension-torsion loading [3 - 9].

If a machine component is subjected to multiaxial loading, normal and shear stresses act on every material plane. The so-called "critical plane criteria" fatigue models are based on reducing the multiaxial stress state into a uniaxial one, on a certain plane. According to these criteria, both the normal and shear stresses contribute with a certain share to the formation of fatigue cracks. Thus, the critical plane can be defined as the plane where a stress (normal or shear) or a mathematical combination of stresses and/or strains reaches a values considered to be critical [3, 10, 11].

Given the above, in the present work a multiaxial load history is adopted, composed of a normal and a shear stress, both variable in time, with various amplitude ratios and phase shift angles. In the first part of the paper, an analysis is carried out regarding the influence of amplitude ratio and phase shift on the positions of the critical planes, which are defined as the planes where the normal or shear stresses reach extreme values.

In the second part of the paper, the critical plane concept is analyzed by applying the Yokobori [12], Matake [13] and McDiarmid [14] models. Finally a comparison between these models is made, based on the correct evaluation of the corresponding equivalent stresses, which can

be used in plotting fatigue curves for tension-torsion loading.

2. Material characteristics and load history

In the calculations, the experimentally determined characteristics of 41Cr4 steel were considered (Table 1).

Table 1 Material characteristics

Material	41Cr4
Ultimate tensile strength, σ_r *[MPa]*	860
Ultimate shear strength, τ_r *[MPa]*	650
Tensile yield strength, σ_c *[MPa]*	770
Shear yield strength, τ_c *[MPa]*	460
Rotating bending fatigue lim.σ_{-1} *[MPa]*	293**
Torsional fatigue limit, τ_{-1} *[MPa]*	180

* Heat treatment: quench hardening at 830 °C followed by annealing at 400 °C;
** for N = 1000000 cycles

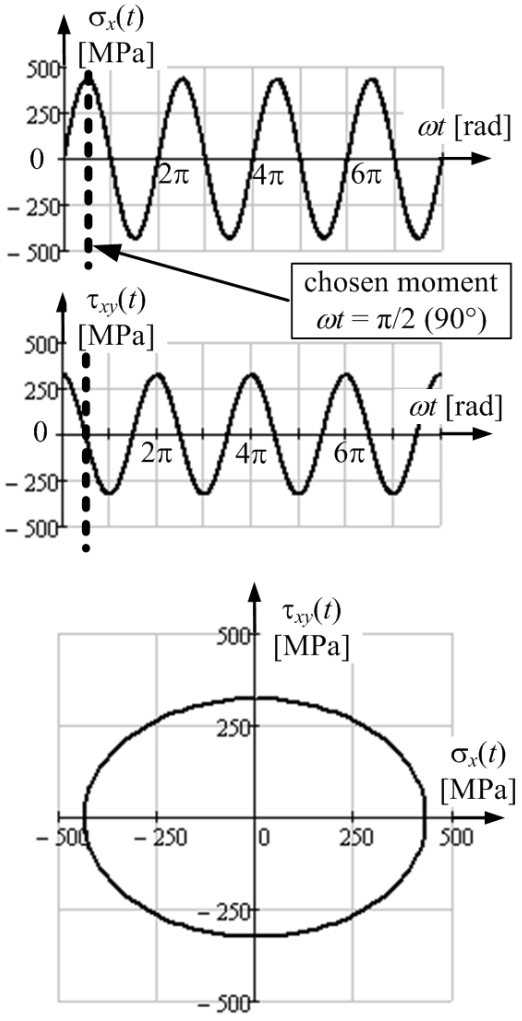

Figure 1 Stress time histories and loading path for A = 0.75 and $\phi = \pi / 2$

Consider a component machined from this material, subjected to cyclic multiaxial tension-torsion (Fig. 1), composed of a normal and of a shear stress (Eq. 1-2), where the subscripts have the meaning: m – mean stress, a – stress amplitude, and ϕ is the phase shift angle.

$$\sigma_x(t) = \sigma_{x,m} + \sigma_{x,a} \cdot \sin(\omega t) \quad (1)$$

$$\tau_{xy}(t) = \tau_{xy,m} + \tau_{xy,a} \cdot \sin(\omega t + \phi) \quad (2)$$

The ratio of the two stresses' amplitudes $A = \tau_{xy,a} / \sigma_a$ and ϕ were given different values.

The variation of A from 0.5 to 1 is obtained by decreasing $\sigma_{x,a}$ from 650 to 325 MPa, while keeping $\tau_{xy,a}$ constant at 325 MPa.

3. Finding the critical plane as the plane with maximum normal or shear stress

Since except for σ_x and τ_{xy}, all the other components of the stress tensor are zero, plain stress is accepted [1, 2], and the mathematical relations for computing normal and shear stresses in any material plane inclined by the angle θ are given in Eq. 3-4.

$$\sigma(t,\theta) = \frac{\sigma_x(t)}{2} + \frac{\sigma_x(t)}{2} \cdot \cos 2\theta + \tau_{xy}(t) \cdot \sin 2\theta \quad (3)$$

$$\tau(t,\theta) = -\frac{\sigma_x(t)}{2} \cdot \sin 2\theta + \tau_{xy}(t) \cdot \cos 2\theta \quad (4)$$

A calculation program has been written in order to compute the angles of the planes where the normal, shear of the shear stress amplitude reach extreme values.

This program was used to compute the values of normal and shear stresses during one whole load cycle, on planes inclined from 0 to 360° and with different values of A and ϕ. Fig. 2 presents the surfaces generated by plotting σ, τ and τ_a as functions of two parameters simultaneously, ϕ and θ, at one chosen moment ωt on the load cycle.

The mathematical functions describing these surfaces were the basis in determining the critical plane positions, regarded as the planes where σ or τ reach extreme values. The values of σ and τ on these critical planes as well as their angles θ are presented in Table 2.

4. Finding the critical plane and equivalent stress based on different models

The idea that all critical plane models are built upon is the reduction of a multiaxial stress state into an equivalent uniaxial one, but on a certain plane [1,2,10]. According to this concept, both normal and shear stresses on the critical plane contribute to the damage process, and they can be combined in a mathematical relation.

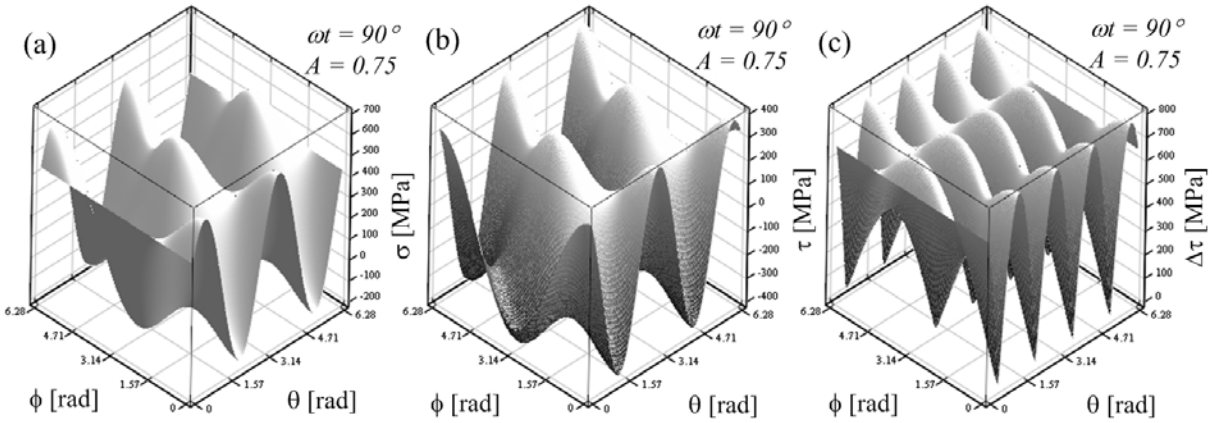

Figure 2 Surfaces generated by σ (a), τ (b) and τ_a (c), as functions of θ and ϕ, for $\omega t = 90°$

These models, besides of determining the critical plane's position, also allow the computing of the number of cycles to failure.

4.1. Yokobori model

According to Yokobori [12], the critical plane is the one with the normal *n* where the shear stress reaches its extreme value. The resulting equivalent stress is also influenced by the normal stress on the same plane (Eq. 5). The material parameter α is a function of the fatigue limits under tension and torsion.

$$\sigma_{Yokobori} = \max_t\left(\tau_n(t)\right) + \alpha \cdot \sigma_{n,\max}; \quad \alpha = 2\left(\tau_{-1}/\sigma_{-1}\right) - 1 \tag{5}$$

4.2. Matake model

Unlike Yokobori, Matake [13] considers the critical plane the one with normal *n* where the shear stress amplitude reaches an extreme value (Eq. 6). α and σ_n have the same significance as above.

$$\sigma_{Matake} = \max_t\left(\tau_{n,a}(t)\right) + \alpha \cdot \sigma_{n,\max}; \quad \alpha = 2\left(\tau_{-1}/\sigma_{-1}\right) - 1 \tag{6}$$

4.3. McDiarmid model

McDiarmid [14] proposed a similar model with Matake, but the parameter α is a function of tension fatigue limit and ultimate tensile strength (Eq. 7).

$$\sigma_{McDiarmid} = \max_t\left(\tau_{n,a}(t)\right) + \alpha \cdot \sigma_{n,\max}; \quad \alpha = \tau_{-1}/2\sigma_r \tag{7}$$

4.4. Finding the critical plane and equivalent stress

The above presented models were applied in case of the load history given in Fig. 1, considering different values for *A* and ϕ, and implemented in the calculation program.

The surfaces generated by plotting the Yokobori, Matake and McDiarmid equivalent stresses as functions of two parameters simultaneously, ϕ and θ, at one chosen moment ωt on the load cycle, are given in Fig. 3a, 3b and 3c. Another set of surfaces, given in Fig. 3e, 3f, and 3g, present the influence of *A* on each equivalent stress, simultaneously with the variation of the plane angle θ.

In case of the Yokobori model, the critical plane has been determined based on Fig. 2b, while for the Matake and McDiarmid models using Fig. 2c, according to Eq. 5-7.

5. Analysis of results

As stated before, the calculations were carried out in case of different values for parameters *A* and ϕ. The values of these parameters together with the corresponding critical plane position θ_{cr} and the values of σ, τ, τ_a and the equivalent stresses $\sigma_{Yokobori}$, σ_{Matake} and $\sigma_{McDiarmid}$ are all given in Table 2, at the chosen moment $\omega t = 90°$.

The results in Table 2 show that in case of the critical plane defined as the one with maximum normal stress, the critical plane position θ_{cr} changes with the increase of the shift angle ϕ (*A* being constant). The critical plane becomes normal to the normal stress's direction ($\theta_{cr} = 0$) when $\phi = \pi/2$.

Analyzing the dependence between ϕ and the plane where τ has extreme values, a major influence of the phase shift angle on the critical plane's position can be seen. On the other hand, the influence of *A* on θ_{cr} is not as strong, the plane position remaining approximately around $\theta_{cr} \cong 160°$. However, it can be clearly seen that θ_{cr} is increasing with the decrease of $\sigma_{x,a}$, even though the increment of θ_{cr} is rather small.

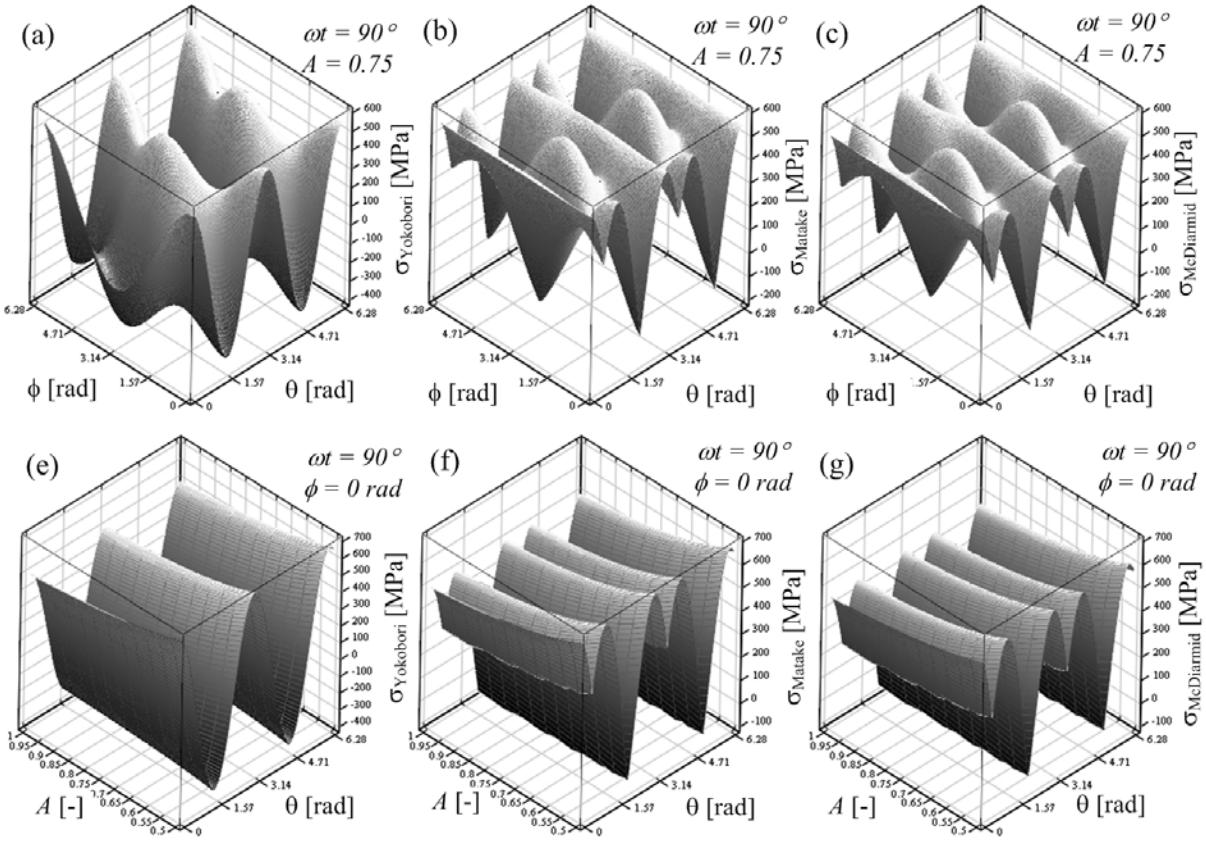

Figure 3 Surfaces generated by plotting $\sigma_{Yokobori}$, σ_{Matake} and $\sigma_{McDiarmid}$ as functions of θ and ϕ (a, b, and c) respectively as functions of θ and A (e, f and g), for $\omega t = 90°$

Table 2 Stress values and critical plane positions for $\omega t = 90°$

No.	Phase shift	Amplitude ratio	Normal stress on critical plane	Shear stress on critical plane	Shear stress amplitude on critical plane	Yokobori stress on critical plane	Matake stress on critical plane	McDiarmid stress on critical plane	Critical plane position
	ϕ [rad]	A [-]	σ [MPa]	τ [MPa]	τ_a [MPa]	$\sigma_{Yokobori}$ [MPa]	σ_{Matake} [MPa]	$\sigma_{McDiarmid}$ [MPa]	
	Critical plane = where σ is max								θ_{cr} [°] (σ_{max})
1	0	0.75	607.23	-5.48	5.48	-	-	-	28.5
2	π / 6	0.75	571.86	-0.73	98.86	-	-	-	26.2
3	π / 4	0.75	532.47	4.68	160.11	-	-	-	22.9
4	π / 3	0.75	487.5	0.95	225.76	-	-	-	18.3
5	π / 2	0.75	433.33	0	325	-	-	-	0
6	π	0.75	607.21	-6.42	6.42	-	-	-	152.3
	Critical plane = where τ is max								θ_{cr} [°] (τ_{max})
7	0	0.50	316.83	459.55	459.55	621.64	-	-	156.9
8	0	0.55	300.48	439.2	439.2	592.93	-	-	159.2
9	0	0.60	274.37	423.04	423.04	563.42	-	-	160.3
10	0	0.65	253.82	410.01	410.01	539.88	-	-	161.5
11	0	0.70	237.69	399.36	399.36	520.96	-	-	162.6
12	0	0.75	210.74	390.56	390.56	498.38	-	-	162.7
13	0	0.80	201.37	383.25	383.25	486.28	-	-	163.9
14	0	0.85	193.2	377.05	377.05	475.9	-	-	164.9
15	0	0.90	174.57	371.74	371.74	461.06	-	-	165
16	0	0.95	171.53	367.27	367.27	455.02	-	-	166.2
17	0	1.00	168.78	363.31	363.31	449.66	-	-	167.2

18	0	0.75	210.73	390.56	390.56	498.38	-	-	162.7
19	π / 6	0.75	220.1	355.18	377.99	467.79	-	-	161.5
20	π / 4	0.75	214.38	315.83	356.77	425.52	-	-	158.1
21	π / 3	0.75	216.91	270.83	319.27	381.81	-	-	153.5
22	π / 2	0.75	217.62	216.66	216.66	328.01	-	-	135.1
23	π	0.75	212.92	390.58	390.58	499.52	-	-	106.6
	Critical plane = where τ_a is max								θ_{cr} [°] ($\tau_{a,max}$)
24	0	0.50	324.71	-459.62	459.62	-	625.75	583.78	67.5
25	0	0.55	297.11	-439.22	439.22	-	591.23	552.82	68.7
26	0	0.60	273.73	-423.05	423.05	-	563.09	527.71	69.9
27	0	0.65	252.42	-410.02	410.02	-	539.17	506.54	71.1
28	0	0.70	232.68	-399.39	399.39	-	518.44	488.36	72.2
29	0	0.75	215.41	-390.6	390.6	-	500.81	472.96	73.3
30	0	0.80	201.37	383.25	383.25	-	486.28	460.24	163.9
31	0	0.85	193.2	377.05	377.05	-	475.9	450.92	164.9
32	0	0.90	179.69	-371.79	371.79	-	463.72	440.49	75.5
33	0	0.95	171.53	367.27	367.27	-	455.02	432.85	166.2
34	0	1.00	162.91	-363.36	363.36	-	446.71	425.65	76.7
35	0	0.75	215.41	-390.6	390.6	-	500.81	472.96	73.3
36	π / 6	0.75	249.61	353.66	379.41	-	507.12	474.85	163.9
37	π / 4	0.75	289.53	307.32	366.15	-	514.28	476.85	165
38	π / 3	0.75	342.72	239.71	349.45	-	524.79	480.49	167.3
39	π / 2	0.75	433.33	0	325	-	546.71	490.69	0
40	π	0.75	213.22	-390.59	390.59	-	499.68	472.11	17.1

Considering now the values of θ_{cr} obtained in case of the critical plane defined as the plane where τ_a reaches an extreme value, no clearly visible dependence can be observed between θ_{cr} and A respectively θ_{cr} and ϕ.

It has been observed that the Matake equivalent stress is always higher than the McDiarmid stress. This can be explained by the difference in defining the material parameter α.

It has also been found that the Yokobori and Matake equivalent stresses always have very close or even identical values, at almost any combination of A and ϕ. This comes as a surprise, since the two models define the critical plane differently. For the same reason, however, the positions of the critical planes predicted by Matake and Yokobori are not in any correlation. If also taken into consideration the critical plane definition proposed by Findley and analyzed by the authors [15], the conclusion can be drawn that critical planes and their positions are not universally accepted and they depend very much on the hypotheses used in each and every criterion.

6. Conclusions

This paper presents the analysis of the influence of phase shift and amplitude ratio on the positions of material planes where certain parameters reach extreme values, adopting cyclic multiaxial load histories. Firstly, the planes where the normal or the shear stresses reach extreme values are considered to be critical. Secondly, the critical plane concept is analyzed from the point of view of some critical plane models, such as Yokobori, Matake and McDiarmid.

It has been found that the phase shift has an important influence on critical plane positions, when critical planes are considered the ones where the normal or shear stresses reach extreme values. On the other hand, the variation of stress amplitudes did not produce sudden shifts in critical plane angles.

The McDiarmid model has proven to be less conservative than Yokobori and Matake. The latter two models, although they define the critical plane differently and are in no correlation with each other regarding the critical plane's angle, they produce very similar equivalent stress values.

It is concluded that in case of the analyzed critical plane models, the positions of the planes considered to be critical depend greatly on their defining hypotheses which vary from one criterion to another, thus they are not in good correlation with each other.

Acknowledgement

This work was partially supported by the strategic grant POSDRU/88/1.5/S/50783, Project ID50783 (2009), co-financed by the European Social Fund – Investing in People, within the Sectoral Operational Programme Human Resources Development 2007-2013.

References

1. Dumitru, I.: *Bazele calculului la oboseala*, Ed. Eurostampa, ISBN: 978-973-687-820-6, Timisoara, 2009 (in Romanian)
2. Socie, D., Marquis, G.: *Multiaxial Fatigue*, SAE International, ISBN-10: 0-7680-0453-5, 2000
3. Dumitru, I., Kun, L.: *On the multiaxial high cycle damage parameters*, Scientific Bulletin of the Petrol-Gas University of Ploiesti, Technical Series, vol. LXIII, nr. 1, 2011, p. 117-126, ISSN: 1224-8495
4. Kun L., Dumitru I., Cotuna E.: *A study on multiaxial high cycle fatigue models*, Proceedings of ModTech2011, vol. I, 2011, pp. 561-564, ISSN: 2069-6736, Chisinau, Republic of Moldova
5. Bernasconi, A., Folletti, S., Papdopoulos, I.V.: *A study on combined torsion and axial load fatigue limit tests with stresses of different frequency*, International Journal of Fatigue, vol. 30, 2008, p. 1430-1440, ISSN: 0142-1123
6. Bernasconi, A., Filippini, M., Folletti, S., Vaudo, D.: *Multiaxial fatigue of a railway wheel steel under nonproportional loading*, International Journal of Fatigue, vol. 28, 2006, p. 663-672, ISSN: 0142-1123
7. Reis, L., Li, B., de Freitas, M.: *Analytical and experimental studies on fatigue crack path under complex multi-axial loading*, Fatigue & Fracture of Engineering Materials & Structures, vol. 29, 2006, pp. 281–289, ISSN: 1460-2695
8. Reis, L., Li, B., de Freitas, M.: *Crack initiation and growth path under multiaxial fatigue loading in structural steels*, International Journal of Fatigue, vol. 31, 2009, p. 1660-1668, ISSN: 0142-1123
9. Susmel, L.: *Multiaxial fatigue limits and material sensitivity to non-zero mean stresses normal to the critical planes*, Fatigue & Fracture of Engineering Materials & Structures, vol. 31, 2008, p. 295-309, ISSN: 1460-2695
10. Karolczuk, A., Macha, E.: *A review of critical plane orientations in multiaxial fatigue failure criteria of metallic materials*, International Journal of Fracture, vol 134, 2005, p. 267-304, ISSN: 0376-9429
11. Dumitru I., Kun L., Dreucean M., Menyhardt K.: *The equivalent stress concept in multiaxial fatigue*, Jorunal of Engineering Studies and Research, vol. 17, no. 2, 2011, p. 53-62, ISSN: 2068-7559
12. Yokobori, T., Yoshimura, T.: *A criterion for fatigue fracture under multiaxial alternating stress state*, Report 2, p.45-54, Tohoku Univ., Sendai, Japan, 1966
13. Matake, T.: *An explanation on fatigue limit under combined stress*, Bulletin of JSME, vol. 20, no. 141, p. 257-263, 1977
14. McDiarmid, D.L.: *A shear stress based critical-plane criterion of multiaxial fatigue failure for design and life prediction*, Fatigue & Fracture of Engineering Materials & Structures, issue 12, vol.17, 1995, p.1475-1484, ISSN: 1460-2695
15. Kun, L., Dumitru, I.: *The influence of phase shift and frequency on critical plane positions under nonproportional cyclic loading*, Scientific Bulletin of the "Politehnica" University of Timisoara, Trans on Mechanics, vol. 55(69), Special Issue S1, 2010, p. 53-58, ISSN 1224 - 6077

Cercetări asupra planelor critice şi a tensiunilor în materiale supuse la incercări ciclice de tracţiune cu torsiune

Rezumat

Evaluarea durabilităţii materialelor la oboseală multiaxială constituie o problemă de mare actualitate. În acest context în ultimii ani s-au extins studiile asupra durabilităţii materialelor la tracţiune cu răsucire folosind echipamente pentru care condiţiile de încercare se pot reproduce în diverse laboratoare. Alegerea regimului de încarcare pentru trasarea curbelor de durabilitate impune o analiză a planelor critice precum şi a tensiunilor normale şi/sau tangenţiale care acţionează în acestea. Aceasta se impune intrucât planele critice în asemenea condiţii de solicitare nu mai sunt cunoscute apriori. Pornind de la acest aspect în prima parte a lucrării se face o analiză a influenţei raportului amplitudinilor tensiunilor componente şi a defazării asupra poziţiei planelor critice, definite ca planele în care tensiunile tangenţiale sau normale ating valori extreme. În partea a doua a lucrării noţiunea de plan critic se analizează pe baza modelelor McDiarmid, Matake şi Yokobori. În final se face o comparaţie între aceste modele prin prisma evaluării cât mai corecte a unor tensiuni echivalente cu ajutorul cărora se pot trasa curbe de oboseală la tracţiune cu torsiune.

Scientific reviewers: **Nicolae FAUR, "Politehnica" University of Timisoara**
Liviu MARSAVINA, "Politehnica" University of Timisoara

SCIENTIFIC BULLETIN OF
THE „POLITEHNICA" UNIVERSITY OF TIMISOARA, ROMANIA
TRANSACTIONS ON MECHANICS
BULETINUL ŞTIINŢIFIC AL
UNIVERSITĂŢII „POLITEHNICA" DIN TIMIŞOARA, ROMÂNIA
SERIA MECANICĂ
Tom 56 (70) ISSN 1224 - 6077 Fasc. S1, 2011

OBTAINING SOLDER ALLOYS FROM Sn-Ni-Cu-P FAMILY IN RIBBON FORM BY MELT-SPINNING METHOD FOR ELECTRONIC COMPONENTS SOLDERING

Georgiana MELCIOIU, Viorel-Aurel ŞERBAN Cosmin CODREAN, Dragoş BUZDUGAN, Florin Marian CORNEA

e-mail: georgianamelcioiu@yahoo.com, viorel.serban@rectorat.upt.ro, cosmin.codrean@mec.upt.ro, dbuzdugan@eng.upt.ro, mfcornea@gmail.com

Mechanical Engineering Faculty Timisoara, Bd. Mihai Viteazul Nr.1, Timisoara, Romania, RO-300222

Abstract. This paper presents the main lead-free solder alloys used to bond the electronic components and defects that occur because of the solder and their consequences. Given the preliminary research to reduce defects in electronic components is proposed a new solder alloy from Sn-Ni -Cu -P family and a technology for obtaining based on melt-spinning method. The alloy developed in ribbon form is characterized structurally by X-ray diffraction and macroscopic images.

Keywords: whiskers, PCB, printed circuit boards, Melt Spinning, solder

1. Introduction

Soldering is a process of permanent joining, made from metal parts with filler material in fluid state used in the electronics industry. Through this process, we obtain solder joints that support small stresses and behave well at temperatures below 450 ºC.

Soldering alloys used in electronic industry are in wire or paste form [1]. During the soldering process, several phenomena take place some a namely:

- wetting
- stretching
- capillarity
- diffusion

Wetting is the phenomenon of interaction between solder and base metal, heated to a temperature of wetting, which is manifested by stretching or solder flow on the surface of the base material. Wetting of a metal alloy melted by the forces due to base-metal alloy contact.

A solid surface can be wetted by a liquid or not.

Drop of liquid placed on a solid surface extends up to a certain limit, called the wetting perimeter.

Stretching shall be carried out when the adhesion between the liquid and solid will be greater than the cohesion of the liquid.

Surface tension, especially the liquid alloy of base metals and alloys, are quite large, leading to the existence of capillary phenomenon is particularly important for bonding electronic parts. Due to capillary, the alloy melt penetrates and fills the narrow spaces between the pieces, often called adhesive bonding ensuring capillary. Capillarity

occurs if gaps are quite small (less than 0,25 mm) and is favored by low roughness surfaces, especially if the form of channels (tread) on polished surfaces capillarity is reduced, the extent of poor, of which reason is recommended that the areas, especially copper, have look "polished" - small rough. Capillarity is the phenomenon lies in the interplay between surface bonded parts is very small, forming a kind of capillary tube.

Diffusion is the phenomenon of solder melt reacts with the metal base.

Speed the diffusion process greatly increases with temperature. "Acceleration" of the diffusion process a piece of metal deposited on the surface increases by heating to several hundred degrees Celsius. Diffusion mechanism in solids is a jump mechanism. Mass transport is realized by successive jumps from one equilibrium position to another. Both forms of diffusion are possible: self-diffusion and interdiffusion. There are two types of diffusion:

- Diffusion through the interstices: in interstitial solid solutions,
- Diffusion through vacant nodes: the substitution solid solutions [2].

The requirements of soldering alloys used are:

- the chemical composition must be guaranteed by the manufacturer;
- the melting temperature must be lower than the base metal melting temperature;
- it must have an optimal surface tension in order to ensure a good adhesion on the surface.
- it must ensure a good mechanical resistance and stiffness;
- it must have a clean surface, smooth, without cracks, stratification or inclusions;
- the linear expansion coefficient should be approximately equal to the base metal coefficient, in order to avoid the formation of cracks or crevices ;
- it must ensure a good corrosion resistance of the joint in the used environment;
- it must have a low cost price [3].

In electronics are used lead or tin based alloys. The bonding of the electronic components has been achieved using Pb-based alloys. The bonding is realized using Sn-Pb-based solders and by adding quantities of Sb, with a melting point between 138 ° C and 325 °C and Ag-Pb-Sn that has a melting point between 235°C and 310°C. Because lead is harmful, soldering electronic components today are made with lead-free solder, based on tin [4].

2. Conditions imposed to soldering of electronic components on printed circuit boards.

The technology used for soldering components passing through the printed circuit (PCB) (THD through-hole devices) is wave soldering. Surface soldering on PCBs components (SMD Surface mount technology) is generally realized through reflow.

The soldering temperature must be low enough during reflow or wave soldering in order to avoid damaging the PCB and the components, but high enough to melt the paste and to solder the PCBs components in a reasonable time for processing [4].

The solder should solidify immediately without forming defects that could affect the product integrity during its use.

Also, the solder must be able to resist to the requirements imposed to the final product, such as: thermomechanical fatigue, thermal shock and vibration.

In the past 10 years, all research has been directed toward lead-free solder alloys. A special importance was given to identify the alloys that meet specific criteria for manufacturing, reliability, toxicity, cost, and availability. These criteria can be understood by examining the metals on production and product reliability.

This includes phase transformations in solders (including melting behavior, and reactions to the solidification interface PCB substrate), wetting behavior and mechanical properties of the alloy [2].

3. Printed circuit board solders defects

The defects, that can be observed under the microscope analyze are different. Electronic components defects, which have as main cause the soldering process, are:

- alloy's defects;
- solder defects;

Solder defects can be:

- an excess of alloy soldering; these defects have spherical appearance;
- a lack of alloy solder-soldering, with low strength;
- false soldering, mainly due to faulty insertion of the terminal components (short or bent terminals as components);
- cold soldering solder major defect

The solder has a high surface roughness and an amount of heat due to an insufficient application or component movement during solder's solidification.

Defects caused by the alloy are:

- needle tin;
- tin pest;
- dendrites;
- growth whiskers [4]

The defects analyzed in this paper are those observed on printed circuit boards, namely alloy whiskers growth (Figure. 1) that occur frequently in tin alloys. Lead-based alloys, like growths, had a lower frequency of occurrence and were less and less.

Tin whisker growths are crystalline structures that grow spontaneously from the surfaces of tin in soldering electronic components.

These growths are usually conductive whiskers electricity. It can be observed that they can grow in length from a few mm to several μm. In rare cases can reach lengths over 10 mm. Growth whiskers are usually 1-2mm length and diameters between 1-5 μm [5, 6].

They produce the short-circuiting of the electronics. The whiskers growth, affects many areas, like:

- aerospace industry
- military industry
- medical industry
- home electronics industry
- energy industry
- IT industry
- automotive industry.

Figure 1 Growths whiskers to a connector pins [5, 6]

From 1940, when the first damage caused by these grows was reported, the researchers have tried various ways of prevention and mitigation. Currently, these growths are more common using solder alloys Sn-based [7].

4. Lead-free alloys based on tin

Lead-free alloys that replace lead alloys used so far, must have the following basic properties:

- as low as possible melting temperature;
- physical properties at least as good as (fluidity, surface tension) as SnPb-based alloys;
- thermal shock resistance;
- a good anti-corrosive or difficult to oxidize.

Other requirements:

- low cost;
- relatively easy to find;
- not toxic

Properties required for good use:

- wet well to the surface and extend well;
- minimal reactivity with flows;
- to form as few internal goals to solidification;
- to build as little granules alloy.

Lead-free solders, which replace SnPb alloys, contain tin as the base metal and one or more of the following metals: Ag, In, Zn, Cu, Bi, and Sb. The solder used in electronic components are based on Sn-Cu, Sn and Sn-Ag.

The properties of Sn-Pb solder alloys depend on the composition of:

- ✓ the Sn alloys containing high (65 - 98% Sn) are great for soldering, stable, but expensive-not be used for soldering in electronics;
  - ✓ Sn-containing alloys increased (50-65% Sn) has the lowest melting temperature (183-220 °C), are great for splices (fluidity and good wetting capacity) and are commonly used in electronic (and electrical)
  - ✓ Sn alloys containing medium (30 -50% Sn) stick well many metals (including iron and iron alloys) and are more commonly used, with higher melting temperatures are relatively little used in electronics;
  - ✓ Sn alloys with low (below 30% Sn) were quite high melting temperatures, not solder well and not used in electronics.[1]

Quite often, the Sn-based alloys are introduced to improve the properties of certain metals. The most common are:

Sn-St alloys increase mechanical strength, less than 0.3% St improves the wetting ability and a decrease over 3.7%;

In small amounts, Sn-Ag alloys (1-5%, usually 2%) provide higher conductivity and superior mechanical property, but are more expensive. They are used in USA. [4].

Sn-Cd alloys and bismuth Bi reduces the melting temperature, but have contradictory effects. They are rarely used.

In electronics, sometimes are used special solders.

Among these are:

- alloys with indium (In). They are expensive, but allow bonding of

aluminum, zinc, titanium, tungsten, glass, ceramics and other materials commonly used in electronics and technology flows are necessary. They require special bonding;

- cadmium-zinc alloys (Cd-Zn), with a very high corrosion resistance; are used as equipment for harsh environments, like marine, tropical, etc.
- alloy of bismuth (Bi) with low melting temperatures of 50 - 150 º C.

The forms of presentation of the solders depend on technology solder used.

- For soldering in bathrooms or wave the equipment using blocks (bars) and alloy bars, usually rectangular shapes.
- For soldering components mounted on a surface using solder paste, made of alloy powder form - particles of 20 - 150 μm, embedded in paste flow on, with possible addition of binder.

The paste is deposited (by screen printing, through templates) on points (surfaces) of solder wiring, then place the pieces and heat. Alloy powder is obtained by chemical precipitation by injection of liquid alloy in a vacuum or inert gas through narrow nozzles, by galvanic deposition or mechanical processing. The best powder particles are spherical particles of optimal size, the percentage of alloy in the paste, paste viscosity and other characteristics depend on the application and solder technology.

- For certain applications, it provides and solder in the form of sheets, ribbon or preformed shapes (preforms, rings, cylinders, spheres) or covered with trying to obtain that flow properties and improved solder alloys. [3]

In this paper is also presented a method, Melt Spinning, used to prevent the appearance of growths whiskers.

5. Obtaining alloys in the ribbon form using Melt Spinning method

This method allows the structure of metastable alloys (amorphous and nanocrystalline). The material is melted by induction in a quartz crucible and is ejected under pressure through a hole in the crucible now on a Cu roll with rotation moving. Figure [2].

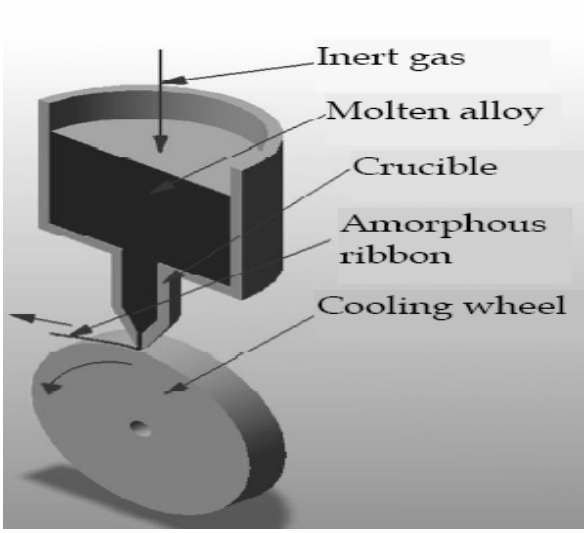

Figure 2 Melt-Spinning Method [2]

Equipment to obtain amorphous materials has the following components: the cooling roller, mechanical transmission, an electric motor, the inductor vertical, cylindrical crucible vertical, medium frequency generator, control panel, which is presented in Figure 3. [8, 9]

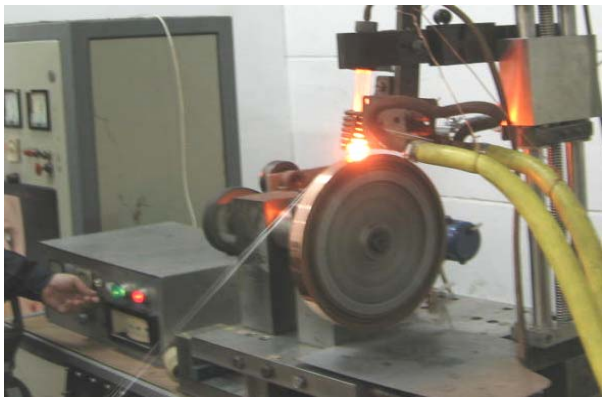

Figure 3 Amorphous alloys equipment performance in the form of ribbon

The following steps should be realized in order to obtain the tapes using this method.

- developing a master alloy with amorphization favorable chemical composition using high purity materials
- melting of master alloy in the crucible
- melt is ejected by applying a controlled pressure on the outer surface of the roller rotation located in Figure 3 [9, 10] .

6. Obtain family solder alloys Sn-Ni -Cu -P

The alloys were developed based on tin-copper for soldering electronic components. It is known that copper alloys obtained by Melt-Spinning shows good brazing properties [9].

The chosen chemical composition must present a metastable structure and good properties for bonding electronic components. Considering the research on electronic components soldering alloy is part of the family chose Sn-Cu-P-Ni, which has the chemical composition: $Sn_{91}Ni_7Cu_1P_1$. The presence of phosphorus is necessary because this component provides a good amorphous [10]. To obtain these amorphous ribbons were made two samples with the following parameters:

- for the first sample was used a pressure of 0.15 atm and a speed of 2100 rot/min
- for the second sample was used for pressure 0.1 atm and a speed of 2100 rot/min

The obtained ribbons are characterized macroscopically with:

- width 4mm
- thickness 18-20 μm, Figure 4

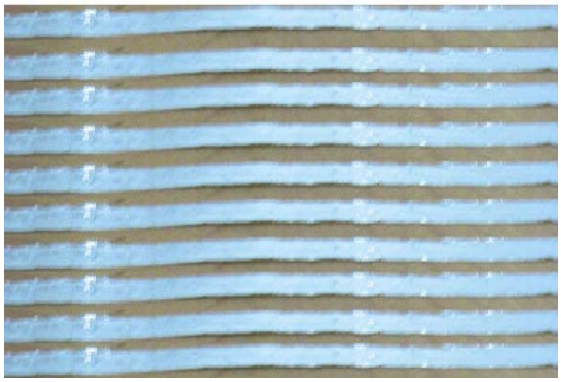

Figure 4 Ribbons Sn-Ni -Cu-P

The structure of the ribbons obtained was performed by X-ray diffraction analysis. This was carried out using DRON 3 diffractometer, with the following parameters:

- voltage U=40 kV
- current intensity I= 30 mA
- anticathode Mo, λ_{kM0}=0,71Å
- speed X-ray tube Xv_d=1°/min

Difractometry of the ribbons is shown in Figure 5 and Figure 6. Structural analysis by X-ray diffraction performed on alloys prepared attest present the crystal structure. We speak of a metastable structure because it is observed that solid solutions prevail. If bands obtained at lower pressure due to a smaller thickness (18 μm) peak intensity is lower, so the finished grade of the structure is higher.

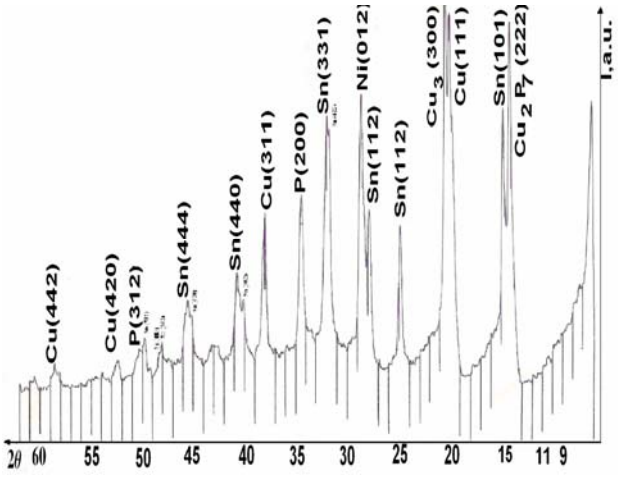

Figure 5 Difractometry of the obtained ribbons for the first sample

Therefore there is potential to obtain a nanocrystalline structure or amorphous in terms of chemical composition and optimization of technological parameters of preparation.

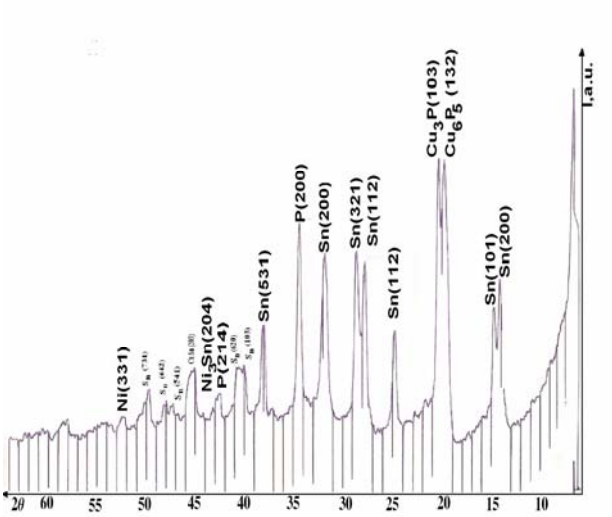

Figure 6 Difractometry of the obtained ribbons for the second sample

7. Conclusions

Since there were damages caused by growth first tried to preventing their whiskers. Due to ban lead in electronic components soldering is harmful and replaced with tin whiskers have been growing these common. Therefore it was tried sticking various components with tin-based alloys. Ribbons obtained with the chemical composition $Sn_{91}Ni_7Cu_1P_1$ will be used for bonding electronic components and solder getting new technologies to prevent the occurrence of these growth whiskers.

Optimization of chemical composition (increased content of phosphorus) and the technological parameters of processing can lead to these alloys with amorphous structure or cvasicrystalline.

References

1. I. N. Trif, L.Feraru, R.Roşca, C.Tanco, *Tehnologii de lipire si brazare in industria*, Editura Agir, Braşov 2007, Vol.4. ISSN:2247-3548 (14.04.2011, www.agir.ro/buletine/959.pdf)
2. M. Judd, K. Brindley, *Soldering in Electronics Assembly,* Planta Tree, 1999 ISBN: 0750635452 (http://www.okian.ro/shop/search/index.php?brand_id=4465)
3. K. Suganuma, *Lead-free soldering in electronics science,tehnology and enviromental impact,* Marcel Dekker, 2004, ISBN:0824741021

4.D. Shangguan, *Lead-free solder interconnect reliability,* ASM International, 2005 ISBN 0871708167

5. J. Brusse, H. Leidecker, *Tin Whiskers* NASA Goddard,

QSS Group, Inc.April, 2006

(5.04.2011,http://nepp.nasa.gov/whisker/reference/tech_papers/2006-Leidecker-Tin-Whisker-Failures.pdf)

6. J. Brusse, H. Leidecker,, *Tin Whiskers* NASA Goddard,

(http://nepp.nasa.gov/WHISKER/)

7. J. Brusse, H. Leidecker., L. Panashchenko *Metal Whiskers A Discussion of Risks and Mitigation,* 2010 Enviromental Technology Technical Symposium and Workshop (http://nepp.nasa.gov/whisker)
8. V A Şerban, C. Codrean, D. Uţu, C. Stoian, *Technological Solutions to Reduce Energy Consumption by Obtaining of Advanced Brazing Alloys* Selected Topics in Energy, Environment, Sustainable Development and Landscaping 2010, Timisoara (www.wseas.us/e-library/.../EELA-26.pdf*)* ISSN: 1792-5924, ISSN: 1792-5940
9. V.A. Şerban, C Codrean, D Uţu and C Opriş, *Amorphous alloys for brazing copper based alloys* The 13th International Conference on Rapidly Quenched and Metastable Materials, Journal of Physics 2009, ISBN. 1742-6596 Journal of Physics: Conference Series 144 (2009) 012098 (http://iopscience.iop.org/1742-6596/144/1/012098)
10. C. Codrean,V. A. Şerban, C. Stoian *New technology for brazing stainless steels with copper based amorphous alloys* Tehnologii inovative de îmbinare a materialelor avansate 2010 ISBN 1453-0384

Obţinerea aliajelor de lipire din familia Sn-Ni - Cu-P sub formă de benzi prin metoda Melt Spinning pentru lipirea componentelor electronice

Rezumat

Lucrarea de faţă prezintă principalele aliaje de lipire fără plumb (lead-free) utilizate la realizarea componentelor electronice, precum şi defectele care apar la aceste componente datorate aliajului de lipire şi consecinţele lor. Având în vedere cercetări preliminare, pentru a diminua defectele apărute la componentele electronice se propune un nou aliaj de lipire din familia Sn-Ni-Cu-P şi o tehnologie de obţinere a acestuia bazată pe metoda melt-spinning. Aliajul elaborat sub

Acknowledgment

This work was partially supported by the strategic grant POSDRU/88/1.5/S/50783, Project ID50783 (2009), co-financed by the European Social Fund – Investing in People, within the Sectoral Operational Programme Human Resources Development 2007 – 2013.

¶

Scientific reviewers: **Mihaela POPESCU, "Politehnica" University of Timişoara, Romania**
Dragoş UŢU, "Politehnica" University of Timişoara, Romania

SCIENTIFIC BULLETIN OF
THE „POLITEHNICA" UNIVERSITY OF TIMISOARA, ROMANIA
TRANSACTIONS ON MECHANICS
BULETINUL ŞTIINŢIFIC AL
UNIVERSITĂŢII „POLITEHNICA" DIN TIMIŞOARA, ROMÂNIA
SERIA MECANICĂ
Tom 56 (70) ISSN 1224 - 6077 Fasc. S1, 2011

POSSIBILITIES TO USE THE AGILENT VEE PRO PROGRAMMING ENVIRONMENT IN ORDER TO PERFORM THE TEST FOR DETERMINATION OF EXPLOSION PRESSURE SPECIFIC FOR APPARATUS WITH THE TYPE OF PROTECTION FLAMEPROOF ENCLOSURE "d"

Lucian MOLDOVAN *, Martin FRIEDMANN **, Mihai MAGYARI ***
*INCD-INSEMEX, str. Gen. V. Milea, nr. 32-34, Petroşani, jud. Hunedoara, lucian.moldovan@insemex.ro
**INCD-INSEMEX, str. Gen. V. Milea, nr. 32-34, Petroşani, jud. Hunedoara, mihai.magyari@insemex.ro
***INCD-INSEMEX, str. Gen. V. Milea, nr. 32-34, Petroşani, jud. Hunedoara, martin.friedmann@insemex.ro

Abstract: This paper presents a possible software to control the test rig apparatus, required for determination of explosion pressure, with the help of Agilent VEE Pro graphical programming environment. Determination of explosion pressure is part of the tests in explosive mixtures, performed in order to evaluate the apparatus with type of protection flameproof enclosure "d".

Keywords: Agilent VEE Pro, determination of explosion pressure, flameproof enclosure "d".

1. Introduction

Evaluation and testing of equipments that compose an explosion-proof system, in purpose of certification, is very important considering the existing explosion risk which has to be minimized to ensure peoples health and security, as well as to prevent goods damage and, not in the last instance, to protect the environment [1].

For the certification of electrical equipment with flameproof enclosure type of protection "d" it is necessary to be subjected to type tests [4]. The type test category includes also the tests in explosive mixtures. The tests in explosive mixtures to which this kind of apparatus must be subjected are [2]:

- determination of explosion pressure (reference pressure);
- overpressure test;
- non-transmission of an internal ignition test.

Each of these tests shall be made with the group specific test gases, respectively subgroup specific gases of which the equipment is related.

The actual methods and test rig to make the tests in explosive mixtures for electrical apparatus with type of protection flameproof enclosure, a series of disadvantages, like [3]:

- the maneuverability and operability are diminished because three computers are used in the same time;
- the malfunction of one of the three computers results in the impossibility of making the tests in explosive mixtures;

- the computers use operating systems for which the manufacturer no longer ensures support (Windows NT 4.0, IBM OS/2 version 3.0 [7], Windows NT Server);
- the test rig integrates a large number of apparatus that leads to high costs for maintenance and also for calibration.

For the functional correlation of logical and analogical assembly of information, sampled from the testing process of flameproof enclosure equipment, a logical and sequential algorithm was created, in order to respect all the standard requirements.

According to the algorithm presented in [1], [2], [3] the test to determine the reference pressure is made according [5], usually in the following steps:

a. the equipment identification data are introduced and saved;
b. the equipment enclosure to be tested is placed in the testing chamber and ventilated until the humidity is reduced to an appropriate level.
c. calibration of oxygen analyzer;
d. the explosive mixture is introduced in the testing sample of equipment at atmospheric pressure and ambient temperature;
e. the test mixture is ignited through a specific device;
f. explosion pressure is measured with the help of pressure transducers;
g. the maximum value of explosion pressure and the pressure curve are visualized and saved;
h. the equipment enclosure is ventilated in order to eliminate burned and unburned gases and to reduce humidity.

After this step the process is restarted from point d to h, until the end of tests.

2. Possibilities to use the Agilent VEE Pro programming environment to perform the test for determination of explosion pressure for flameproof enclosure "d" apparatus

Agilent VEE is a Visual Engineering Environment that allows programming by creating intuitive “block diagrams.” Selection and editing of objects from pull-down menus and connecting them to each other by wires to specify the program’s flow, mimicking the order of tasks need to be performed represent the way Agilent VEE Pro works. The open development environment of Agilent VEE allows to easily use other applications and tools. With access to .NET classes and assemblies, Agilent VEE can programmatically perform everyday tasks and interact with other applications [1], [9].

The DT VPI [8] component represents the interface for data acquisition products made by Data Translation, which together with Agilent VEE incorporate a programming environment used to elaborate a new management technology for tests in explosive mixtures of equipments designed to be used in explosive areas.

According to the flowchart for test analysis and control of tests in explosive mixture for a flameproof enclosure type of protection equipment [1] the input-output variables were identified [2].

Based on this algorithm, the sequence regarding determination of reference pressure was identified and three programs were created using the Agilent VEE Pro 8.5 graphical programming environment and a Data Translation 9804 [10] data acquisition board. Also, the Data Translation DT-VPI 6.3 component was installed in the Agilent VEE Pro graphical programming environment as an interface for the Data Translation acquisition systems.

The programs were launched in execution in simulated conditions, with only the data acquisition system connected to computer. The simulation was made by introducing some virtual instruments in the programs, in order to substitute the variables obtained when using real apparatus [3]. The created software instruments has integrated also the necessary functions to connect the measuring and control apparatus (pressure transducers, charge amplifiers, flow controllers to make the explosive test mixture, temperature and humidity transmitter, oxygen analyzer) to the data acquisition system.

The first of the three programs, P1_Program_grupa_de_explozie [3] has the purpose of recording the identification data for the equipment subjected to tests and to choose the test that will be subsequently made, or creation of the test report. The introduced data are saved into a .xls file type.

The graphical interface of the virtual instrument created for the program P1_Program_grupa_de_explozie, is presented in Figure 1.

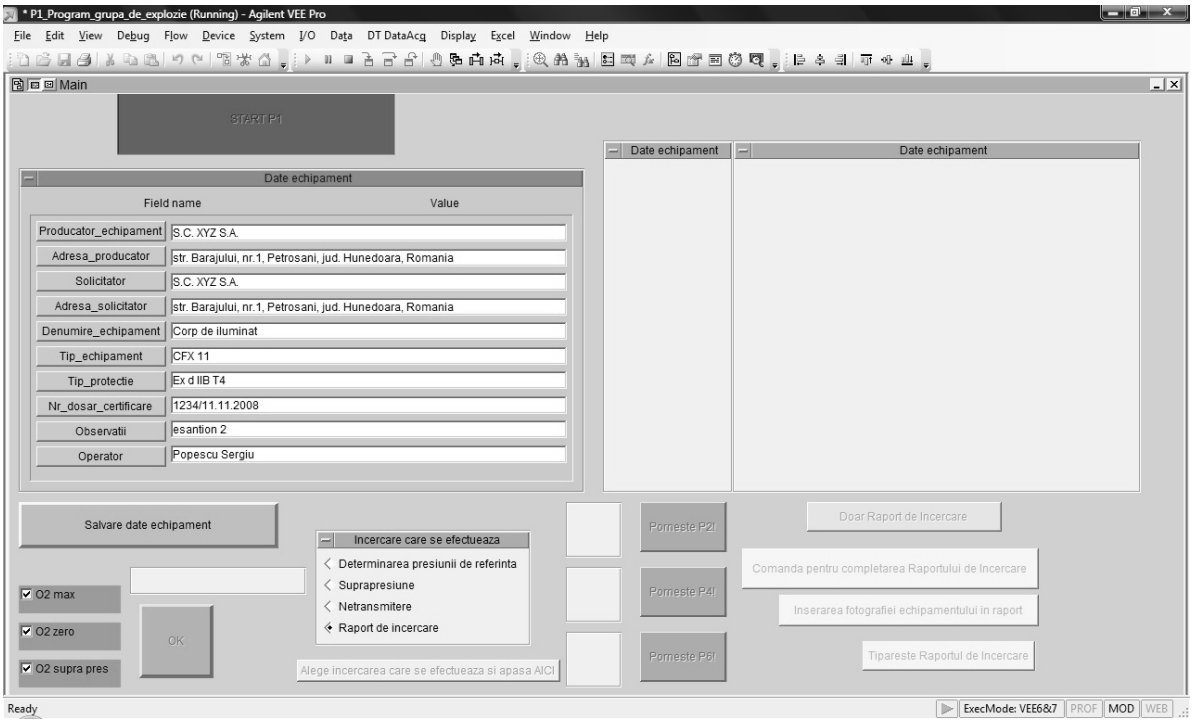

Figure 1 Graphical interface of the virtual instrument created for the program P1_Program_grupa_de_explozie

The second program, P2_Program_determinare_presiune_de_referinta [3] has the purpose to command and control the installation in order to make the test for determination of explosion pressure, and also to save the required information (mixture pressure, temperature, humidity, mixture concentration) in the same .xls file type in which the equipment identification data were introduced, but in other sheet (Figure 2).

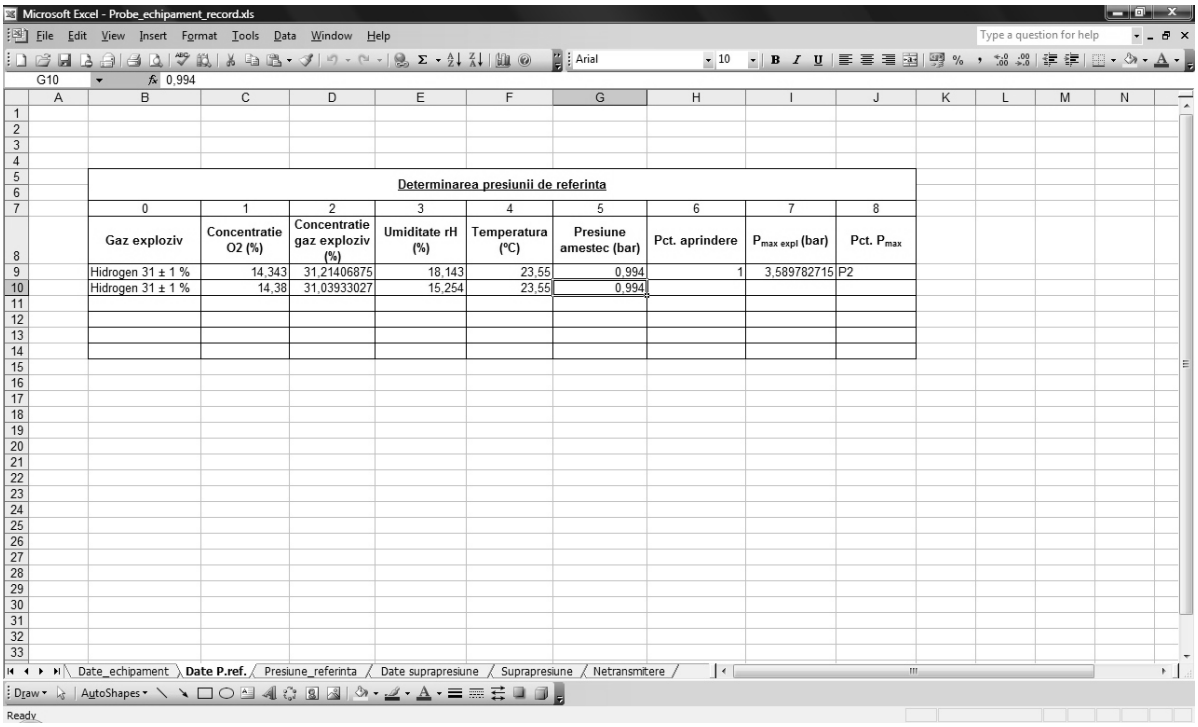

Figure 2 Program P2 – Explosive mixture parameters (fişier tip „.xls”)

The graphical program created to control the subsystem P2_Program_determinare_presiune_de_referinta, with « Users Objects » integrated functions, is presented in Figure 3.

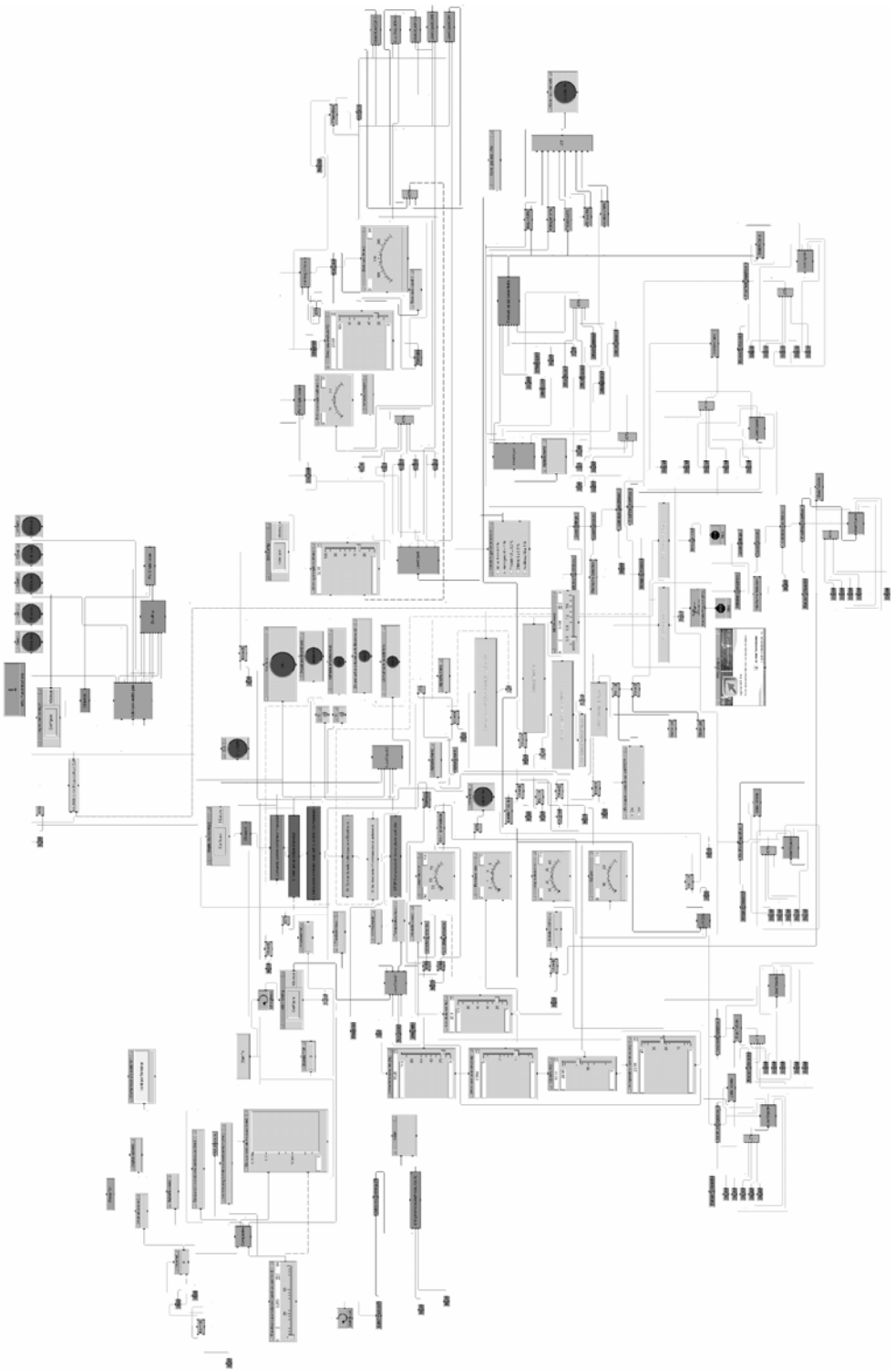

Figure 3 Graphical program of P2_Program_determinare_presiune_de_referinta subsystem

The graphical interface of the virtual instrument created for the program P2_Program_determinare_presiune_de_referinta, is presented in Figure 4.

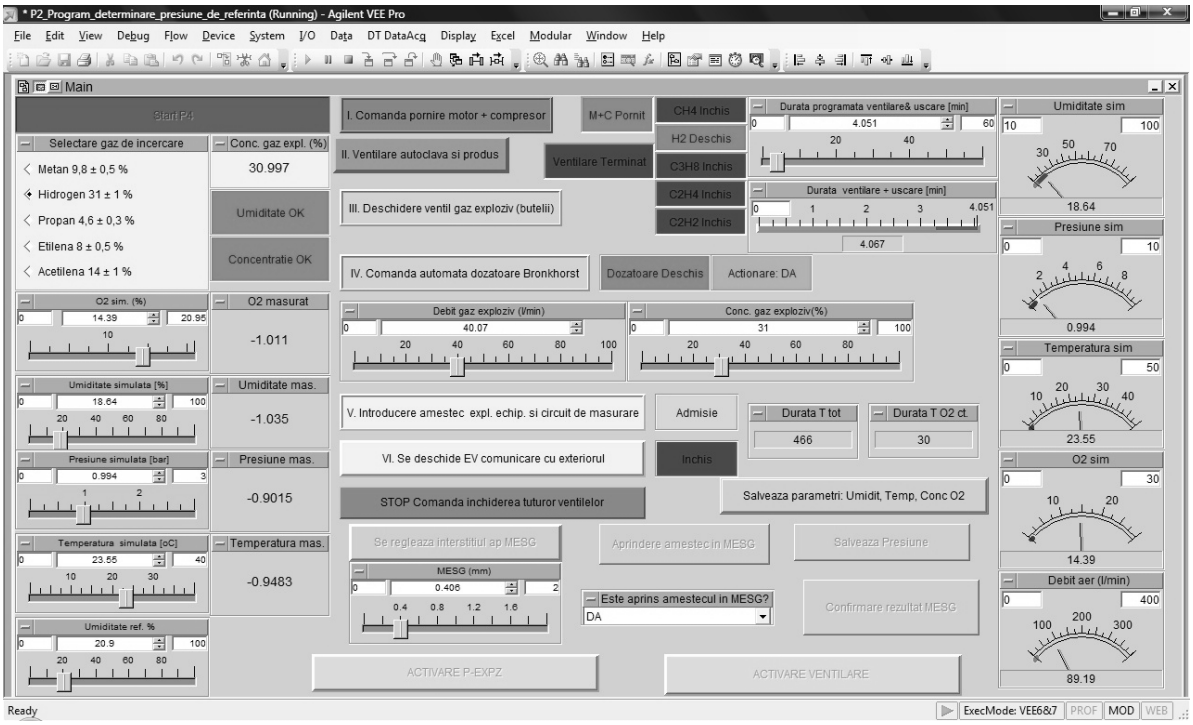

Figure 4 Graphical interface of the virtual instrument created for the program P2_Program_determinare_presiune_de_referinta

The third program, P3_Program_explozie_la_pres_de_referinta [3] has the purpose to command ignition of explosive mixture from a certain point, recording of data resulted in the test for determination of explosion pressure (the point from which the ignition was initiated, the maximum recorded pressure, the values resulted from the pressure curve for the three pressure transducers used). Also, from this program, the equipment and testing chamber adequate ventilation can be made, and to select the appropriate option to continue the equipment test program.

The graphical interface of the virtual instrument created for the program P3_Program_explozie_la_pres_de_referinta is presented in Figure 5.

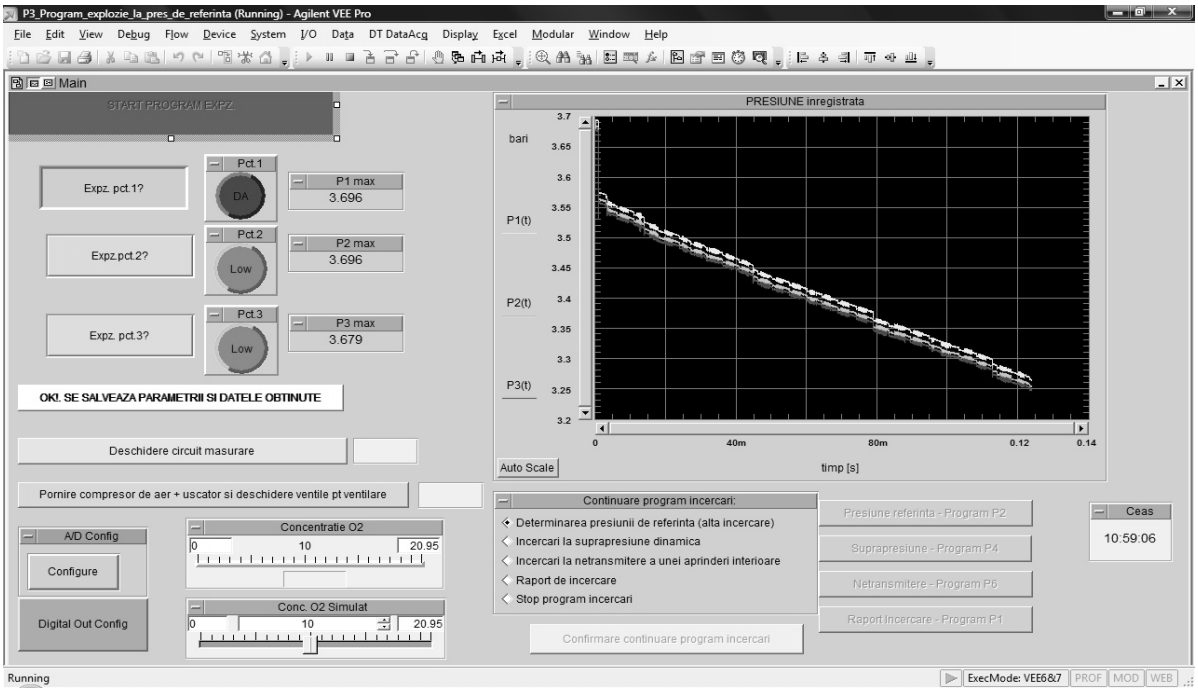

Figure 5 Graphical interface of the virtual instrument created for the program P3_Program_explozie_la_pres_de_referinta

3. Conclusions

The main advantages of the system that uses the new software are:

- full process automation;
- a better management of test that results from the use of a single computer instead of three computers;
- uses the most part of the apparatus existing in the actual test rig;
- reduces the number of apparatus existing in the test rig (the oscilloscopes and a part from the control and command side for flow controllers are not needed);
- possibility of implementing this solution on actual and commonly used operating systems like Windows Vista, Windows XP;

4. References

1. Moldovan, L., Zoller, C., *Possibilities to improve the test methods for equipments used in explosive areas*, Revista Minelor, nr. 12 / 2009, p. 33-40, ISSN 1220-2053
2. Moldovan, L., Friedmann, M., *Identification of input-output variables of the command and control system for testing flameproof protected equipments designed for use in explosive atmospheres*, International Symposium "Young people and multi-disciplinary research", 2009, p.41-48, Timişoara, ISSN 1843-6609
3. Moldovan, L., *The improvement of evaluation and testing methods for electrical apparatus designed to be use in potentially explosive atmospheres*, Doctoral Thesis, 2009
4. SR EN 60079-0:2007 – *Electrical apparatus for explosive gas atmospheres*. Part 0: General requirements
5. SR EN 60079-1:2008 - *Explosive atmospheres - Part 1: Equipment protection by flameproof enclosures "d"*"
6. INSEMEX-LIEx, *PI-Ex-01.1 Test procedure to verify flameproof equipments – Tests in explosive mixtures,* Edition 6, 2008
7. Schönhoff, M., Oppermann M. – *Ventilsteuerung für OS/2, Benutzerhandbuch,* PTB Braunschweig, 1999
8. Data Translation, *DT VPI™ UM-16150-C, User's Manual*, Version 6.0, Third edition, 2000
9. * * * *Agilent VEE Pro User's guide*, Ninth edition, 2005
10. * * * *Data Translation (UM-17473-U), DT 9800 Series* ; User's Manual, 2007

Posibilități de utilizare a mediului de programare Agilent VEE Pro la realizarea încercării de determinare a presiunii de explozie specifică aparaturii cu tip de protecție capsulare antideflagrantă "d"

Rezumat

Această lucrare prezintă un posibil software pentru controlul aparaturii din standul de încercare, necesar determinării presiunii de explozie, cu ajutorul mediului de programare grafică Agilent VEE Pro. Determinarea presiunii de explozie face parte din încercările în amestecuri explozive, realizate pentru evaluarea aparaturii cu tip de protecție capsulare antideflagrantă "d".

Scientific reviewers: **Sorin BURIAN[*], INCD-INSEMEX Petroşani**
Sorin SICOI[**], INCD-INSEMEX Petroşani

SCIENTIFIC BULLETIN OF
THE „POLITEHNICA" UNIVERSITY OF TIMISOARA, ROMANIA
TRANSACTIONS ON MECHANICS
BULETINUL ŞTIINŢIFIC AL
UNIVERSITĂŢII „POLITEHNICA" DIN TIMIŞOARA, ROMÂNIA
SERIA MECANICĂ
Tom 56 (70) ISSN 1224 - 6077 Fasc. S1, 2011

THE NECESSITY OF IMPLEMENTING MODERN PROTECTION SYSTEMS INTO THE NATIONAL ENERGETIC SYSTEM

Păsculescu Vlad[*], Şuvar Marius[**], Păsculescu Dragoş[***]
[*] INCD INSEMEX Petroşani, G-ral V.Milea Street, no.32-34, Petroşani, Hunedoara, insemex@insemex.ro
[**] INCD INSEMEX Petroşani, G-ral V.Milea Street, no.32-34, Petroşani, Hunedoara, insemex@insemex.ro
[***] University of Petroşani, Universitatii Street, no. 20, 332006, Petrosani, Hunedoara, pdragos_74@yahoo.com

Abstract. The energetic systems are considered critical infrastructures, infrastructures that the society will become increasingly dependent on. Romania is favoured because these infrastructures are designed and developed now when such structures exist globally. Most of the existing equipment have lifetime limit or cannot meet the requirements of operating the system with a high safety level and cannot meet at the same time the requirements for interconnecting to the UCTE – Union for the Co-ordination of Transmission of Electricity - European Structure. Due to exceeding the lifetime and due to decreasing the reliability of the equipment, they need to be replaced with modern protection equipment. This paper presents the advantages, disadvantages and perspectives of implementing numerical protection systems into the National Energetic System.

Keywords: National Energetic System, Union for the Co-ordination of Transmission of Electricity, numerical protection system

1. Introduction

A series of faults can occur in high voltage networks: mono-phase short-circuit, two-phase short-circuit, three-phase short-circuit as well as other faults given by the phase-breaks, lasting over-loads, voltage decrease, frequency decrease and by synchronous machinery phase-swinging.

A series of protections against faults are used in the National Energetic System. Depending on the controlled variables and depending on how they work, these may be categorized into the following: current protections, voltage protections, directional protections, distance protections with filters, with transmission channels, comparative-longitudinal protections, numerical protections, gas relays protections.

Following the analysis of faults that may occur in high voltage electrical networks and the protections that are currently used, this paper presents the advantages and disadvantages of implementing modern numerical protection systems into the National Energetic

2. Advantages of using modern protection systems

Modern numerical protections with advanced techniques and technologies ensure the efficient operation of the entire coordination and control protection system, fact that is an essential contribution for safe electric energy supply.

The numerical protection system has the more advantages than classical protections with contact-relays:

- It removes protection operation delays due to the movable elements of classical protection relays;

- It removes the malfunctioning caused by the contact imperfections of conventional relays;
- Higher sensibility, rapidity and reliability than classical relays that have been until now; the moment;
- Feature for fault detection in electrical systems;
- The persistence time of minor damages is very much shortened so that the protected elements damages are almost insignificant;
- Reparation times are shortened because the numerical protection system provides the user with the diagnosis of the fault that occurred, by recording all events that occurred from the protection starting until the release of the damaged element from the electrical system;
- The numerical protection system needs much less space than the needed space for contact-relays protection systems;
- It removes malfunctioning caused by periodical preventive verifications of classical relays and replace these verifications with simple periodical testing of the numerical equipment to view the default settings;
- It provides a wide variety of protection functions, some of them unable to be applied with the help of classical relays (e.g. balancing function for two voltages or the over-temperature function by achieving the thermal table, etc.)

The implementation of the numerical protection system, of complex automation and of the computer for monitoring events has a great influence upon the reduction of staff from an electrical station.

The operation activity of installations comprises the monitoring of protection operation, the monitoring of the installations that operate under automatic control or by manual processing of various electric installations.

The main working place consists of the main operation room and the control panels from within the electrical installations, with local inspections being carried out on each shift, following fixed routes by monitoring temperature, local apparatus pressure and the notification of different regimes and abnormal phenomena.

The high number of interferences and faults is always present in the energetic system, most times it is unexpected, and the direct intervention of operating staff in case of interferences or faults in the electric system has as main purpose interference removal with minimum consequences upon used power or in case of danger to isolate the fault from the electric system in maximum safety conditions.

Commands in these critical situations are given from the main operation cab, but when in need the commands can be given from the local command equipment or from the relay chambers located within the station.

In this kind of situations, the protection and automation take over most operations but the human factor (staff) has the role of deciding upon main manoeuvres and verifies command accomplishment on site.

Unlike classical relay protection systems, the modern numerical protection system has the advantage of providing an important number of functions: acquisition, storing and processing, automation, monitoring and dialogue. Hard structure ensures numerical protection systems modelling providing a high flexibility and safety level.

These modern protection systems are provided with permanent self-testing functions regarding the status of protection elements, with diagnosis and staff alert through signalling systems or on site in the protection cab in which the relay is installed, or by signals transmitted to the control room.

Specialized staff equipped with a portable computer can set and adjust the starting values, the characteristic parameters and the temporizations of each protection.

Modern numerical protection systems have high reliability in operation and in most cases this reliability can be doubled because of the existence of two parallel hardware systems that operate according to the principle “one of two” in case distance controlling is implemented, these two systems complementing each other and in case of the malfunctioning of one of them, the other hardware system stays in operation.

The use of microprocessors in the numerical relays technique in order to achieve the protection of electrical systems improved quality and in some cases it improved some facilities of the new systems:

- High reliability, easy debugging and maintenance, self-testing;
- Flexibility of adjustments through numerical algorithms for tracking events in time;
- The possibility of archiving adjustments and inspection tests;
- Operating system available through a local keyboard or through a computer that has installed the software related to that protection;
- Compact design, protection to electromagnetic fields, possibilities of interconnection with surveillance systems, centralized command and control;

- Reasonable purchase costs through the provided facilities in case of proper operation;

Figure 1 presents the upgraded control room of a power station.

Figure 1 Power station upgraded control room

Numerical protection systems, through their internal function blocks, prove to have a major influence in compliance with the conditions required by the interconnection with the energetic systems of the European Union (UCTE – Figure 2)

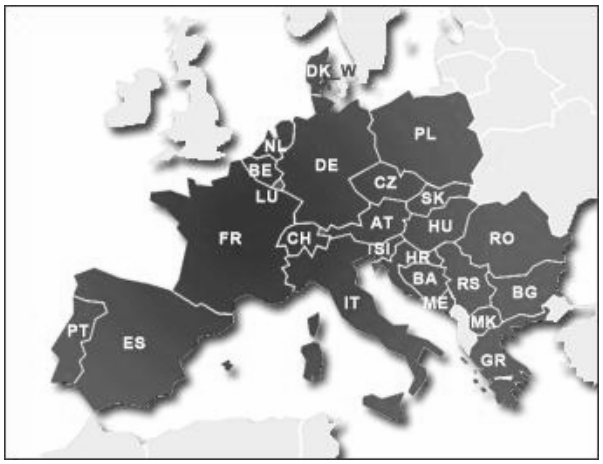

Figure 2 UCTE – Union for the Co-ordination of Transmission of Electricity - European Structure

3. Disadvantages of using modern protection systems

The devices are more complex and reliable this being reflected in their performances and maintenance, but also in high costs. The price must not stand against purchasing more reliable and advanced equipment, but they must not include facilities or functions that are not mandatory.

During the replacing of protection there can occur the following:

- Providing a data sheet that is understandable for all participating workers;
- Breaching the terms of execution which has a negative effect upon the foreign experts that have a well-established schedule for a large geographic area;
- At the level of the National Energetic System, breaching the approved withdrawal program may lead to the modifying of other terms from other inspection and modernization programs, as well as lead to the decrease of the safety level related to the operation of the system in some areas;
- Problems regarding the reception of workings due to non-conformities in the quality domain;
- Quality suffers because of the rush in which the workings are executed under the pressure of deadlines and because of the quality of the human factor and of the technologies used by workers;
- Documentation does not come in Romanian which makes global understanding difficult and also generates difficulties in clearly establishing the obligatory character of some operations that need to be carried out related to the operation and maintenance of the equipment.

4. Conclusions

Based on the above mentioned facts we can conclude: introducing and developing modern numerical protection systems in the National Energetic System will obviously improve the operation of protection systems in terms of event complexity increasing and at the same time being in compliance with EU Directives (UCTE).

Taking into account the above mentioned facts regarding replacing, substantiation and supervising digital protection systems that have as main purpose stability improvement and the ensuring of selectivity, will fully contribute to the understanding of the need of replacing classical protection equipment from the electrical power stations.

Having an age of approximately 100 years, the energetic domain has continuously progressed. Energetic systems are considered to be critical infrastructures on which the society will become more and more dependent on. Romania has the advantage that these infrastructures are designed and developed at the moment when they already exist worldwide, when the requirements regarding safe conditions operation are being set up and the specific risk management is defined. Being a partner of the European Structures (UCTE), our National

Energetic System must have a strategy for implementing modern equipment in power stations.

Currently, we are going through a stage in which technical innovations modify the architecture of power stations and their operation concept, change the cooperation relations continentally and as well change human destiny. Most of the old equipment is domestic manufactured, except for most protection relays, and they have made possible the operation of the energetic system in tough conditions for a long period of time.

For such an important sector domain like the energetic one, the equipment is purchased from the world market. This one provides state-of-the-art and complex services. In order to diminish the risks generated by the market dynamics, the modernization strategy must be a flexible one that shall take into account the diversity and volatility of the offers together and not separated.

Upgrading the stations, protections, equipment is a must for the operating in safe conditions of the National Energetic System. Most of the existing equipment have lifetime limit or cannot meet the requirements of operating the system with a high safety level and cannot meet at the same time the requirements for interconnecting to the UCTE – Union for the Co-ordination of Transmission of Electricity - European Structure.

References

1. Păsculescu, M., Romanescu, A., Păsculescu, D., Tătar, A.: *The determination and simulation of a short circuit currents of a defect on the 110kV Rods of a Power Station,* Proceedings of 3rd WSEAS International Conference on Manufacturing Engineering, Quality and Production Systems (MEQAPS '11), p.30-34, ISBN: 978-960-474-294-3, Transilvania University of Braşov, May 2011, Braşov,
2. Păsculescu, D., Romanescu, A., Păsculescu, V., Tătar, A., Fotău, I., Vajai, G.: *Presentation and simulation of a modern distance protection from the national energy system,* Proceedings of 10th International Conference of Environment and Electrical Engineering (EEEIC 2011), p. 647-650, IEEE Catalog Number: CFP1151I-CDR, ISBN 978-1-4244-8781-3, May 2011, Rome, Italy
3. Păsculescu, D., Romanescu A.,: *Presentation and Simulation of homopolar modern protection from National Energetic System*, Revista Minelor, Vol.16, No.12, 2010, p. (16-19), ISSN 1220-2053, Deva, Romania (in Romanian: Prezentarea şi simularea unei protecţii homopolare moderne din sistemul energetic national)
4. Păsculescu, D., Romanescu A.,: *Fault analysis in high voltage networks through modern numerical terminals*, Revista Minelor, Vol.17, No.2, 2011, p. (45-47), ISSN 1220-2053, Petroşani, Romania (in Romanian: Analiza defectelor în reţelele de înaltă tensiune prin intermediul terminalelor moderne numerice)
5. Romanescu, A.: *Improving the protections of high voltage lines from the National Energetic System by using modern equipment*, PhD thesis, University of Petroşani, Petroşani, Romania, 2011 (In Romanian: Perfecţionarea protecţiilor unei linii de înaltă tensiune din SEN utilizând echipamente moderne)

Necesitatea implementării sistemelor moderne de protecție în Sistemul Energetic Național

Rezumat

Sistemele energetice sunt considerate infrastructuri critice, infrastructuri de care societatea va deveni din ce în ce mai dependentă. România este favorizată de faptul că aceste infrastructuri se proiectează şi se realizează acum, când astfel de structuri există pe plan mondial. Echipamentele existente, în marea lor majoritate, au durată de viaţă la limită sau nu mai pot răspunde cerinţelor impuse de funcţionarea sistemului cu un grad mare de siguranţă şi să răspundă totodată cerinţelor de interconectare la Structura Europeană UCTE - Uniunea pentru Coordonarea Transportului Energiei Electrice. Datorită depăşirii duratei de viaţă şi a scăderii fiabilităţii echipamentelor este nevoie ca acestea să fie înlocuite cu echipamente moderne de protecţie. Această lucrare prezintă avantajele, dezavantajele şi perspectivele implementării sistemelor numerice de protecţie in Sistemul Energetic Naţional.

Scientific reviewers: **Fotău Ion*, University of Petroşani, Romania**
Pădure Alexandru, University of Petroşani, Romania**

SCIENTIFIC BULLETIN OF
THE „POLITEHNICA" UNIVERSITY OF TIMISOARA, ROMANIA
TRANSACTIONS ON MECHANICS
BULETINUL ŞTIINŢIFIC AL
UNIVERSITĂŢII „POLITEHNICA" DIN TIMIŞOARA, ROMÂNIA
SERIA MECANICĂ
Tom 56 (70) ISSN 1224 - 6077 Fasc. S1, 2011

DEVELOPMENT OF METHODS FOR DETERMINING THE SAFETY PARAMETERS OF CONVEYOR BELTS USED IN POTENTIALLY EXPLOSIVE ATMOSPHERES

Florin PĂUN[*], Leonard LUPU[*], Adrian JURCA[*], Niculina VĂTAVU[*], Emilian GHICIOI[*], Mihaela PĂRĂIAN[*]

[*] INCD-INSEMEX, Institutul naţional de cercetare-dezvoltare pentru securitate minieră şi protecţie antiexplozivă Petroşani, str. G-ral Vasile Milea, nr. 32-34, cod 332047, Petroşani, jud. Hunedoara, insemex@insemex.ro

Abstract. Conveyor belts are used from a long period of time in the industry branches where potentially explosive atmospheres could occur.
Dangerous phenomena in direct connection with the use of conveyor belts are the ones regarding static electricity discharges, sparks influence over the coating layer and/or resistance casing of the disconnected conveyor belt, propagation of a flame along the length of a conveyor belt that was exposed to a energy source relative high like a fire or due to blockage of a conveyor belt as a result of the driving mechanism still operating, that generate a local heating of the conveyor belt in contact with the driving drum, rollers or any other heating source generated by friction.
Determining the safety parameters characteristic of the conveyor belts by employing test methods allows assessment of the safety level as well as certification of their explosion protection quality when used in environments with explosion danger.

Keywords: static electricity, explosive atmosphere, explosion protection, tests, electrostatic discharges

1. Introduction

Belt conveyors have been used for a long time in most of the industrial branches as well as there where the likelihood of explosive atmospheres occurrence exists.

Unlike normal environments, in the ones with potentially explosive atmospheres the fire/explosions hazard occurs, as consequence of various technological processes or accidental leaks.

In order to mitigate explosion risk in these environments with potentially explosive atmospheres, both equipment and its component (conveyor-transportation belt) must be of special construction so as not to generate electric sparks, impact or friction mechanical sparks, static electricity, hot surfaces or any other energy sources that could ignite the atmosphere.

The conveyor belt, as component of the conveyor, non-metallic, made of rubber or polymers with or without insertions, during operation may build up static electricity charges, thus gaining an electrostatic potential. On the other side, due to belt blockage and excessive rubbing between it and conveyor's driving drum, high temperatures can be developed that could lead to igniting the conveyor belt and further to its burning.

All these phenomena, strictly related to conveyor belts operation, show a high influence on the safety level in technological areas where they are operating.

Having in view this aspect, identifying these phenomena is imposed as necessary; likelihood and frequency of occurrence determination as well as determination of those parameters upon which the safety level depends.

In these conditions it can be stated that both electrostatic potential and resistance to flammability as well as flame retardation process are all part of the safety parameters category, specific to conveyor belts when used in environments with potentially explosive atmospheres.

2. Dangerous phenomena generated during belt conveyors operation

One of these dangerous phenomena that occur during operation of a conveyor belt is static electricity through the electrization mechanisms as for example electrization through contact or influence (induction).

Static electricity may appear during conveyor belt operation due to the friction phenomenon, that is nothing else but a particular case of contact electrization which often is responsible of major electrization that lead to high risks in presence of an explosive atmosphere or other sensitive safety devices.

Due to a continuous separation of the surfaces of contacts, for example a driving shaft and a belt or a driving drum and a belt, the surface in motion may acquire a considerable amount of charges and it may become an ignition risk. The amount of acquired charges depends upon the conveyor belt's material and the materials of rollers and driving drum.

The main factors that determine the degree of electrization of materials/products by rubbing are: materials nature, rubbing frequency/duration and environmental conditions.

Largely due to the frequency of occurrence both in conveyor belt operation and other situations, static electricity is a often occurring phenomenon in practice. Starting from the explosion prevention and protection principle, static electricity should be avoided; otherwise it may represent an fire and explosion hazard.

The main electrostatic charging source is *contact charging*. If two bodies, not charged previously, come into contact, this generally will produce a charge transfer in the area of contact.

At separation, each surface will have an equal amount of charges, but with opposite polarity. Conductive objects can become charged by induction if they are placed in an electric field generated by other charged objects or by conductors in vicinity having a high potential.

Any object can become charged if on it charged particles or ionized molecules are built up.

Other hazardous phenomena that may be in connection with conveyor belt using and operating, are the ones related to influence of sparks on the coating and/or on the resistance casing of the conveyor belt disconnected; flame propagation along a belt exposed to a high source of energy as for example a fire or, due to conveyor belt blockage as consequence of the driving mechanism continuous operating that leads to a local heating of the belt through contact with the driving drum, rollers or any other friction heating source.

3. Determination of the conveyor belt safety parameters by employing test methods

Conveyor belts testing for certification purposes is especially important having in view existing explosion risks that has to be minimized, for ensuring safety of life and human health and in order to avoid damages to goods and environment, as well as for a free circulation of products when they comply with the essential safety and health requirements at European level.

In order to have a basis for comparison, tests must be carried out, with well established methods, that take into account specific influencing factors, and that may ensure adequate repeatability and reproducibility.

3.1. Test method to determine electrostatic potential generated by a running light conveyor belt in operation

Light conveyor belts with a inner conductive layer shall undergo the tests provided in SR EN ISO 21178:2007 (SR EN ISO 21179:2007) and the admittance condition is not to generate electrostatic charges that could generate a surface potential greater than 500 V.

In special conditions of use, electrostatic high amount of static charges that generate a surface potential greater than 500 V may be produced through the rubbing between the belt and the conveyed products or by rubbing between the transported products themselves, or by displacement of belt over the rollers or return drum, in this case dangerous products conveyed are the ones in bulk.

The test is carried out on a new conveyor belt, unused and not submitted to test earlier than

five days since manufacturing date; it shall show no traces of contamination or surface faults.

The conveyor belt to undergo the test shall have the length of (2500 ± 50) mm and width of (100 ± 1) mm and shall have no ends. During the tests two results are important and have to be taken into consideration, namely the maximum value reached by the surface potential and a value taken as a constant (for example when after 10 minutes the charge accumulated is below 10%).

In order to determine the electrization potential a special test stand is required, through it a test sample (conveyor belt) having the above mentioned sizes is statically charged while rubbing on drums with a velocity of 5 m/s, ensuring a certain tension in the belt and under specific environment conditions.

Temperature and relative humidity in the test room are relevant and they have to be measured and recorded.

In its motion, the belt sample accumulates charges of electrostatic kind as consequence of its friction on the two drums, thus generating an electrostatic field.

In relation to the device used for recording, either electrostatic intensity *E* in volts per meter or, if the measuring device has a direct potential *U* reading, this value in volts can be recorded.

Figure 1 shows the tests stand for determination of the electrostatic potential generated by a running light conveyor belt.

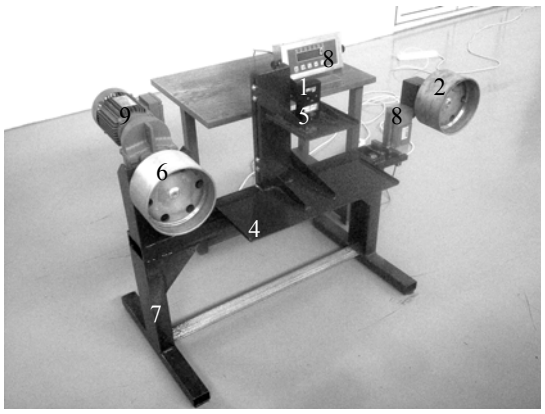

Keyword
1-electrostatic field measuring/recording device;
2-return drum;
4-metallic plate, 600mm×200mm
5 - metallic plate 200mm×200mm;
6-driving drum;
7-metallic frame;
8-tensiometric cell and digital indicator;
9-motor gear.

Figure 1 Test stand for determination of the electrostatic field generated by a light transporting belt in operation

3.2. Test method for determination of flammability at fire simulation (propane burner)

The tests consist in determination of conveyor belt characteristics regarding flame resistance. The test is carried out on two belt samples, each of 200 mm length and 1200 mm width or on all width if the conveyor belt has a width lesser than 1200mm; the test samples have to be kept away from moisture 24 hours before the test, at a positive room temperature in order to avoid any residual bending.

The test samples are placed on a trestle (fig.3) which is placed in a gallery with a cross section area of maximum 6 m^2, and then the propane burner is placed under the trestle (fig. 2). The exposure time on flame is 10 minutes then they are let to self extinguish subsequently the length of undamaged belt has to be measured.
The admittance condition for the conveyor belts in categories 4A, 4B, 5A, 5B and 5C submitted to tests according to method A of SR EN 12881-1:2003 is the undamaged belt length has to be greater than 100 cm on the tested belt.

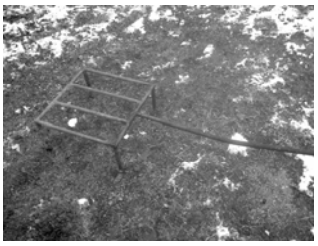

Figure 2 Burner for the flammability test of conveyor belts

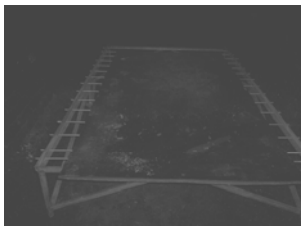

Figure 3 Burner trestle to support the conveyor belt sample

Both the test stand for determination of electrostatic field generated by a light running conveyor belt and the one for flammability test had been carried out within a research project in the "NUCLEU" Program, where the test accreditation had also been provided, having in view extending the testing capacity and implicitly conformity assessment, knowing that proving product conformity - conveyor belts, with the European harmonized standards ensures the assumption of complying with the particular European directive's requirements, respectively the ATEX Directive 94/9/CE, since INCD-INSEMEx is a Notified Body at Brussels for conformity certification.

4. Conclusions

The conveyor belts having as intended use environments with potential explosive atmospheres have to comply with the essential safety and health requirements regarding explosion protection and prevention.

In order to assess conveyor belts conformity with the applicable safety requirements, laboratory tests are required, according to applicable standards.

Developing tests methods within the test laboratory contributes to extending the test capacity, at the same time offering a practical applicability as consequence of various requests coming from manufacturers, beneficiaries and/or market inspection and surveillance bodies that don't dispose of their own test facilities and have to perform verifications in order to ensure production consistency within the quality assurance system or at request of other bodies with competency in market control and surveillance.

Development of the safety parameters specific to conveyor belts, through test methods, allows an assessment of the safety level as well as certification of their explosion protection quality when used in environments with explosion hazards.

5. References

1. Florin P. şa, Proiect: *„Dezvoltarea facilităţilor de cercetare privind riscul sau frecvenţa probabilă de producere a unor fenomene periculoase în funcţie de circumstanţele specifice ale aplicaţiilor din atmosfere cu pericol de explozie a benzilor transportoare (DFCBT)”,* Program: Dezvoltarea capacităţii naţionale de evaluare, prevenire şi limitare a riscurilor generate de aplicaţiile industriale desfăşurate în medii cu pericol de explozie şi/sau toxicitate în domeniul securităţii şi sănătăţii personalului, protecţiei mediului, resurselor minerale şi materialelor / RISC, contract nr. 45N/2007
2. ***, SR EN 12882:2009 *Benzi transportoare de uz general. Cerinţe de securitate electrică şi de protecţie împotriva inflamabilităţii*
3. ***, SR EN 14973+A1:*2008 Benzi transportoare pentru utilizare instalaţii subterane. Cerinţe de securitate electrică şi inflamabilitate*
4. ***, SR EN 21183-1:2007 *Benzi uşoare de transport. Partea 1: Caracteristici şi aplicaţii principale*
5. ***, SR EN ISO 21179:2007 *Benzi uşoare de transport. Determinarea câmpului generat de o bandă uşoară de transport în funcţionare*

Dezvoltarea metodelor de determinare a parametrilor de securitate ai benzilor transportoare folosite in atmosfere potential explozive

Rezumat

Benzile transportoare se utilizează de o perioadă lungă de timp, în ramurile industriale în care există probabilitatea prezenţei atmosferelor potenţial explozive.

Fenomene periculoase care pot fi în legătură directă cu utilizarea benzilor transportoare sunt cele referitoare la descărcarea energiei electrostatice, influenţa scânteilor asupra stratului acoperitor şi/sau asupra carcasei de rezistenţă a benzii transportoare oprite, propagarea unei flăcări în lungul unei benzi care a fost expusă la o sursă de energie relativ ridicată cum ar fi un foc sau datorită blocajului unei benzi transportoare ca urmare a funcţionării în continuare a mecanismului de acţionare care provoacă o încălzire locală a benzii prin contact cu tamburul de antrenare, role sau orice altă sursă de căldură prin frecare.

Determinarea parametrilor de securitate specifici benzilor transportoare, prin aplicarea metodelor de încercare, permite aprecierea nivelului de securitate precum şi certificarea calităţii de protecţie la explozie a acestora atunci când sunt utilizate în medii cu pericol de explozie.

Scientific reviewers:	**Drd.ing. Sorin BURIAN, cercet.şt.II, INCD-INSEMEX, Petroşani, jud. Hunedoara** **Ing. Sorin SICOI, cercet.şt.II, INCD-INSEMEX, Petroşani, jud. Hunedoara**

SCIENTIFIC BULLETIN OF
THE „POLITEHNICA" UNIVERSITY OF TIMISOARA, ROMANIA
TRANSACTIONS ON MECHANICS
BULETINUL ŞTIINŢIFIC AL
UNIVERSITĂŢII „POLITEHNICA" DIN TIMIŞOARA, ROMÂNIA
SERIA MECANICĂ
Tom 56 (70) ISSN 1224 - 6077 Fasc. S1, 2011

JUDICIOUS PLACEMENT OF FANS ALONG THE VENTILATION COLUMN AT THE FRONT CASTEL AMONTE FEEDING PIPE USING DIAGRAMS IN THE Q-L SYSTEM SIZING

Florin RĂDOI*, Constantin LUPU*, Doru CIOCLEA*, Ion GHERGHE*, Corneliu BOANTĂ*
*INCD INSEMEX, National Institute for Research and Development in Mine Safety and Protection to Explosion,
G-ral V.Milea Street, no.32-34, Petroşani, Hunedoara, insemex@insemex.ro

Abstract. Similar to the general ventilation mode with the help of mine ventilation installation, auxiliary ventilation is widely used in all mines, irrespective of the useful mineral substance, and is intended to provide safe and sound working conditions in underground.

It is a difficult job to design an efficient suction system because several parameters should be known. Each suction hole shall be designed so that it doesn't allow a recycling of toxic and/or explosive gases, but it catches coarse particles that might clog up even the ventilation pipes.

To be able to take suitable measures for a good partial ventilation, there shall be determined the specific parameters related to the ventilation columns R_0 (joint aerodynamic resistance) and k_0 (joint coefficient of air leakage through non-sealed areas). These parameters are very important because they give the efficiency of partial ventilation installations. The higher the aerodynamic resistance R_0 is, the smaller the maximum length of the conveyed air to the coal face is.

It is well-known the fact that as the ventilation columns have a higher length, the fan shall have a higher flow rate due to the non-sealed areas along the tube column. This is the reason why the conveyance of large air flow rates along coal faces is difficult to settle.

Keywords: Ventilation, ventilation part, adduction.

1. Introduction

Partial ventilation installations are unique for all preparatory mining works, as well as for the assembly of mining works with the purpose of prospecting and geological exploitation.

In terms of structure and conditions of use, the partial ventilation installations are essentially different from the main ventilation installations, being characterized by the following particularities:

- the variation range of the aerodynamic resistance at which should operate a partial ventilation installation is extremely high (from R = 0 in the initial mining work phase, up to R_{max} corresponding to the final length of the mining work), in a relatively short period;
- continuous and significant changing of the functional parameters (air flow, pressure) relative to the advancing of the mining work;
- the installation is achieved gradually and the accuracy of its execution on the whole length directly influences the ventilation efficiency.

There are used ventilation columns made of metallic tubes with diameters of 400 mm, 630 mm, 760 mm, 800 mm and 900 mm. As a

tightening instrument for the columns from the tubes there are used rubber gaskets that are fixed with flanges and screws, respectively fixed with rubber sleeves.

The ventilation of the main adduction gallery Surduc – Nehoiaşu, front Castel Amonte is achieved in suction system through a partial ventilation installation with the length of 3.160 m, that is made of a column of metallic tubes tightened together with flat rubber gaskets, with ϕ = 900 mm, two cascade placed pneumatic fans, type VP 500 and one surface placed centrifugal fan, type V 496/5.

2. Establishing the underground required airflow

The main atmosphere pollution sources in the underground mining work consist of the gases emitted by the deposit (methane), the gasses that result from the Diesel engine operated machinery (exhaust) and the ones resulting from the blasting operations.

Since the aeration of the main adduction of Surduc – Nehoiaşu, front Castel Amonte is achieved in suction system through a partial ventilation installation, that is made of a column of metallic tubes with ϕ = 900 mm, two cascade placed pneumatic fans, and one surface placed centrifugal fan, the airflow calculation has been achieve after the following criteria:

a) After the amount of explosives: Q_{fp} = 76 m^3/min;

b) After the absolute gas flow: Q_{fp} = 125 m^3/min;

c) After the minimum air speed: Q_{fp} = 67 m^3/min;

d) After the number of Diesel engine locomotives: Q_{fp} = 236 m^3/min.

The airflow that is planned for the working face (Q_{fp}) is going to be the flow with the maximum value, flow that results from one of the above criteria namely „after the number of Diesel engine locomotives".

Q_{fp} = 236 m^3/min.

3. Aeration solutions for the front Castel Amonte main adduction gallery

In order to establish the aeration solutions there have been considered the following elements:

- the coal face necessary airflow, resulting from the operation of the machinery powered by Diesel engines, considering that de CO concentration from the exhaust gases does not exceed 0,08% vol;
- the aerodynamic parameters of the existing ventilation column with diameter of 900 mm;
- the characteristic pressure curve of the fan - $H_v = f(Q)$;
- the unitary aerodynamic resistance of the ventilation column - R_O
- the unitary coefficient of air loss through leakages - K_0.

The values of the aerodynamic parameters specific for the ventilation columns (R_0 şi K_0), taken into account for achieving the nomograms, have been determined based on the measurements carried out in 2010, measurements having the value of 0,003038 kμ/m respectively of 3,326 $\times 10^{-4}$ m/s/m at 1 mm H_2O.

3.1 Cascade placement of the fans on the ventilation column

The nomograms have been drawn up taking into account the means from the existing equipment for the achievement of partial ventilation (ventilation columns made of metallic tubes with ϕ 900 mm, tightened with flat rubber gaskets, the connection of the tubes being done with flanges and screws respectively centrifugal fan V 496/5). Additional nomograms have been drawn up for type VE ϕ 800 – 30 Kw fans and for type dESN 9-300-30 Kw Korfmann fans.

Figure 1 presents the nomogram for a value of R_0 = 0,003038 kμ/m of the unitary aerodynamic resistance and for a value of K_0 = 3,3326 × 10^{-4} m^3/s/m at 1 mm H_2O of the unitary coefficient of air loss through leakages.

Figure 2 and figure 3 present the nomogram for the column with the diameter ϕ = 900 mm, for a value of R_0 = 0,003038 kμ/m of the unitary aerodynamic resistance (medium value resulted from the measurements) and for a value of K_0 = $1{,}8\times10^{-4}$ m^3/s/m at 1 mm H_2O (very good tightness level) of the unitary coefficient of air loss through leakages.

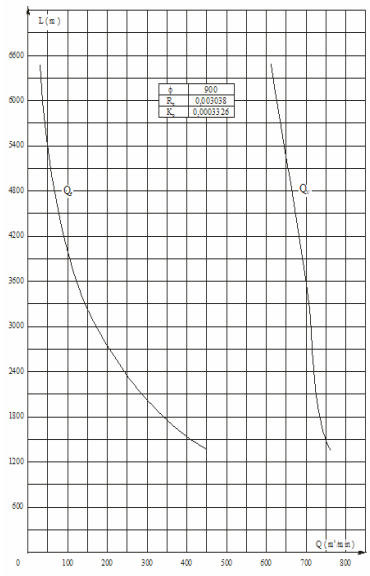

Figure 1 Nomogram centrifugal fan V 496/5

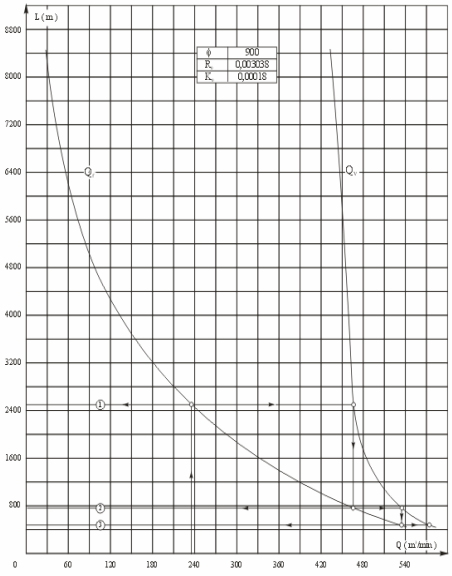

Figure 2 Nomogram axial fan VE 800-30 kw

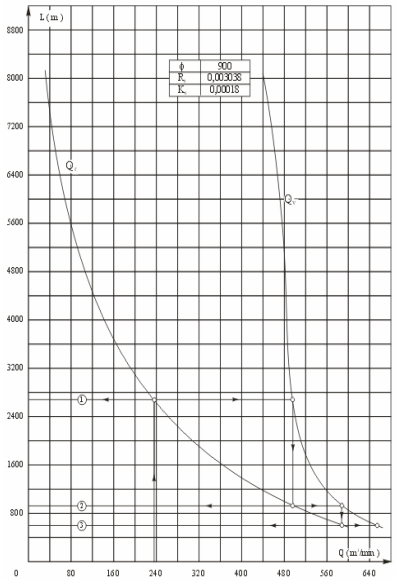

Figure 3 Nomogram axial fan type Korfman dESN 9-300-30 kw

From the analysis of the nomograms presented in Figures 1 ÷ 3 mainly result the following aspects:

- For the present situation, columns with the diameter ϕ = 900 mm, R_0 = 0,003038 kμ/m and $K_0 = 3{,}326 \times 10^{-4}$ $m^3/s/m$ at 1 mm H_2O, in case of using the centrifugal fan V 496/5 the necessary airflow from the working face (236 m^3/min) can not be achieved for the final length of 3500 m of the mining work;
- For the column with the diameter of ϕ = 900 mm, R_0 = 0,003038 kμ/m and $K_0 = 1{,}8 \times 10^{-4}$ $m^3/s/m$ at 1 mm H_2O, in case of using the type VE ϕ 800 – 30 kW fan, respectively using dESN 9-300-30 Kw fans, the necessary airflow at the coal face (236 m^3/min) can be achieved by the two types of fans with their cascade placement:

* with 3 VE 800-30 kW fans, at a total length of the column of 3720 m;

* with 3 dESN 9-300-30 Kw fans , on a total column length of 4200 m.

Figure 4 (fig. a - e) presents and example of VE 800-30 kW fans placement on the 900 mm diameter ventilation column based on the nomogram presented in Figure 2.

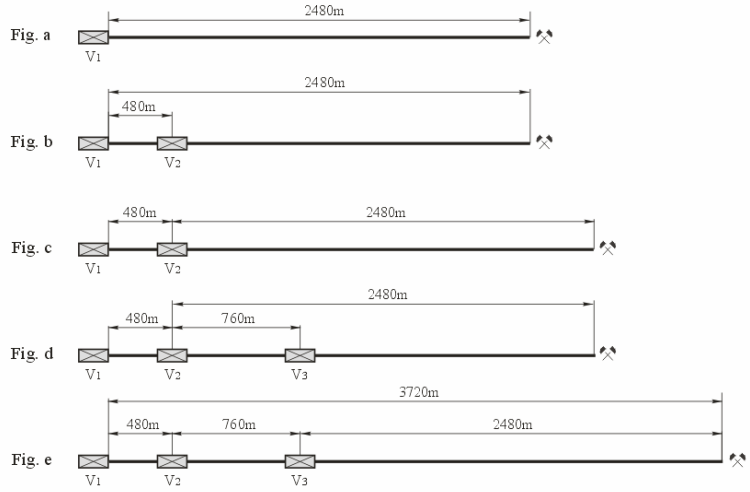

Figure 4 VE 800-30 kw fan placement of ventilation tubes on steel column diameter 900 mm (Q = 236 m/min)

With one fan, the 236 m^3/min airflow reaches a length of 2480 m of the ventilation column, with 2 fans it reaches 2960 m, with 3 fans it reaches 3720 m.

During the mining work diggings the fans are placed like this (Figure 4) :

- fan no. 1 is place at the and of the ventilation column assuring the achievement of the planned flow up to a length of the column of 2480m (fig.a, Figure4);
- fan no. 2 is placed at a distance of 480m from fan no.1 (fig. b, Figure 4). Fan no. 2 will circulate air on a length of 2480 m (fig. b, Figure 8). When the mining work has been dug up to 2960m length, fan no.3 is installed (fig. c, Figure 8) ;
- fan no.3 is place at a distance of 760m from fan no.2 (fig.d, Figure 4) and will circulate air on a length of 2480m (fig.e, Figure 4).

Finally, fan no.3 will circulate air on a column length of 2480 m, fan no.2 on a length of 760 m, fan no.1 on a length of 480 m (fig.e, Figure 4).

Table 1 presents the column lengths for each fan that can circulate the necessary airflow for the working face (236 m^3/min) as well as the maximum length that this flow can reach based on the elaborated nomograms (column diameter ϕ 900 mm).

Table 1

No.	Fan type	Ro kμ/m	Ko m^3/s/m la 1 mm H_2O	Required air flow at the working face Q_{fp} (m^3/min)	Column length related to each fan			Maximum length to reach L_{max} (m)
					L_1	L_2	L_3	
1.	V 496/5	$3{,}038 \times 10^{-4}$	$3{,}326 \times 10^{-4}$	236	2480	-	-	2480
2.	VE ϕ 800 – 30 kW	3,038x10	1,8x10	236	480	760	2480	3720
3.	dESN 9-300-30 Kw	3,038x10	1,8x10	236	600	920	2680	4200

By analyzing the data presented in table 1 there can be observed that the necessary airflow from the working face (236 m^3/min) depends on the unitary coefficient of air loss through column leakages K_0 as well as on the aerodynamic resistance of the tubes column R_O

The greater the aerodynamic resistance R_0 the smaller the maximum length of the circulated airflow to the working face.

Cascade using of fans with different features or with different parameters is not recommended.

4. The use of a single fan for achieving the ventilation of the front Castel Amonte main adduction gallery

It is known that once with increasing the length of the ventilation columns, the necessary flow at the fan grows because of the increasing of air loss through the leakages of the tubes column. On this grounds, the circulation of high air flows in the work faces from within the mining works with very long lengths raise issues that are hard to solve.

Considering that the final length of the tubes column will be 3500 m, the necessary parameters of the fan will have the maximum values. In these conditions it is necessary for the ventilation to be achieved in more phases, using more fans that correspond to these gallery digging phases. The necessary airflow at the working face (Q_f) has been considered to be 236 m^3/min (for the dilution of the exhaust gases from the 45 HP locomotives.)

The calculation of the parameters necessary for the fan have been made by giving „k" 2 values:

- k = 0,0003326 (medium value resulted from the measurements);
- k = 0,00018 (very good tightness level).

The following values for airflow and for depression necessary to be met by a fan resulted after performing calculations:

- for k = 0,0003326 m^3/s/m at 1 mm H_2O and R_0 = 0,003038 kμ/m at a length of the working of 3500m, there would be necessary a fan that achieves a 17,905 m^3/s (1074 m^3/min) airflow and a depression of 614 mm H_2O. Actually, these parameters necessary for the fan, using the K_0 coefficient as determined by the measurements are possible to achieve by using a single fan;
- for k = 0,00018 m^3/s/m at 1 mm H_2O and R_0 = 0,003038 kμ/m (medium value resulted from the measurements), at a length of the working of 3500 m there would be necessary a fan that achieves a11,493 m^3/s (690 m^3/min) airflow and a depression 408 mm H_2O.

Practically, to achieve the ventilation of the Front Castel Amonte main adduction gallery, the improvement of their tightness is necessary in order obtain a coefficient „K_0" up to $1,8 \cdot 10^{-4}$ m^3/s/m at 1 mm H_2O.

It results that for the aeration of the Front Castel Amonte main adduction gallery there can be used the following:

- a high pressure centrifugal fan type MZRU 1000 respectively type MZRU 1120 at the actual tightening level of the metallic column or type MZRM 900, 1000, 1120 for a very good tightening level of the metallic tubes column;
- axial fans VE ϕ 800 - 30 kW, respectively axial fans type Korfmann dESN 9-300-30 Kw type with their placement in cascade, in the conditions of ensuring a very good tightening level.

5. Conclusions

1. Irrational placement of the fans on the ventilation columns leads to air recircuiting on the mining work path.
2. The suction ventilation system requires depression only related to the gallery atmosphere, in the column on its entire length.
3. For the aeration of the Front Castel Amonte main adduction gallery there have been considered two aeration solutions as follow:
   - cascade placement of the fans on the partial ventilation column;
   - usage of a single fan on the ventilation column in order to ensure the airflow at the working face.
4. From the analysis of the nomograms presented in the paper for a 236 m^3/min air flow necessary at the work face resulted the following:
   - for ventilation columns with R_0 = 0,003038 Kμ/m and $K_0 = 3,326 \times 10^{-4}$ m/s/m at 1 mm H_2O the necessary air flow can not be achieved at the work face in case of using the centrifugal fan V 496/5;
   - for ventilation columns with R_0 = 0,003038 Kμ/m and $K_0 = 1,8 \times 10^{-4}$ m/s/m at 1 mm H_2O), the necessary air flow can be achieved as it follows:
     - with 3 fans, type VE 800-30 kW at a total column length of 3720 m;
     - with 3 fans, type dESN 9-300-30 Kw on a total column length of 4200m.
5. In case of using a single fan on the metallic tubes column, following the calculations, for a value of R_0 = 0,003038 Kμ/m of the unitary aerodynamic resistance there would be obtained the following parameters necessary for the fan:
   - for K_0 = 0,0003326 m^3/s/m at 1 mm H_2O (Q_v = 1074 m^3/min, h_v = 614 mm H_2O);
   - for K_0 = 0,00018 m^3/s/m lat 1 mm H_2O (Q_v = 690 m^3/min, h_v = 408 mm H_2O).
6. For the aeration of the Front Castel Amonte main adduction gallery there can be used the following:
   - a high pressure centrifugal fan type MZRU 1000 respectively type MZRU 1120 at the actual tightening level of the metallic column or type MZRM 900, 1000, 1120 for a very good tightening level of the metallic tubes column;
   - axial fans VE ϕ 800 - 30 kW, respectively axial fans type Korfmann dESN 9-300-30 Kw type with their placement in cascade, in the conditions of ensuring a very good tightening level.

References

1. I. Matei, R. Moraru ş.a.: *Environmental Engineering and underground ventilation*, Technical Publishing House, Bucharest, 2000 (in Romanian, Ingineria mediului şi ventilaţia în subteran)
2. I. Gherghe: *Checking in situ aerodynamic parameters characterizing ventilation plant used in the main gallery of the supply front of the Castel*

Amonte AHE Siriu – Surduc, INSEMEX Study – 2010 (in Romanian, Verificarea in situ a parametrilor aerodinamici care caracterizează instalațiile de aeraj utilizate pe galeria principală de aducțiune front Castel Amonte din cadrul A.H.E. Siriu – Surduc, Studiu INSEMEX)

3. I Matei ş.a.: *Guidelines for the design of ventilation installations partially*, M.M.P.G., 1986 (in Romanian, Ghid pentru proiectarea instalațiilor de aeraj parțial)
4. Dr. Am Patterson: *The Mine Ventilation* Practitioner's Data Bock , M.V.S. of South Africa - 1992

Amplasarea judicioasă a ventilatoarelor pe coloana de aeraj în cadrul aducțiunii front Castel Amonte utilizând nomogramele pentru dimensionare în sistem Q-L

Rezumat

Similar atribuțiilor aerajului general, realizat prin intermediul instalațiilor principale de ventilație, aerajul parțial cu pondere foarte mare în existența oricărei mine, indiferent de natura substanței minerale utile care se extrage are drept scop asigurarea condițiilor de securitate şi confort în lucrările miniere de deschidere şi pregătire, în faza de execuție a acestora.

Proiectarea unui sistem aspirant eficient este un proces foarte complex care implică cunoaşterea unui număr mare de factori. Fiecare gură de aspirare trebuie astfel proiectată încât să nu permită prafului, respectiv gazelor toxice şi/sau explozive să fie recircuitate, dar în acelaşi timp, devine necesară captarea particulelor grosiere care colmatează până şi conductele de aeraj.

Pentru identificarea unor soluții de realizarea a aerajului par□ial trebuie determina□i parametrii specifici aferenți coloanelor de aeraj R_0 (rezistența aerodinamică unitară) şi K_0 (coeficientul unitar al pierderilor de aer prin neetanşeități). Aceşti coeficienți prezintă o deosebită importanță practică deoarece determină în cea mai mare măsură eficiența instalațiilor de aeraj parțial. Cu cât rezistența aerodinamică R_0 este mai mare cu atât lungimea maximă de vehiculat a debitului de aer către frontul de lucru este mai mică.

Este ştiut că odată cu creşterea lungimii coloanelor de aeraj, debitul necesar la ventilator creşte datorită majorării pierderilor de aer prin neetanşeitățile coloanei de tuburi. Din aceste motive vehicularea debitelor mari de aer în fronturile de lucru din lucrările miniere cu lungimi mari, ridică probleme greu de rezolvat.

Scientific reviewers: **Emilian GHICIOI*,INCD INSEMEX,Petroşani,Romania**
Ion TOTH, INCD INSEMEX, Petroşani, Romania**

SCIENTIFIC BULLETIN OF
THE „POLITEHNICA" UNIVERSITY OF TIMISOARA, ROMANIA
TRANSACTIONS ON MECHANICS
BULETINUL ŞTIINŢIFIC AL
UNIVERSITĂŢII „POLITEHNICA" DIN TIMIŞOARA, ROMÂNIA
SERIA MECANICĂ
Tom 56 (70) **ISSN 1224 - 6077** **Fasc. S1, 2011**

DISTRIBUTION OF LOADS OF CYCLOID SPEED REDUCER

Marko RISTIĆ[1], Milorad KOČIĆ [1], Ana ALIL[1], Olivera ILIĆ[1], Jelena IGNJATOVIĆ[1]
[1]Institute Gosa, Belgrade, Serbia, marko.ristic@institutgosa.rs

Abstract: Cycloidal speed reducer belongs to the generation of modern planetary gears. It main features are: high transmission ratio, compact design, long and reliable working life, high efficiency, possibility of accepting big short-term overloads, wide application in various industries,...
The main element of cycloidal speed reducer is certainly cycloid disc whose profile is equidistant of shortened epitrochoid. Analytical and numerical models of cyclo speed reducer are developed in aim to analiyse the distribution of stress of some elements of cyclo speed reducer. The results are presented in the form of images, tables and charts.

Keywords: cycloidal speed reducer, cycloid disc, force analysis

1 Introduction

In accordance with modern development trends in the area of complex machine constructions, high power transmission gears with high transmission ratios and low losses are becoming a necessity. Considering the limitations imposed on standard transmission gears regards to their power and dimensions, planetary gears have started to be applied as a substitution for complex transmission gears. The cycloidal speed reducer belongs to a group of new generation planetary gears. They are broadly used in the modern industry. The most common applications are in the areas of robot industry, satellite technology, tool machines, elevators, the process industry, transporters, etc. Cycloidal speed reducers have found a broad use due to a number of excellent characteristics they possess such as long and reliable work life, large range of possible transmission ratios, extremely reliable functioning in dynamical load conditions, compact design, and high efficiency coefficient. Single-stage cycloidal speed reducer is shown in Figure 1.

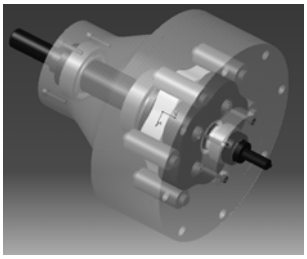

Figure 1 Single-stage cycloidal speed reducer

1.1 Operating principle of cycloidal speed reducer

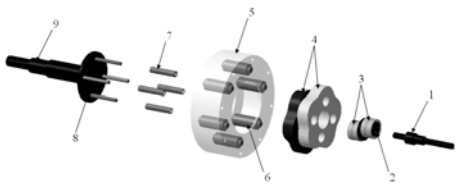

Figure 2 Operating principle of single-stage cycloidal speed reducer

An exploded view of a one-stage cycloidal speed reducer of traditional design is shown in Fig. 2, where two cycloid discs, relatively turned to each other for an angle of 180˚, are used for each stage. The working principle is as follows: eccentric (2) is rotating with the same number of revolutions and in the same direction as the input shaft (1). Cycloid discs (4) are situated on the eccentric through bearings (3). Cycloid discs are conjugated with ring gear rollers (6) located within the body of the ring gear (5). The result of this conjugation is the complex motion of the cycloid discs consisting of a rotation that originates from the eccentric, in the direction of the input shaft rotation and rotation of cycloid discs around their own axes in the opposite direction. Output rollers (7), which carrier (8) is tightly connected to the output shaft (9), go through the circular openings of the cycloid discs and transfer their motion to the output shaft.

2. Analysis of the load that occurring at Cycloid speed reducer

Cycloid speed reducer is a very complex system, both in terms of geometry, and in terms of its kinematic and dynamic structure. A key element of cycloid speed reducer is cycloid discs, and will therefore have a very central place on the further analysis. Figure 3 shows the forces acting on cycloid discs which is rotated an angle β with respect to the starting position.

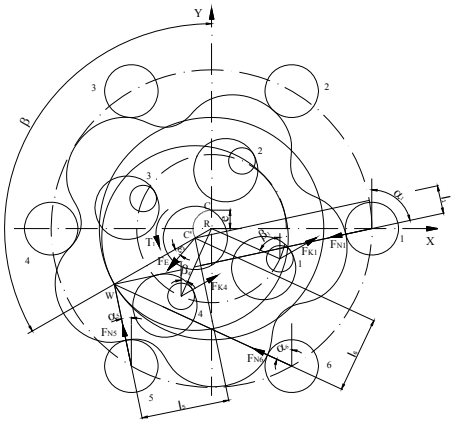

Figure 3 Cycloid disc in contact with housting rollers and output rollers

Forces on cycloid disc are:

F_E – bearing reaction,

F_{Ni} – force between housing roller *i* and cycloid disc,

F_{Kj} – force between output roller *j* and cycloid disc,

T_1 – input torque.

The following equations can be expressed, based on Figure 2:

$$T_1 = F_E\, e \cos(\beta + \varepsilon) \tag{1}$$

$$T_1 = \frac{r_i}{z} \sum_{j=1}^{q} F_{Kj} \sin(\beta_j + \beta) \tag{2}$$

$$-\sum_{i=1}^{p} F_{Ni} \sin\alpha_i + \sum_{j=1}^{q} F_{Kj} \sin\beta - F_E \sin(\beta + \varepsilon) = 0 \tag{3}$$

$$-\sum_{i=1}^{p} F_{Ni} \cos\alpha_i - \sum_{j=1}^{q} F_{Kj} \cos\beta - F_E \cos(\beta + \varepsilon) = 0 \tag{4}$$

$$\sum_{i=1}^{p} F_{Ni}\, l_i - \sum_{j=1}^{q} F_{Kj}\, r_i \sin(\beta_j + \beta) = 0 \tag{5}$$

where:

e – eccentricity,

β – swivel angle of the input shaft,

ε – angle between the force F_E and eccentricity direction,

r_i - radius of output rollers pitch circle,

z - number of teeth of cycloid disk (gearing ratio of the cycloidal speed reducer),

β_j – angular position of the output roller – j ,

α_i – angle which force F_{Ni} makes with vertical,

l_i - lever arm of force F_{Ni} ,

p - number of the housing rollers that carry the load,

q - number of the output rollers that carry the load.

Values α_i and l_i are calculated according to Figure 2, based on the following expressions:

$$\alpha_i = \operatorname{arctg} \frac{\sin\beta + \dfrac{r}{r_2}\sin\gamma_i}{\cos\beta - \dfrac{r}{r_2}\cos\gamma_i} \tag{6}$$

$$l_i = r_1 \sin(\alpha_i - \beta) \tag{7}$$

Angle γ_i (angular position of the housing rollers) is calculated based on the following expression:

$$\gamma_i = \frac{360(2i-1)}{2(z+1)} \quad (8)$$

r - radius of housing rollers pitch circle,
r_1 - base circle radius of the cycloid disc,
r_2 - base circle radius of the housing rollers.

Forces F_{Ni} and F_{Kj} are proportional to their respective distances from the centre of rotation:

$$\frac{F_{Ni}}{l_i} = const. \quad (9)$$

$$\frac{F_{Kj}}{\sin(\beta_j + \beta)} = const. \quad (10)$$

Only for ideal (theoretical) case all cycloid disk teeth are in contact with appropriate rollers and half of them carry load. In reality, cycloidal speed reducer has machining tolerances due to which number of teeth in contact is lower than in ideal case, that is, the load per one tooth is increased.

3 Analiyse the distribution of stress of cyclo speed reducer

Analysis load distribution was done for concrete one-stage cycloidal speed reducer with next characteristics:

Input power: $P = 1{,}1\,\text{kW}$

Input rpm: $n = 1410\,\text{min}^{-1}$

Gear ratio (number of cycloid disc teeth): $u = 5$ ($z_1 = 5$)

input torque: $T_1 = 3{,}725\,\text{Nm}$

Table 1 Values of normal force depending on the number of teeth in contact

In contact	F_{N1},[N]	F_{N5},[N]	F_{N6},[N]
1 teeth	1750,47	/	/
2 teeths	212,29	/	572,04
3 teeths	97,23	303,48	261,99

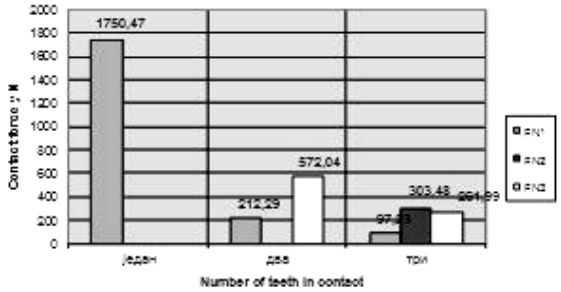

Figure 4 Contact force changes depending on the number of teeth in contact

As it could be expected, with the number of teeth which at the same time carry the load decreases the value of certain contact force on the teeth cycloid discs.

He also performed the analysis of stress-state elements deform cycloid speed reducer. For this purpose software package INVENTOR was used. In the very numerical analysis, elements cycloid speed reducer were considered elastic, deformable bodies.

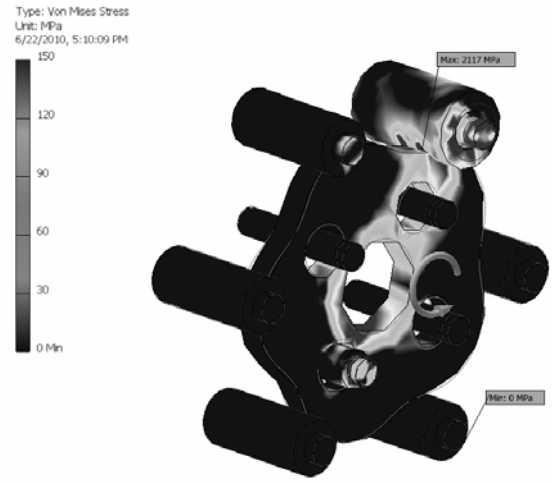

Figure 5 Von Mises Stress

Cycloid discs not only carry the load from the input torque, but it also acts as the output torque and power to the eccentric and analysis done in the case. Figure 4 shows the distribution of stress $(\sigma_{VonMises})$ and also the from picture it can be concluded that the maximum stress occurs on the ring gear rollers.

4 Conclusions

M. Lehmann [1] is described the procedure for force distribution at cycloidal speed reducer for theoretical case (when friction don`t exist) in detail. Malhotra [2] is defined some simplified model for force analysis but without friction, too. Complete geometric and kinematic analysis of cycloid disc tooth profile is described in papers [3]. Gorla, Davoli and others [4] give out the results of theoretical and experimental analysis of cycloidal speed reducer efficiency. Stress and strain state at cyclo speed reducer elements are presented in papers [5,6,7]. Meng and others [8] defined a mathematical model of transmission performance of 2K-H pin-cycloid planetary mechanism including the friction. The development of appropriate analytical and

numerical model by which can analyze the stress state of the basic elements of cycloid speed reducer and analysis the forces acting on cycloid speed reducer presented in [9]. In the paper, also is described and presented a two-step cycloid speed reducer new concept [10], is also presented and the distribution of loads, acting on it, as well as experimental results obtained through the specific example of this type cycloid speed reducer.

References

1. M. Lehmann: *Calculation and measurement of forces acting on cycloidal speed reducer* (in German), PhD Thesis, Technical University Munich, Germany, 1976.
2. S.K. Malhotra, M.A. Parameswaran*: Analysis of a cycloidal speed reducer*, Mechanism and Machine Theory, Vol.18, No 6, pp. 491-499, 1983.
3. Y.W. Hwang, C.F. Hsieh*: Geometry design and analysis for trochoidal-type speed reducers:* with conjugate envelopes, Transactions of the CSME/de la SCGM, Vol. 30, No. 2, pp. 261-278, 2006.
4. C. Gorla, P. Davoli, F. Rosa, C. Longoni, F. Chiozzi, A. Samarani: *Theoretical and experimental analysis of a cycloidal speed reducer*, Journal of Mechanical Design (ASME), Vol. 130, pp. 112604-1-112604-8, 2008.
5. M. Blagojevic, N. Marjanovic: *The force distribution on two stage cyclo speed reducer with new concept*, in: 9th International Conference on Accomplishements in Electrical and Mechanical Engineering and Information Technology, Banja Luka, pp. 51-56, 2007.
6. M. Blagojevic: *Stress and strain state of cyclo speed reducer`s elements under dynamic loads*, PhD Thesis, Faculty of Mechanical Engineering Kragujevac, Serbia, 2008.
7. M. Blagojevic, V. Nikolic, N. Marjanovic, Lj. Veljovic: *Analysis of cycloid drive dynamic behavior*, Scientific Technical Review, Vol.LIX, No. 1, pp. 52-56, 2009.
8. Y. Meng, C. Wu, L. Ling: *Methematical modelling of the transmission performance of 2K-H pin cycloid planetary mechanism*, Mechanism and Machine Theory, Vol. 42, pp. 776-790, 2007.
9. M. Kocic: *Distribution of loads of cycloid speed reducer*, MSc Thesis Faculty of Mechanical Engineering Kragujevac, Serbia, 2010.
10. M. Blagojevic, N. Marjanovic, Z. Djordjevic, B. Stojanovic, A. Disic: *A new design of a two-stage cycloidal speed reducer*, Journal of Mechanical Design,Vol.133.

Rezumat

In terms of kinematic and dynamic Cycloid speed reducer have very good performance. Cycloid speed reducer belong to a group of planetary gear power. Given the numerous advantages that have (a compact design, quiet operation and bezšuman, easy installation and maintenance, efficient operation and saving energy, etc..) Cyclo mechanisms eventually assume the role of the market. Today, every industry is interested in the mechanisms of cyclo inserted in its facilities, particularly in industrial robots, which are a reflection of economic and economic growth in the twenty-first century.

The results obtained in this work are defined and directions for further research in this area:

- Development of a functional model cikloreduktora and analysis of the same in order to confirm schematically obtained in this work.
- Development of numerical models in which the analysis to include the phenomena of friction, wear, fatigue fracture, and so on.

Acknowledgments

This paper is the result of research within the project TR 34028, which is financially supported by Ministry of Science and Technology of Serbia, Messer Tehnogas and PD TE – KO Kostolac.

Scientific reviewers: **Slavica Ristic, Institute Gosa, Belgrade**
Boris Katavić, Institute Gosa, Belgrade

SCIENTIFIC BULLETIN OF
THE „POLITEHNICA" UNIVERSITY OF TIMISOARA, ROMANIA
TRANSACTIONS ON MECHANICS
BULETINUL ŞTIINŢIFIC AL
UNIVERSITĂŢII „POLITEHNICA" DIN TIMIŞOARA, ROMÂNIA
SERIA MECANICĂ
Tom 56 (70) **ISSN 1224 - 6077** **Fasc. S1, 2011**

NUMERICAL SIMULATION OF THE COLD-WATER PRESSURE TEST AND OPERATING CONDITIONS FOR AIR RESERVOIR

Marko RISTIĆ[1], Mirjana PRVULOVIĆ [1], Milan PROKOLAB[1], Stevan BUDIMIR[1], Miroslav RADOSAVLJEVIĆ[1], Dragan JOVANOVIĆ[1], Zlatan MILUTINOVIĆ[1]
1

[1]Institute Gosa, Belgrade, Serbia, marko.ristic@institutgosa.rs

Abstract: In this paper, is performed a comparative analysis of stresses in the pressure vessel wall, based on strength calculation, numerical simulations using software package CATIA and cold-water pressure tests results. It was analyzed a stress distribution in the wall of vessel, in case of operating pressure and test pressure. It was considered a cylindrical reservoir, designed to keep air. During the test, neither strain nor improper side effects on the vessel has been identified. Using the software package CATIA it was done a modeling of the pressure vessel for a real geometry, taking into account a form of vessel head, geometry of connections, supports and welded joints, since they are critical zones for the occurrence of stress concentration. Results by the analysis show that the highest achieved stresses are in the torus part of the head and around the connections. Comparative analysis has shown that there is a good agreement between the results obtained on the basis of strength calculations, test results and numerical simulations, hence applied methodology can be successfully used in the tests during exploitation and designing of the pressure vessel.

Keywords: numerical simulation, CATIA software package, cold – water pressure test

1 Introduction

In recent years, numerical simulation has been used very often in various studies [1-4] and calculations of stress distribution for mechanical structures.

In this paper, is performed a comparative analysis of stresses in the pressure vessel wall, based on strength calculation, numerical simulations using software package CATIA and cold-water pressure tests results. It was analyzed a stress distribution in the wall of vessel, in case of operating pressure and test pressure.

It was considered a cylindrical reservoir, designed to keep air. During the test, neither strain nor improper side effects on the vessel has been identified.

Using the software package CATIA it was done a modeling of the pressure vessel for a real geometry, taking into account a form of vessel head, geometry of connections, supports and welded joints, since they are critical zones for the occurrence of stress concentration. Results by the analysis show that the highest achieved stresses are in the torus part of the head and around the connections.

Comparative analysis has shown that there is a good agreement between the results obtained on the basis of strength calculations, test results and numerical simulations, hence applied methodology can be successfully used in the tests during exploitation and designing of the pressure vessel.

2 A brief reviews of the used methods

2.1 Calculation of the strength

It is considered vertical steel vessel, volume 8,6 m^3. Operating fluid is pressure air (6 bar, 50 ^{0}C). Pressure vessel is made of structural steel 355 J2G3 (EN 10025).
Strength calculation of parts of the pressure vessel has been done in accordance with valid national standards (SRPS M.E2.250, SRPS M.E2.252, SRPS M.E2.253, etc.).

2.2 Numerical simulations

Numerical simulation of stress distribution on the same model and same condition is presented. Finite element method (FEM) was chosen to simulate operating conditions (boundary conditions and load). The CATIA (Computer Aided Three-dimensional Interactive Application) software package has been used for generating finite element meshes, composed of tetrahedron type, three-dimensional finite elements. FEM is based on a physical discretization of the considered parts of a continuum of finite dimensions and simple shapes called finite elements (FE). All finite elements are connected by common nodes to form the original structure. The basic types of finite elements are: one-dimensional (rods, beams, pipe fittings), two-dimensional (triangular, rectangular, membranes, plates and shells), three-dimensional (tetrahedron, prism, axisymmetric and others). In FEM studied domain (the strain body) is shared by using fictitious line on a number of finite elements. Set of finite elements for the entire domain make a network of finite elements. Stress and strains are described by interpolation functions and a finite number of parameters in the nodes. They are the basic parameters of the FEM. When the basic relations in the FEM are setting up, using the same principles and procedures, that are valid beyond the classical discrete models, they relate force and stress and stress and strain. By grouping the basic equations finite elements gets the equation structure in matrix form.

Numerical simulation has been done for both operating and testing pressure.
Stress analysis tank is made with FEM. It is an efficient and reliable numerical procedure for modelling both, linear and nonlinear behaviour of materials and structures . Numerical method FEM has been used in order to confirm the ability of testing tank pressure to predict the crack of spacemen. Elastoplastic, numerical analysis of the tank made of structural steel is made. The primary aim was to obtain the maximum strain that correspond to the calculation. The finite tetrahedron type element and model specimen with finite element mesh are shown in fig 1.

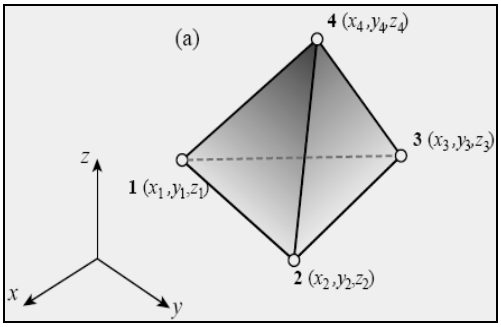

Figure 1 Finite element type tetrahedron

Finite element mesh is consisted of 92,890 elements and 18,5958 nodes with three degrees of freedom, so the system has a total of 557,874 equations. A global stiffness matrix system of finite element meshes in this case has 33297 x 33297 elements. Using equations which link displacement and strain, and the equations of deformation and stress, stress distribution is determined. External load were entered into the model on the front surface of the board, while the other plate wedged. In Figure 2 is shown the model of thank with the finite element mesh.

Numerical simulation of operating pressure
Firstly is done numerical simulation of testing pressure which is P=8bar and results are shown .

Figure 2 Model specimen with finite element mesh after tensile test

The highest stress in the bottom of the thank, is $2.24 \cdot 10^8$ N/m^2 (Fig. 3). Numerical results demonstrate a good agreement with control calculation which value is $2.36 \cdot 10^8$.(N/m^2). The zoomed part of bothom of thank with Von Miss stress distribution is presented in fig4.

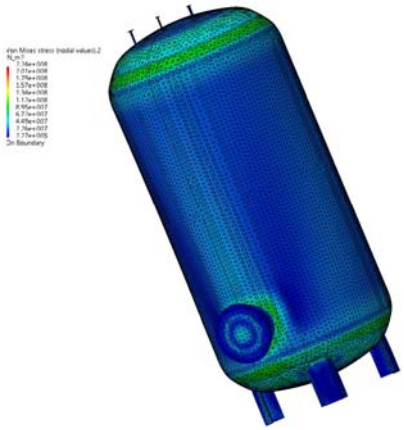

Figure 3 Preasure test simulation with the testing pressure, specimen with the Von Mises stresses

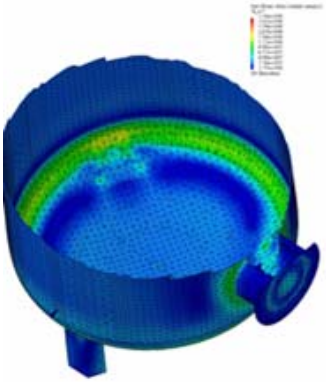

Figure 4 Increase part of specimen with the field of stress, calculation preformed with testing pressure

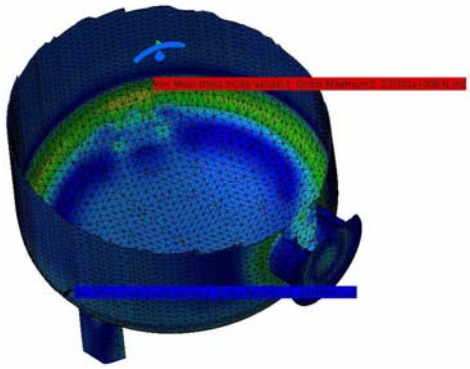

Figure 5 Point with maximum and minimum of stress, bottom of thank with testing preasure

Numerical simulation operating pressure

After testing pressure simulation, is done simulation of working pressure to see of the value of stress in this condition, working pressure is P=5bar. Figure 6, 7

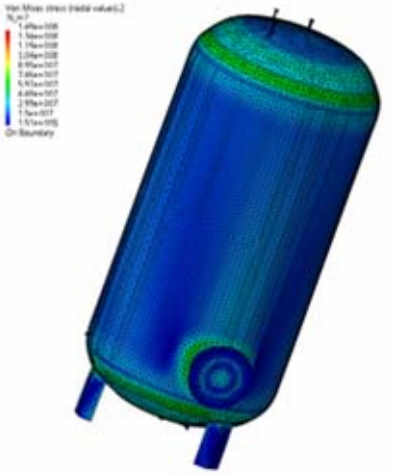

Figure 6 Preasure test simulation with the working preasure , specimen with the Von Mises stresses

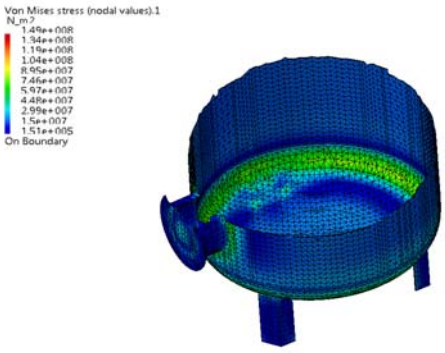

Figure 7 Increase part of specimen with the field of stress, calculation preformed with working pressure

2.3 Cold-water pressure testing

This testing has been performed in accordance with standard SRPS M.E2.201. Needed preparation took place before testing. Value of the test pressure is 8 bar. Examination has been done at ambient temperature 17 ^{0}C. Test medium is cold water. During the performed testing it has not been seen the signs of a destruction, plastic deformation, leaking on the weld joints.

Results and discussion

Strength calculation shows that stresses in the wall of pressure vessel have permitted values for both operating and testing conditions. A greatest stress values are obtained on the torus part of the head, around hole and near the connections. The same conclusion can be made on the basis of the results of the numerical simulations.
Maximal value of stress is 249 N/mm^2 based on the standard strength calculation.

Conclusion

Distribution of stresses in the wall of the pressure vessel obtained by used numerical simulation shows a good agreement with the results of the standard strength calculation also for operating and test conditions.
Pressure vessel is properly designed due to stress value is lower than the yield stress of the applied material.
Maximal value of stress has been achieved around connections, supports and torus part of the head.
Numerical simulations can be very useful in the determination of the stress state on the real structures especially after reconstruction during life-time of the constrictions.

References

1. M.A.Guerrero, C.Betagon, J.Belzunce, *Fracture analysis of a pressure vessel made of high strength steel* (HSS), Engineering Failure Analysis, Vol.15, Issue 3, April 2008, pp. 208-219.
2. N. Vanderesse, E. Miarie, A. Chabod, *Microtomographic study and finite element analysis of the porosity harmfulnesin a cast aluminium alloy,* International Journal of Fatigue, Vol.33, Issue 12, December 2011, pp. 1514-1525.
3. M. Radosavljevic, M. Prvulovic., N. Markovic and others, Project,: *Control calculation of the strenght and making of attest and technical documentations of the pressure vessel* (In Serbian), 2004.
4. M. Kutin, S. Ristic, M. Puharic, M. Ristic: *Tensile features of hole in plate specimen testing by thermography and conventional method*, Third Serbian (28th Yu) Congress on Theoretical and Applied Mechanics Vlasina lake, Serbia, 5-8 July 2011.

Rezumat

In this paper performed a comparative analysis of stresses in the pressure vessel wall, based on strength calculation, numerical simulations using software package CATIA and cold-water pressure tests results. It was analyzed a stress distribution in the wall of vessel, in case of operating pressure and test pressure.
It was considered a cylindrical reservoir, designed to keep air. During the test, neither strain nor improper side effects on the vessel has been identified.
Using the software package CATIA it was done a modeling of the pressure vessel for a real geometry, taking into account a form of vessel head, geometry of connections, supports and welded joints, since they are critical zones for the occurrence of stress concentration. Results by the analysis show that the highest achieved stresses are in the torus part of the head and around the connections.
Comparative analysis has shown that there is a good agreement between the results obtained on the basis of strength calculations, test results and numerical simulations, hence applied methodology can be successfully used in the tests during exploitation and designing of the pressure vessel.

Acknowledgments
This paper is the result of research within the project TR 34028, which is financially supported by Ministry of Science and Technology of Serbia, Messer Tehnogas and PD TE – KO Kostolac.

Scientific reviewers: **Slavica Ristic, Institute Gosa, Belgrade**
Boris Katavić, Institute Gosa, Belgrade

SCIENTIFIC BULLETIN OF
THE „POLITEHNICA" UNIVERSITY OF TIMISOARA, ROMANIA
TRANSACTIONS ON MECHANICS
BULETINUL ŞTIINŢIFIC AL
UNIVERSITĂŢII „POLITEHNICA" DIN TIMIŞOARA, ROMÂNIA
SERIA MECANICĂ
Tom 56 (70) ISSN 1224 - 6077 Fasc. S1, 2011

JOINING ALUMINUM ALLOY WITH GALVANIZED STEEL BY CMT PROCESS

Radu Alexandru ROŞU*, Doru Romulus PASCU*, Sorin DRĂGOI*
* National Institute of Research and Development in Welding and Material Testing, ISIM Timişoara,
e-mail:rrosu@isim.ro

Abstract. Galvanized steel sheets are used frequently in different sectors, especially in construction and automotive. Welding of galvanized sheets is difficult due to degradation of the zinc layers which leads to evaporation of zinc in the weld area. The paper presents the results of eight variants of galvanized steel-aluminum alloy heterogeneous joining. For the experimental program was used DX51D+Z150-N-A-C (EN 10327/2004) galvanized steel sheets and aluminum alloy sheets EN AW 1200 (SR EN 1706: 2000) with the thickness of 1 mm. Macro and microscopic analysis carried out in characteristic areas present not welding defects. The mechanical characteristics of strength and deformability shows that joints made are adequate.

Keywords: heterogeneous joints, mechanical tests, microstructure

1. Introduction

In recent years, in the automotive industry are used more and lighter materials to reduce the fuel consumption of the cars. This involves the use of aluminum and magnesium alloys, due of their characteristics (lower density than steel, good corrosion properties). Using these types of alloys becomes inevitable to realize similar and dissimilar joints. A relatively new method of making such connections is CMT method [1].

CMT welding is a favorable possibility for solving specific problems for welding galvanized sheets by the low linear energy transfer used and the precise control of welding materials [2]. At the same time, using filler materials with a lower melting temperature compared with the base material will leads to reducing the effects which appear frequently at this kind of materials. The CMT process can be used also to heterogeneous joints such as metal-ceramic materials by depositing a layer of various alloys (Ti, Zr, Mo-Mn alloys, etc.), on the ceramic material components [3].

2. Materials used

For realization of galvanized steel-aluminum alloy heterogeneous joints were used the following materials:

- galvanized steel sheet DX51D+Z150-N-A-C (EN 10327/2004) of 1mm thick
- aluminum alloy sheet EN AW 1200 (SR EN 1706: 2000) of 1 mm thick

As filler material it was used AlSi5 electrode wire with the diameter of 1.2 mm using cc^+ polarity. Table 1 shows the chemical composition of the wire electrode AlSi5 EL-DIN 1732.

Table 1 Chemical composition of AlSi5 wire electrode

Filler material	Chemical composition [%]			
	Si	Mn	Fe	Al
AlSi5	4,5-5,0	<0,5	<0,5	rest

The mechanical characteristics of the deposited material by melting the wire electrode EL-AlSi5 are presented in Table 2.

Table 2 Mechanical characteristics EL-AlSi5 wire electrode

Yield strength $Rp_{0,2}$ [N/mm^2]	Hardness		Mechanical resistance, Rm [N/mm^2]	Elongation, A_s[%]
	HB	HV		
70-90	48-60	51-63	110-160	Min. 15

2. Experimental program

In Table 3 are presented the parameter values used to realize galvanized steel - aluminum alloy heterogeneous joints.

Table 3 Parameters values used in the experimental program

Variant no.	$I_S[A]$	$U_a[V]$	$v_{as}[m/\min]$	$v_s[mm/\min]$
1	67,2	11,7	3,70	800
2	88,6	15,2	4,37	800
3	88,6	15,2	4,35	1000
4	62,6	11,3	3,64	1000
5	61,0	11,3	3,47	800
6	69,3	14,3	4,35	800
7	70,1	14,5	4,39	1000
8	63,6	11,6	3,69	1000

3. Structural examinations

3.1 Macroscopic examinations on the cross-sections of the heterogeneous joints made on the analyzed variants showed no welding defects such as cracks (Figure 1)

Figure 1 Macroscopic analysis

3.2 Microscopic examinations were performed in the heterogeneous joints areas (WELD, BM, HAZ) according to EN 1321:2006.

On the base metal (unalloyed steel) it was observed ferrito-pearlitic structure the pearlite placing at the grain boundaries (Figure 2).

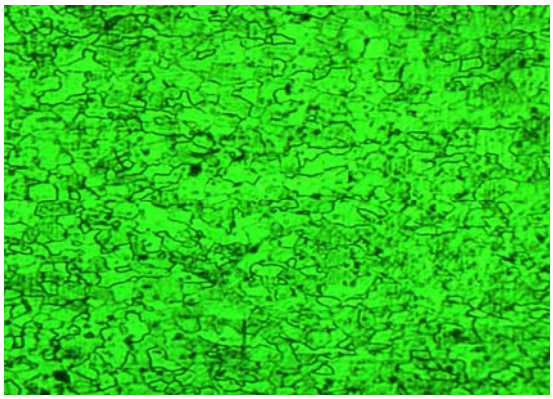

Figure 2 Unalloyed steel, 100x

The base metal (aluminum alloy) structure consists of α solid solution rich in aluminum, intermetallic compounds and oxides of Al-Si (Figure 3).

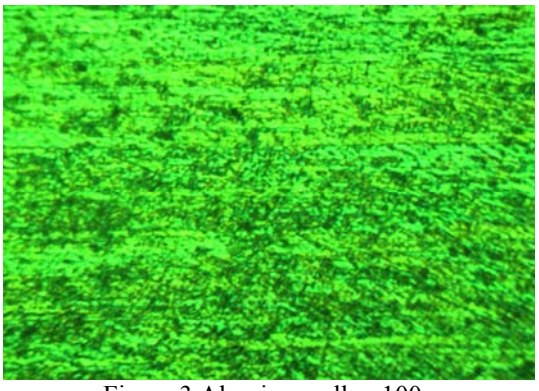

Figure 3 Aluminum alloy 100x

In the interface between the galvanized steel and weld zone are observed zinc layers of different thicknesses which separate the two areas (Figure 4).

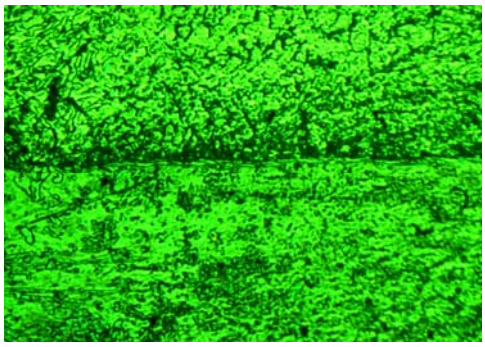

Figure 4 Interface, braze welding variant 1, 100x

In the welds are observing dendritic structures with specific structures of aluminum-magnesium alloys, α solid solution and intermetallic compounds of silicon and magnesium (Figure 5).

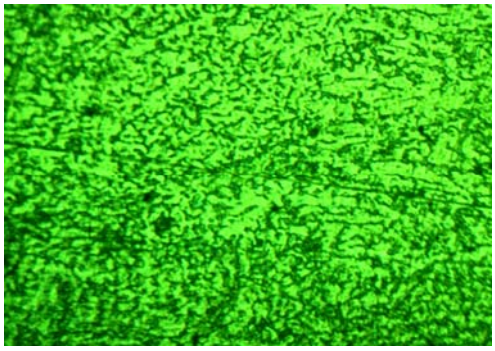

Figure 5 Weld, braze welding variant 1, 100x

In the heat affected zones (HAZ) in aluminum alloy is observed aluminum-rich structures (α structure) with fine particles of intermetallic compounds of aluminium-silicon, aluminum-magnesium (Figure 6)

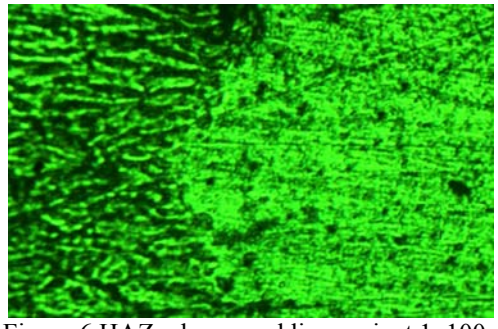

Figure 6 HAZ_{Al} braze welding variant 1, 100x

3.3 Mechanical tests

Tensile test was performed on flat specimens according to en 12797:2002 and the results are presented in Table 4.

Table 4 Breaking force values

Variant	Breaking force value F_{max}, [N]	
	Minimum value	Maximum value
1	1090	1110
2	1120	1130
3	1090	1100
4	1150	1170
5	1140	1150
6	1110	1130
7	1060	1150
8	1150	1150

Tensile test breaks occurred in base metal (aluminum alloy). Bending test was performed on specimens according to EN 12797:2002, the minimum and maximum bending angle are summarized in Table 5.

Table 5 Bending angle values

Variant	Bending angle, α [°]	
	Minimum value	Maximum value
1	91	98
2	90	111
3	110	138
4	92	119
5	101	104
6	95	115
7	91	112
8	90	107

After bending test at 90° all specimens were broken in the weld zone, certifying corresponding deformation characteristics.

HV1 hardness test was performed according to EN ISO 6507-4:2005 in the characteristic areas, the results and the values of structural hardening estimator ΔHV1 [5] calculated with the relationship 1 are listed in Table 6.

$$\Delta HV1 = \frac{HV1_{max} - HV1_{min}}{HV1_{max}} \cdot 100 \quad [\%] \quad (1)$$

Where:

- $HV1_{max}$ is the maximum hardness in o zone of the heterogeneous joint
- $HV1_{min}$ is the minimum hardness determined in another zone of the heterogeneous joint

It is considered that if $\Delta HV1 \geq 50\%$ in the analyzed zones were developed accentuated phenomena of fragile structures with high risk apparition of fragile breaking.

Table 6 HV1 hardness values

Joining variant	HV1 hardness				Estimator ΔHV1 [%]	
	BM_{steel}	WELD	HAZ_{Al}	BM_{Al}	BM_{steel}-Weld	WELD- HAZ_{Al}
1	143	42	28	27	70	33
2	159	71	32	26	55	54
3	148	52	27	26	64	48
4	162	60	34	27	62	43
5	143	39	29	26	72	25
6	135	51	27	25	69	47
7	131	45	30	25	65	33
8	145	37	27	26	74	27

In Figure 7 is shown the variation of ΔHV1 local hardening estimator function of the analyzed variant.

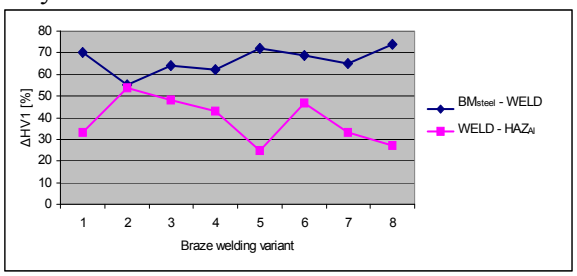

Figure 7 ΔHV1 function of the analyzed variant

ΔHV1 estimator calculated in the zones BM_{steel}-WELD (represented with blue) show generally high values over 50% certifying that in these areas were developed increased structural hardening phenomena. ΔHV1 estimator calculated in the areas WELD-HAZ_{Al} is below 50% (except variant 2) certifying that there were not developed important structural hardening phenomena.

4. Conclusions

1. CMT process is used more and more in many applications where are required to realize joints of heterogeneous materials.
2. Macro-microscopic examinations revealed no welding defects such as cracks or microcracks the zinc layer is not continue being partially degraded on aluminum alloy-galvanized steel interface
3. Mechanical tests performed on aluminum alloy-steel joints showed that the breaking occurred in the base material (aluminum), the breaking angle is over 90°, evidencing a high deformability.
4. Local hardening estimator values calculated in the area BM_{steel}-WELD have values over 50% certifying the apparition of accentuated structural hardening phenomena, the estimator values calculated in the areas WELD-HAZ_{Al} is below 50% (except variant 2) certifying that there were not developed important structural hardening phenomena.

References

1. Feng J.C., He P., Kackl H.: *Distribution of Zn and Interfacial Microstructure of Braze Welding CMT Joints between Aluminum and Galvanized Steel,* Solid State Phenomena, vol. 127, 2007, p43 ISSN 1012-0394
2. Lu Z., Huang P.: *ARC welding method for bonding steel with aluminum,* Mechanical Engineers, vol. 4, pp. 134–146, 2009, ISSN 0025-6501
3. Feng J., Zhang H., He P.: *The CMT short-circuiting metal transfer process and its use in thin aluminium sheets welding*, Materials and Design, Vol. 30, 2009, pp. 1850–1852, ISSN: 0261-3069
4. Roşu R., . Pascu D. R, Drăgoi S., Braze welding by electric arc in protective inert gas environment, PN 103, Phase 3, ISIM, 2011, Timişoara, Romania
5. Safta I. (2006). *Technological resistance tests of the welded or brazed joints*, Publisher Sudura, Timişoara, ISBN: 973-9359-38-4

Îmbinarea aliajelor de aluminiu cu oţel galvanizat prin procedeul CMT

Rezumat. Tablele din oţel nealiat galvanizate sunt utilizate in mod frecvent în diferite sectoare industriale, in primul rând, in construcţii de automobile şi tubulatură. Sudarea prin topire a tablelor acoperite este dificilă datorită degradării stratului galvanizat ca urmare a creşterii temperaturii ce conduce la evaporarea zincului in zona sudurii. În lucrare sunt prezentate rezultatele obţinute la ISIM Timişoara privind realizarea a opt variante de îmbinări eterogene aliaj de aluminiu-tablă zincată. In cadrul programului experimental s-a folosit aliaj de oţel zincat DX51D+Z150-N-A-C (EN 10327/2004) şi tabla de aliaj de aluminiu EN AW 1200 (SR EN 1706 : 2000) cu grosimea de 1mm. Analizele macro şi microscopice efectuate în zonele caracteristice îmbinărilor nu prezintă defecte de sudare. Caracteristicile mecanice de rezistenţă, deformabilitate atestă faptul că îmbinările realizate sunt corespunzătoare.

Scientific reviewers: **Mihaela POPESCU, Politehnica University of Timisoara**
Victor BUDĂU, Politehnica University of Timisoara

SCIENTIFIC BULLETIN OF
THE „POLITEHNICA" UNIVERSITY OF TIMISOARA, ROMANIA
TRANSACTIONS ON MECHANICS
BULETINUL ŞTIINŢIFIC AL
UNIVERSITĂŢII „POLITEHNICA" DIN TIMIŞOARA, ROMÂNIA
SERIA MECANICĂ
Tom 56 (70) ISSN 1224 - 6077 Fasc. S1, 2011

FUNCTION APPROXIMATION FOR THE HYSTERESIS OF FLUIDIC MUSCLES

József SÁROSI
Technical Institute, Faculty of Engineering, University of Szeged
Mars tér 7., Szeged, H-6724, Hungary
e-mail: sarosi@mk.u-szeged.hu

Abstract. Numerous researchers have investigated the relationship of the force, length and pressure to find a good approximation and theoretical approach for the equation of force generated by pneumatic artificial muscles (PAMs). Some of them report several mathematical models, but significant differences have been noticed between the theoretical and experimental results. Accordingly we have generated and introduced a new model and algorithm that gives us simple yet accurate description of this actuator. This paper presents this new function approximation for the hysteresis of Fluidic Muscles manufactured by Festo.

Keywords: Pneumatic Artificial Muscle, Force Equation, Matlab, Genetic Algorithm

1. Introduction

Many researchers have tried to find an actuator similar to human muscles. The most promising actuator in this field of research is undoubtedly the McKibben pneumatic muscle actuator. The McKibben muscle was invented in the 1950's by physician Joseph L. McKibben to help the movement of polio patients and to motorize pneumatic arm orthotics. There exist several types of artificial muscles that are based on the use of rubber or some similar elastic materials, such as the McKibben muscle, the Rubbertuator made by Bridgestone company, Air Muscle made by Shadow Robot company, Fluid Muscle made by Festo company, Pleated PAM developed by Vrije University of Brussel, ROMAC (RObotic Muscle ACtuator), Yarlott and Kukolj PAM and some others [1, 2].

A pneumatic actuator consists of an internal rubber bladder surrounded by a braided shell with flexible yet nonextensible threads according to a helical weaving that is attached at either ends. When inflated, the internal bladder tends to expand, with a consequent increase in the angle between the helical woven fibres of the braid and the axis of the tube and a decrease in axial length [3].

The layout of this paper is as follows. Section 2 (Materials and Methods) is devoted to demonstrate the model of force as a function of pressure and length (contraction). Section 3 (Experimental Results) presents several experimental results and finally, section 4 (Conclusions and Future Work) gives the investigations we plan.

Fluidic Muscles DMSP-10-250N-RM-RM (with inner diameter of 10 mm and initial length of 250 mm), DMSP-20-200N-RM-RM (with inner diameter of 20 mm and initial length of 200 mm) and DMSP-20-400N-RM-RM (with inner diameter of 20 mm and initial length of 400 mm) produced by Festo company were selected for our study.

2. Materials and Methods

The general behaviour of PAM with regard to shape, contraction and tensile force when inflated depends on the geometry of the inner elastic part and of the braid at rest (Figure 1), and on the materials used [1].

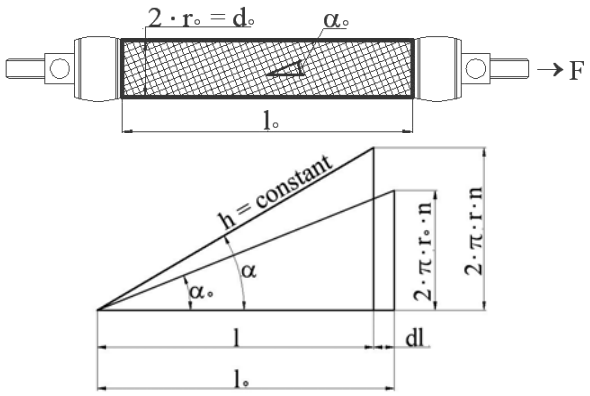

Figure 1 Geometry parameters of PAM

On the basis of [4], [5] and Figure 1, the force can be calculated:

$$F = -p \cdot \frac{dV}{dl} \tag{1}$$

$$2 \cdot p \cdot \pi \cdot r \cdot l \cdot dr - p \cdot \pi \cdot r^2 \cdot (-dl) - F \cdot (-dl) = 0 \tag{2}$$

$$F = -2 \cdot p \cdot \pi \cdot r \cdot l \cdot \frac{dr}{dl} - p \cdot \pi \cdot r^2 \tag{3}$$

$$\cos\alpha_0 = \frac{l_0}{h} \text{ and } \cos\alpha = \frac{l}{h} \tag{4}$$

$$\sin\alpha_0 = \frac{2 \cdot \pi \cdot r_0 \cdot n}{h} \text{ and } \sin\alpha = \frac{2 \cdot \pi \cdot r \cdot n}{h} \tag{5}$$

$$\frac{l}{l_0} = \frac{\cos\alpha}{\cos\alpha_0} \text{ and } \frac{r}{r_0} = \frac{\sin\alpha}{\sin\alpha_0} \tag{6}$$

$$r = r_0 \cdot \frac{\sqrt{1-\cos^2\alpha}}{\sin\alpha_0} = r_0 \cdot \frac{\sqrt{1-\left(\frac{l}{l_0} \cdot \cos\alpha_0\right)^2}}{\sin\alpha_0} \tag{7}$$

$$\frac{dr}{dl} = -\frac{r_0 \cdot l \cdot \cos^2\alpha_0}{l_0^2 \cdot \sin\alpha_0} \cdot \frac{1}{\sqrt{1-\left(\frac{l}{l_0} \cdot \cos\alpha_0\right)^2}} \tag{8}$$

$$F(p,\kappa) = p \cdot \pi \cdot r_0^2 \cdot (a \cdot (1-\kappa)^2 - b) \tag{9}$$

Where $a = \frac{3}{tg^2\alpha_0}$, $b = \frac{1}{\sin^2\alpha_0}$, $\kappa = \frac{l_0 - l}{l_0}$, $0 \le \kappa \le \kappa_{max}$, and V the muscle volume, F the pulling force, p the applied pressure, r_0, l_0, α_0 the initial inner radius and length of the PAM and the initial angle between the thread and the muscle long axis, r, l, α the inner radius and length of the PAM and angle between the thread and the muscle long axis when the muscle is contracted, h the constant thread length, n the number of turns of thread and κ the contraction.

Equation 9 is based on the admittance of a continuously cylindrical-shaped muscle. The fact is that the shape of the muscle is not cylindrical on the end, but rather is flattened, accordingly, the more the muscle contracts, the more its active part decreases, so the actual maximum contraction ration is smaller than expected [4].

Tondu and Lopez in [4] consider improving equation 9 with a correction factor (ε), on the one hand, it does not pay attention to the material that the muscle is made of, and on the other hand, it predicts for various pressures the same maximal contraction. This new equation is relatively good for higher pressure ($p \ge 2$ bar). Kerscher et al. in [5] suggest achieving similar approximation for smaller pressure another correction factor (μ) is needed, so the modified equation is:

$$F(p,\kappa) = \mu \cdot p \cdot \pi \cdot r_0^2 \cdot (a \cdot (1-\varepsilon \cdot \kappa)^2 - b) \tag{10}$$

Where $\varepsilon = a_\varepsilon \cdot e^{-p} - b_\varepsilon$ and $\mu = a_\kappa \cdot e^{-\kappa \cdot 40} - b_\kappa$.

The significant differences between the theoretical and experimental results were analyzed and proved in [6, 7, 8]. Therefore we have introduced a new approximation algorithm:

$$F(p,\kappa) = (a \cdot p + b) \cdot e^{(c \cdot \kappa + d)} + (e \cdot p + f) \cdot \kappa + g \cdot p + h \tag{11}$$

The unknown *a, b, c, d, e, f, g* and *h* parameters can be found using genetic algorithm.

The accuracy of equation 11 was demonstrated in [6, 7, 8], too.

3. Experimental Results

The precise positioning of PAMs requires accurate determination of the dynamic model of pneumatic actuators. Therefore the hysteresis in the tension-length (contraction) cycle of PAMs was analyzed.

Chou and Hannaford in [9] report hysteresis to be substantially due to Coulomb friction, which is caused by the contact between the bladder and the shell, between the braided threads and each other, and the shape changing of the bladder. Some experiments were made to illustrate the hysteresis (Figure 2).

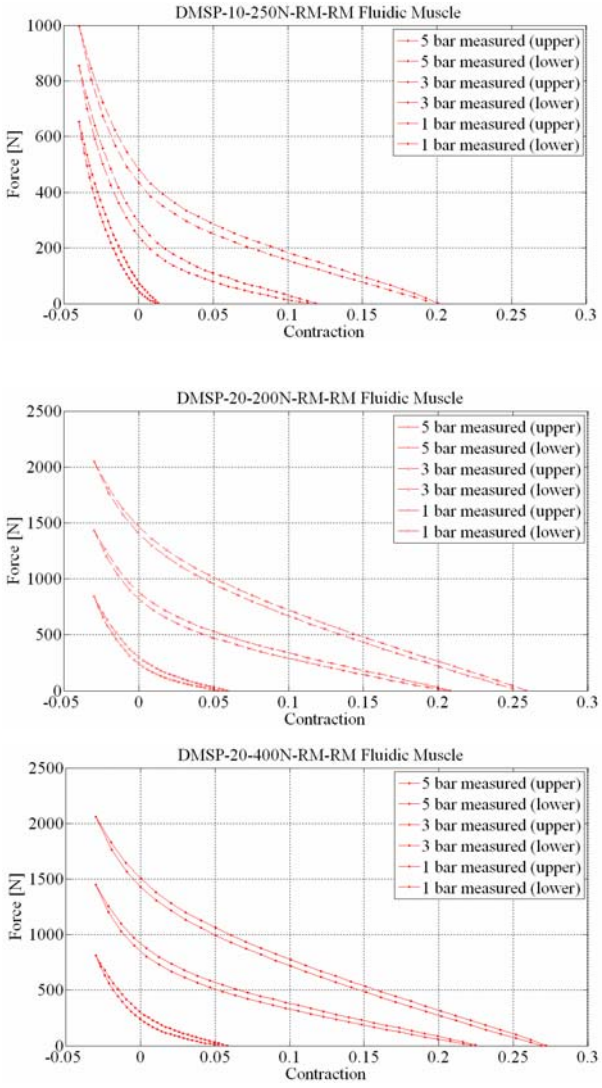

Figure 2 Hysteresis in the tension-length (contraction) cycle

The unknown parameters were found using genetic algorithm in Matlab environment (Figure 3).

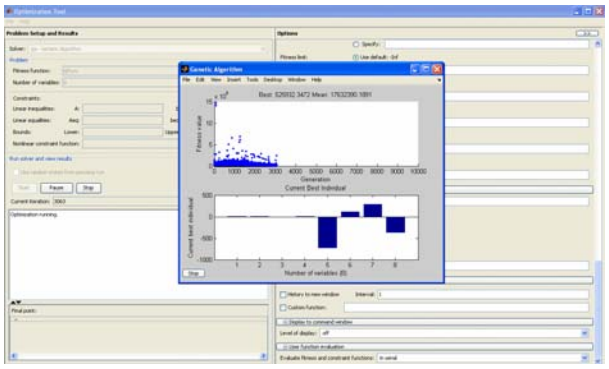

Figure 3 Determination of unknown parameters in Matlab environment

To prove versatility of equation 11, comparisons were done between the measured data and force model. The accurate fitting is demonstrated in Figure 4.

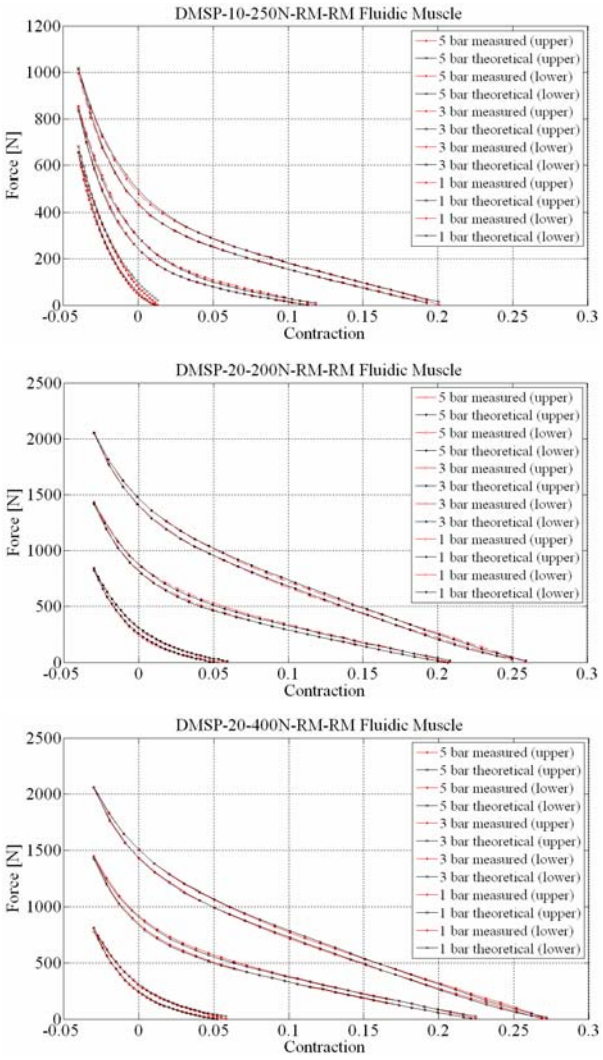

Figure 4 Approximation of hysteresis loop

4. Conclusions and Future Work

In this work a new equation based on purely statistical approach was shown for the hysteresis in the tension-length (contraction) cycle of PAMs. With the help of it precise curve fitting can be proven for any Fluidic Muscles. Our goal is to develop a new mathematical model for pneumatic artificial muscles on the basis of our approximation model.

References

1. Daerden F.: *Conception and realization of pleated artificial muscles and their use as compliant actuation elements*. PhD Dissertation, Vrije Universiteit Brussel, Faculteit Toegepaste Wetenschappen Vakgroep Werktuigkunde, 1999, p. 5-33
2. Daerden F., Lefeber D.: *Pneumatic artificial muscles: actuator for robotics and automation.* European Journal of Mechanical and Environmental Engineering, Vol. 47, 2002, p. 10-21
3. Plettenburg D. H.: *Pneumatic actuators: comparison of energy-to-mass ratio's*. Proceedings of the 2005 IEEE, 9th International Conference on Rehabilitation Robotics, Chicago, IL, USA, 28 June - 1 July, 2005, p. 545-549
4. Tondu B., Lopez P.: *Modeling and control of McKibben artificial muscle robot actuator*. IEEE Control System Magazine, Vol. 20, 2000, p. 15-38
5. Kerscher T., Albiez J., Zöllner J. M., Dillmann R.: *FLUMUT - Dynamic Modelling of Fluidic Muscles using Quick-Release.* 3rd International Symposium on Adaptive Motion in Animals and Machines, Ilmenau, Germany, 25-30 September, 2005, p. 1-6
6. Sárosi J., Szépe T., Gyeviki J.: *New Mathematical Model for Pneumatic Artificial Muscles*. Hungarian Agricultural Engineering, Vol. 22/2009, 2010, p. 49-52, ISSN 0864-7410
7. Sárosi J., Szépe T., Gyeviki J.: *Approximation Algorithm for the Force of Pneumatic Artificial Muscles*. Factory Automation 2010, Kecskemét, Hungary, 15-16 April, 2010, p. 101-104, ISBN 978-963-7294-83-9
8. Sárosi J., Szabó G., Gyeviki J.: *Investigation and Application of Pneumatic Artificial Muscles*. Biomechanica Hungarica, Vol. 3, No. 1, 2010, p. 208-214, ISSN 2060-4475
9. Chou C. P., Hannaford B.: *Measurement and modeling of McKibben pneumatic artificial muscles*. IEEE Transactions on Robotics and Automation, Vol. 12, No. 1, 1996, p. 90-102

Scientific reviewers: **János GYEVIKI, Faculty of Engineering, University of Szeged**
István BÍRÓ, Faculty of Engineering, University of Szeged

SCIENTIFIC BULLETIN OF
THE „POLITEHNICA" UNIVERSITY OF TIMISOARA, ROMANIA
TRANSACTIONS ON MECHANICS
BULETINUL ŞTIINŢIFIC AL
UNIVERSITĂŢII „POLITEHNICA" DIN TIMIŞOARA, ROMÂNIA
SERIA MECANICĂ
Tom 56 (70) ISSN 1224 - 6077 Fasc. S1, 2011

DEVELOPMENT AND INVESTIGATION OF A BALANCING SYSTEM USING FLUIDIC MUSCLES

József SÁROSI[*], Zénó SZABÓ[**]
[*]Technical Institute, Faculty of Engineering, University of Szeged
Mars tér 7., Szeged, H-6724, Hungary
e-mail: sarosi@mk.u-szeged.hu
[**]Technical Institute, Faculty of Engineering, University of Szeged
Mars tér 7., Szeged, H-6724, Hungary
e-mail: sazeno@mk.u-szeged.hu

Abstract. The most significant disadvantage of pneumatic systems is nonlinearity. Due to the nonlinear behavior pneumatic artificial muscles (PAMs) are difficult to control, therefore a fast and robust control necessary to achieve the desired motion. Several control ways have been applied to control different humanoid or robot arms, manipulators, prosthetic and therapy devices driven by pneumatic artificial muscles. The early control methods were based on classical linear controllers and then some modern control strategies have been developed (e. g. adaptive, fuzzy, neural network, sliding-mode, others). This paper presents the investigation of a balancing system using Fluidic Muscle actuators and sliding-mode control.

Keywords: Pneumatic Artificial Muscle, Balancing System, Sliding-mode Control, LabVIEW

1. Introduction

Pneumatic actuators have been considered as a substitute of electric motors because of their high power/weight and power/volume ratio. Comparatively new type of pneumatic actuators the pneumatic artificial muscle, which possesses all the advantage of traditional pneumatic actuators. For this reason, they are common used in robotic systems as actuators of industrial robots or rehabilitation robots, etc. PAMs were introduced by Garasiev in the 1930's, but these muscles were limited to use because of limited material technology at that time. Later, in 1950's McKibben invented braided pneumatic actuator to help the movement of polio patient. In 1980's Bridgestone proposed a redesigned and more powerful version of McKibben muscle named Rubbertuator. Until now different types of PAM have been developed and applied [1, 2].

Pneumatic muscle actuators consist of a rubber bladder enclosed within a helical braid that is clamped on both ends. When the bladder is pressurized the volume increases and the braid and clamps act to shorten the overall length of the actuator. During this movement the muscle converts pneumatic energy into mechanical form [3].

The layout of this paper is as follows. Section 2 (Materials and Methods) is devoted to demonstrate the experimental setup (hardware and software environment). Section 3 (Experimental Results) presents some experimental results and

finally, section 4 (Conclusions and Future Work) gives the investigations we plan.

Fluidic Muscles type DMSP-10-250N-RM-RM (with inner diameter of 10 mm and initial length of 250 mm) produced by Festo company were selected for this study.

2. Materials and Methods

Different experimental setups have been developed to investigate pneumatic systems [4, 5, 6, 7, 8, 9].

Our new balancing system is shown in Figure 1. The PAMs were installed vertically and can be controlled by a proportional valve type MPYE-5-M5-010-B made by Festo. The positioning was measured with a BDF-6360-3-05-2500-65 type (produced by Balluff) rotary incremental encoder with 0.036° resolution. A National Instruments data acquisition card (NI 6251/M) read the signals of incremental encoder into the PC. Between the DAQ card and encoder an I/O device type SCB 68 was attached with a special connecting cable.

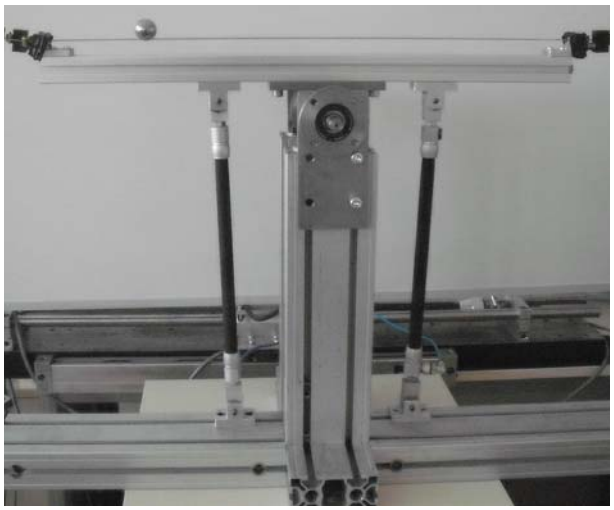

Figure 1 Balancing system

Because of the difficulties caused by the nonlinear properties of pneumatic systems a LabVIEW based sliding-mode control was designed. The design of a sliding-mode controller consists of three main steps. One is the design of the sliding surface, the second step is the design of the control which holds the system trajectory on the sliding surface, and the third and key step is the chattering-free implementation.

Good descriptions of our control system and experimental results of accurate positioning (0.01 mm) can be found in [10, 11].

In this study the purpose of positioning is to use the antagonistic muscles to balance the bearing in a desired position. With the use of sliding-mode control the positioning error can be minimized.

The Figure 2 shows data acquisition and positioning that can be achieved in LabVIEW environment. Aside from the current position the desired position and the control signal can also be set. The data can be saved into a text file.

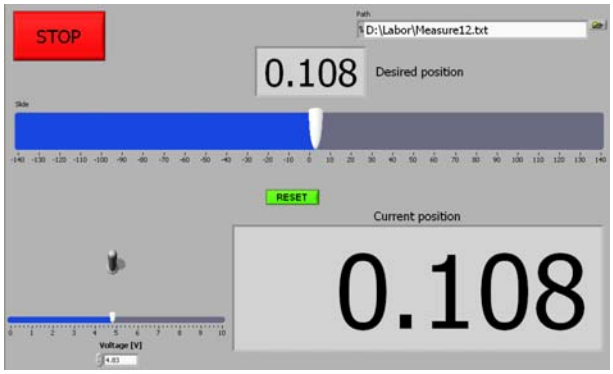

Figure 2 Front panel of LabVIEW program

3. Experimental Results

Positioning was done in room temperature on the pressure of 6 bar, the sampling time was 10 ms. When choosing the slope of the sliding surface the optimum between two concurrent properties must be found (speed, accuracy). The smaller the slope the faster the trajectory reaches the sliding surface, but it will take longer to set. The angle of the sliding surface was set to 26.56° ($tg\alpha = 0.5$). The time function of the position and control signal is shown in Figure 3 and Figure 4. To show the accuracy of positioning a short interval has been magnified (Figure 5 and Figure 6). If an error occurs, the system responds immediately. The position error of the LabVIEW-based sliding-mode control is within 0.036°. This means that the accuracy of the system is limited by the applied rotary incremental encoder.

The control program (control signal [V]) was based on Table1.

Table 1 Control program

Fast Forward	Slow Forward	In Position	Slow Backward	Fast Backward
4	4.8	5	5.2	6

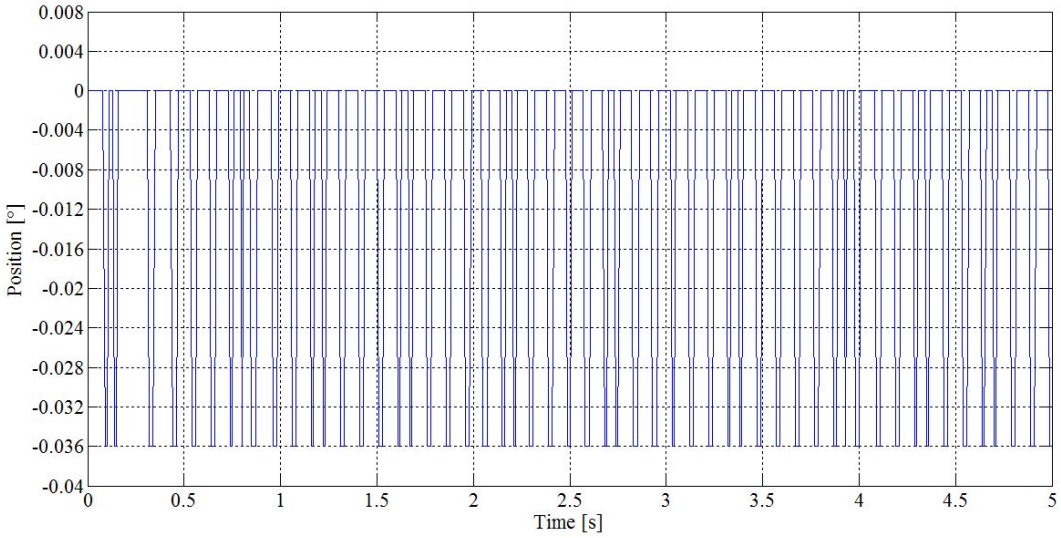

Figure 3 Position as a function of time

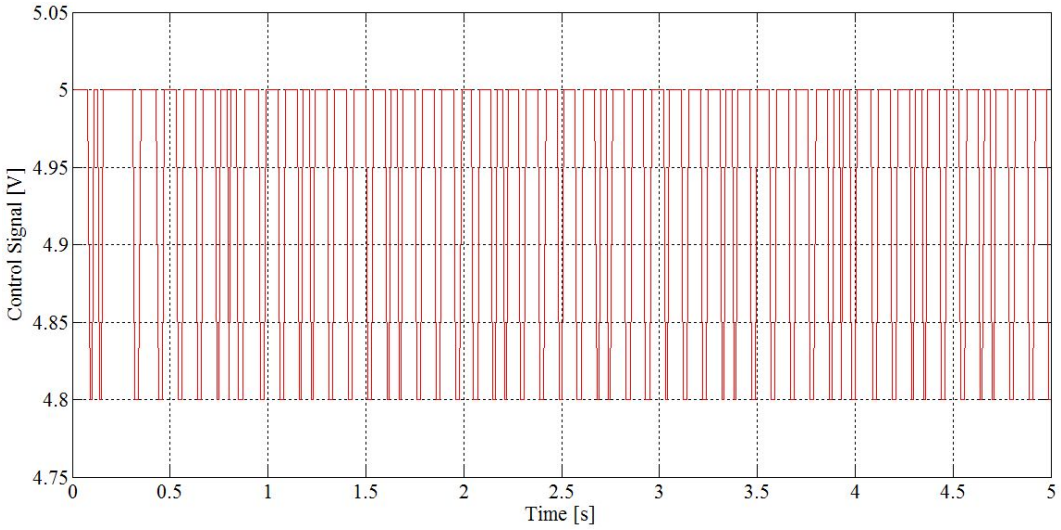

Figure 4 Control signal as a function of time

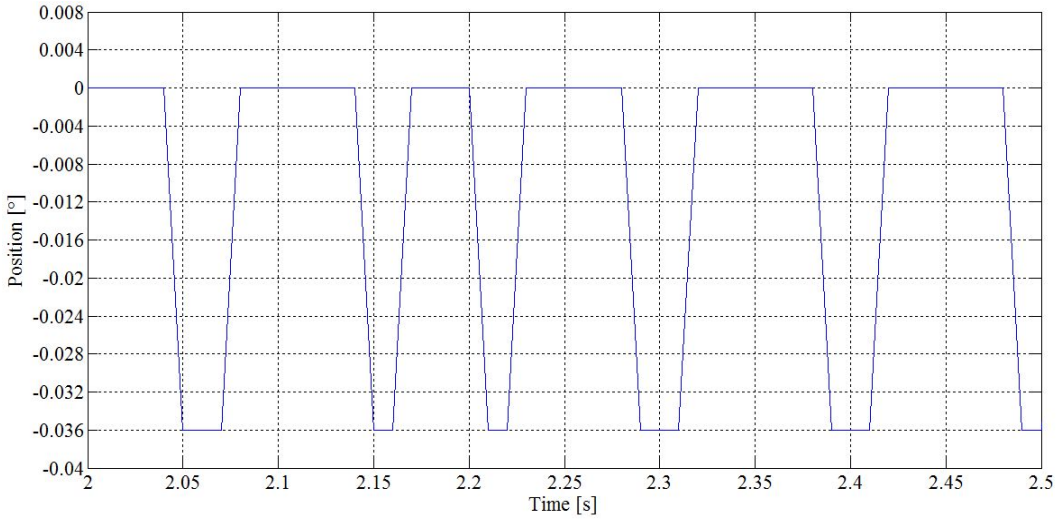

Figure 5 Position as a function of time (enlarged)

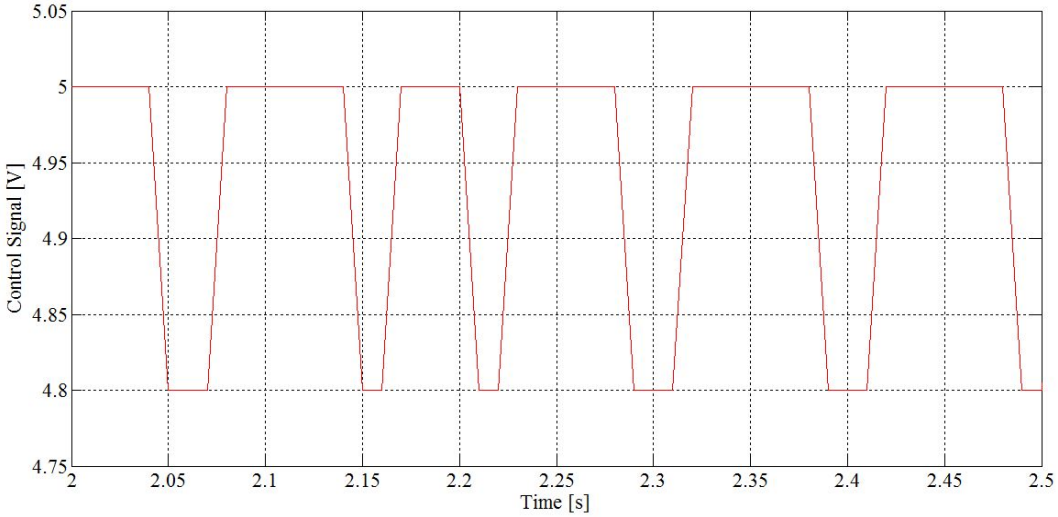

Figure 6 Control signal as a function of time (enlarged)

4. Conclusions and Future Work

In this work a new balancing system using Fluidic Muscles was described. For precise positioning (0.036°) a LabVIEW based sliding-mode control was designed. The experimental results show en excellent control performance and that the sliding-mode control is an effective methods to develop an accurate mechanism using pneumatic muscle actuators.

References

1. Laksanacharoen S.: *Artificial Muscle Contsruction Using Natural Rubber Latex in Thailand*. 3rd Thailand and Material Science and Technology Conference, Bangkok, Thailand, 10-11 August, 2004, p. 1-3
2. Ramasary R., Juhari M. R., Mamat M. R., Yaacob S., Mohd Nasir N. F., Sugisaka M.: *An Application of Finite Modelling to Pneumatic Artificial Muscle*. American Journal of Applied Sciences, Vol. 2, No. 11, 2005, p. 1504-1508
3. Bharadwaj K., Hollander K. W., Mathis C. A., Sugar T. G.: *Spring Over Muscle Actuator for Rehabilitation Devices*. 26th Annual International Conference of the IEEE EMBS, San Francisco, CA, USA, 1-5 September, 2004, p. 2727-2729
4. Chou C. P., Hannaford B.: *Measurement and modeling of McKibben pneumatic artificial muscles*. IEEE Transactions on Robotics and Automation, Vol. 12, No. 1, 1996, p. 90-102
5. Tondu B., Lopez P.: *Modeling and control of McKibben artificial muscle robot actuator*. IEEE Control System Magazine, Vol. 20, 2000, p. 15-38
6. Sárosi J., Gyeviki J., Szabó G., Szendrő P.: *Laboratory Investigations of Fluid Muscles*. International Journal of Engineering, Annals of Faculty of Engineering Hunedoara, Vol. 8, No. 1, 2010, p. 137-142, ISSN 1584-2665
7. Sárosi J., Gyeviki J.: *Experimental Setup for the Positioning of Humanoid Upper Arm*. Analecta Technica Szegedinensia, Review of Faculty of Engineering, Vol. 2010/2-3, 2010, p. 222-226, ISSN 1788-6392
8. Krishna S., Nagarajan T., Rani A. M. A.: *Review of Current Develepoment of Pneumatic Artificial Muscle*. Journal of Applied Sciences, Asian Network for Scientific Information, Vol. 11, 2011, p. 1-7
9. Földi L., Béres Z., Sárközi E.: *Novel Cylinder Positioning System Realised by Using Solenoid Valves*. Sustainable Construction and Design, Vol. 2, No. 1, 2011, p. 142-151, ISSN 2032-7471
10. Sárosi J., Gyeviki J., Véha A., Toman P.: *Accurate Position Control of PAM Actuator in LabVIEW Environment*. IEEE 7th International Symposium on Intelligent Systems and Informatics, Subotica, Serbia, 25-26 September, 2009, p. 301-305, ISBN 978-1-4244-5349-8
11. Sárosi J., Gyeviki J., Szabó G., Szendrő P.: *Pneumatikus izmok pozícionálása csúszómód szabályozással*. Gép, Vol. 60, No. 8, 2009, p. 45-48, ISSN 0016-8572 (Positioning of Pneumatic Muscles using Sliding-mode Control)

Scientific reviewers: **János GYEVIKI, Faculty of Engineering, University of Szeged**
István BÍRÓ, Faculty of Engineering, University of Szeged

SCIENTIFIC BULLETIN OF
THE „POLITEHNICA" UNIVERSITY OF TIMISOARA, ROMANIA
TRANSACTIONS ON MECHANICS
BULETINUL ŞTIINŢIFIC AL
UNIVERSITĂŢII „POLITEHNICA" DIN TIMIŞOARA, ROMÂNIA
SERIA MECANICĂ
Tom 56 (70) ISSN 1224 - 6077 Fasc. S1, 2011

MODERN METHOD FOR OPTIMIZATION OF THE VENTILATION NETWORKS

Marius ŞUVAR[*], Vlad PĂSCULESCU[**], Doru CIOCLEA[***], Ion GHERGHE[****]
[*]INCD INSEMEX Petroşani, G-ral V.Milea Street, no.32-34, Petroşani, Hunedoara, insemex@insemex.ro
[**]INCD INSEMEX Petroşani, G-ral V.Milea Street, no.32-34, Petroşani, Hunedoara, insemex@insemex.ro
[***]INCD INSEMEX Petroşani, G-ral V.Milea Street, no.32-34, Petroşani, Hunedoara, insemex@insemex.ro
[***]INCD INSEMEX Petroşani, G-ral V.Milea Street, no.32-34, Petroşani, Hunedoara, insemex@insemex.ro

Abstract. The ventilation systems represent the primary protection in the exploitation of the underground minerals. In order to optimize the ventilation networks associated with the complex mining works within a mine there are used modern methods and means that comprise specialized software and high performance computing equipment. Such software is Ventsim Visual Advanced, software which allows the 3D modeling in solid system of the ventilation network. The software also provides a range of facilities for handling, navigation and real-time simulation of the ventilation network.

Keywords: Specialized software, 3D modeling, ventilation network

1. Introduction

The solving of a complex ventilation network of a mine cannot be done manually, and usage of a specialized software and advanced IT equipment is a must. As an important consideration for underground mining operations, ventilation network design and monitoring has been computerised.

Associated to mine networks, mine ventilation networks exist having vital role in ensuring optimal microclimate conditions.

The fundamental requirement of ventilation is to provide controlled air distribution within the underground mining operations to satisfy statutory and safety requirements with respect to ventilation quantity and quality. [1]

2. General Considerations

Mining ventilation is the primary protection in underground coal mining. Underground ventilation achievement has the following purposes:

- To ensure an oxygen concentration of more than 19% volume in each point of the ventilation network;
- To accomplish taking over of the rock massif temperature in order to ensure the normal microclimate conditions;
- To dilute explosive/toxic/asphyxiant gases with the purpose of avoiding explosion type events;

In order to ensure the underground occupational health and safety conditions, through the applied ventilation systems, there is necessary to be provided an optimum air flow at each branch level. For this kind of approach there are necessary complex logical-mathematical calculation devices, equipment that have to have high processing capacity. [2]

There has been developed specialized software worldwide, software that ensures an optimum distribution of air flows by solving the ventilation network.

3. Ventsim Visual Advanced

Ventsim Visual Advanced is software designed in Australia which provides special facilities for ventilation modeling (Figure 1).

It represents a mature approach on ventilation networks solving, applied for the first time in Australia starting with the year 1993 (first version), and continuing to be used in over 500 locations (mining facilities, government agents, consultants from all over the world) . The software was designed as an aid in order to view and achieve the ventilation networks. [3]

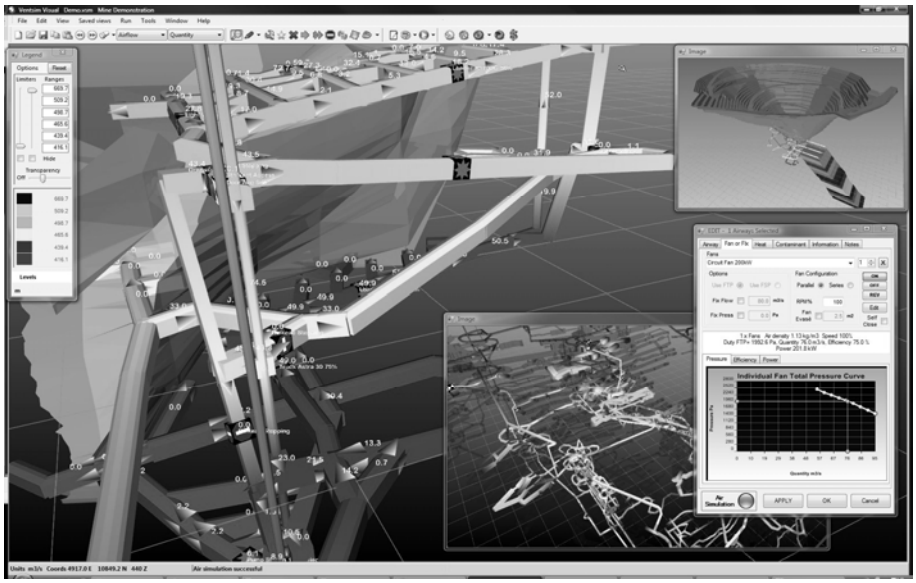

Figure 1 Ventsim Visual Advanced Software

The main technical characteristics of Ventsim Visual Advanced are the following [4]:

- Solid or single-core 3D graphics;
- Fast tridimensional viewing regardless of the data complexity;
- It ensures the animation of air currents and fans;
- It uses 60 data types regarding air;
- Processing capacity: 30 000 branches; (Figure2).

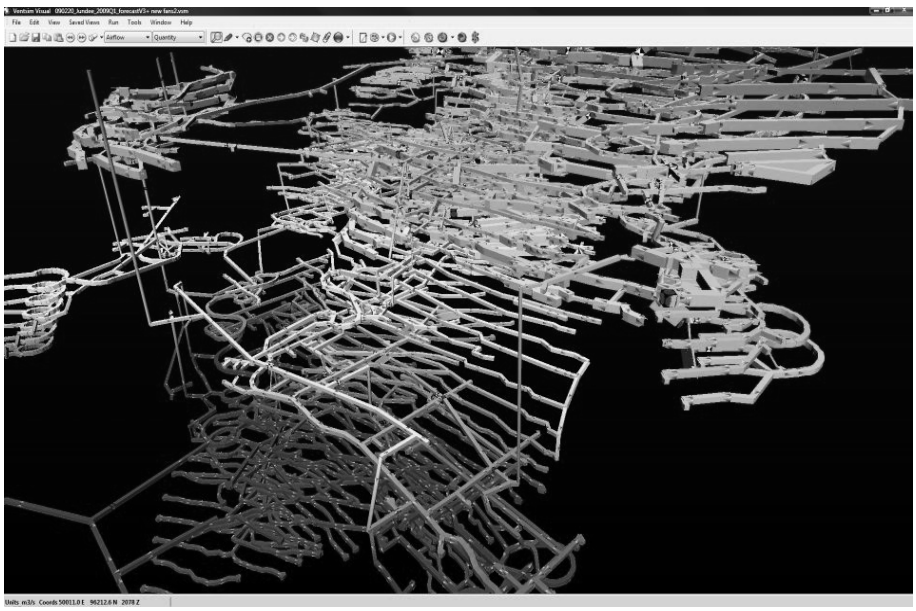

Figure 2 Complex ventilation network

- It uses the multi-pass HC simulation method for weight rate;
- It ensures direction reversibility of air flowing;
- It takes into account air compressibility;
- It can import DXF and solid DXF files;

- It ensures the possibility of air flowing direction changing at fan level;
- It ensures modeling in case of fan switching on/off;
- It ensures modeling under the conditions of air currents heating/cooling;
- It takes rock temperature and humidity into account;
- It calculates the natural air-draught using thermodynamics in order to simulate the effects of natural ventilation;
- It presents gas expansion at the mine workings level;
- It simulates blasting effects;
- It simulates the dispersion of diesel-particles at the ventilation level;
- It highlights air recirculation;

It ensures the ventilation economical calculation

The software offers the possibility to import data generated by other CAD applications from the mining domain, 3D graphic forms, terrain textures as well as other elements that can help for ventilation systems viewing.

4. Ventilation network modelling for Lupeni Mine

4.1. Presentation of Lupeni Mine ventilation network

The ventilation network related to Lupeni Mine (Figure 3) is the biggest and the most complex one from Jiu Valley coal basin. Fresh air enters the underground through the alignment of four vertical shafts as following: shaft with skip, shaft "Stefan", shaft no.12 and auxiliary shaft south. The ventilation network also comprises: 3 blind pits: P.O. no.10, P.O. no.15 and P.O. no 21; directional galleries; inclined planes; risings and transversal galleries. The ventilation network is extended in depth at 4 main levels: level 650, level 480, level 400 and level 300. The return air is evacuated through 2 main ventilation stations: central rising and shaft no.1 east. [2,5]

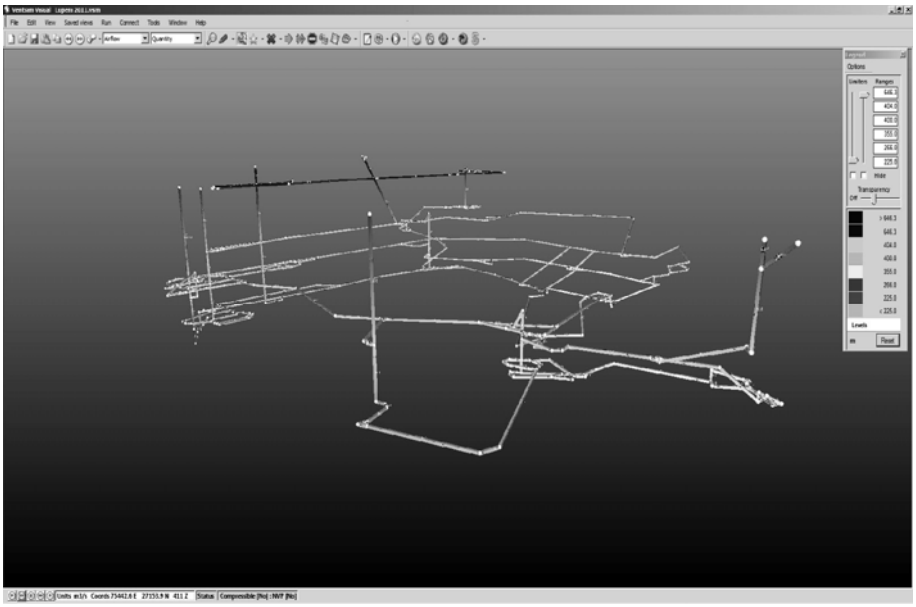

Figure 3 Lupeni Mine ventilation network

4.2. Modelling the ventilation network using Ventsim Visual Advanced

In order to accomplish the modelling of Lupeni Mine ventilation network there need to be carried out the following tasks:

- marking the junctions on the spatial map related to Lupeni Mine;
- collecting the geodesic coordinates related to the marked junctions;
- making depresiometric measurements for each branch of the ventilation network;
- calculating the specific parameters and preparing them in an accessible format, format compatible with Ventsim Visual Advanced software;
- input the data into Ventsim database;
- modelling the ventilation network;
- adjusting/balancing the ventilation network;

Following the modelling of Lupeni Mine results a number of 404 junctions and 519 branches. (Figure 4)

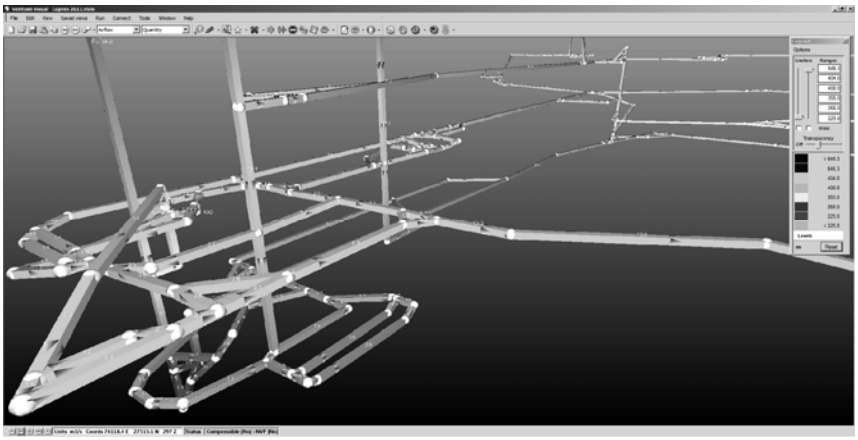

Figure 4 Lupeni Mine ventilation network (in detail)

5. Conclusions

Mining ventilation is the primary protection in underground coal mining;

Solving ventilation networks involves ensuring the optimum flows at branch level and leads the increase of the underground safety level;

Using specialized software like Ventsim Visual Advanced along with powerful IT equipment leads to the optimum management of mining ventilation;

Ventsim Visual Advanced provides solid or single-core 3D graphics and it is an extremely useful tool for the technicians;

Following the modelling of Lupeni Mine results a number of 404 junctions and 519 branches;

Using Ventsim Visual Advanced there can be modelled, solved and simulated any kind of ventilation network regardless of its complexity.

References

1. Gillies, S., Mayes, T.I., Wei Wu, H., Kizil, M.S., Wang, N.: *The development of real time airflow monitoring and control system, The University of Queensland.* Available at: http://www.ventsim.com/files/UQ%20Developement%20of%20Realtime%20Monitoring%20System.pdf Accessed: 2011-10-04A
2. Cioclea, D.: *Diminishing explosion hazard in Jiu Valley hard coal mines through computerized management of the ventilation networks* .Sectorial project, 2010-2011 (in Romanian, Diminuarea pericolului de explozie la minele de huilă din Valea Jiului prin gestionarea computerizată a rețelelor de aeraj, Project Sectorial 2010-2011)
3. XXXXX Ventsim Visual User Guide – Standard and Advanced Versions (Version 2.0)
4. XXXXX Ventsim Visual 3D Software – Information Sheet
5. Gherghe, I*.: Proration of ventilation networks from Jiu Valley in terms of their restructuring and following the closure of an inactive area*, INSEMEX Study, MENER Project, 2002-2004 (in Romanian, Raționalizarea rețelelor de aeraj ale minelor din Valea Jiului în condițiile restructurării acestora ca urmare a închiderii unei zone inactive).

Metodă modernă pentru optimizarea rețelelor de aeraj

Rezumat

Sistemele de aeraj reprezintă protecția primară la exploatarea substanțelor minerale utile în subteran.

Pentru optimizarea rețelelor de aeraj asociate rețelei complexe de lucrări miniere din cadrul unei mine, se utilizează metode şi mijloace moderne care cuprind programe software specializate precum şi echipamente de calcul performante.

Un astfel de program este şi Venstim Visual Advanced, care permite modelarea tridimensională în sistem solid a rețelei de aeraj.

De asemenea, programul asigură o serie de facilități privind manevrarea, navigarea şi simularea în timp real a rețelei de aeraj

Scientific reviewers: **Emilian GHICIOI*,INCD INSEMEX, Petroşani, ROMANIA**
Ion TOTH, INCD INSEMEX, Petroşani, ROMANIA**

SCIENTIFIC BULLETIN OF
THE „POLITEHNICA" UNIVERSITY OF TIMISOARA, ROMANIA
TRANSACTIONS ON MECHANICS
BULETINUL ŞTIINŢIFIC AL
UNIVERSITĂŢII „POLITEHNICA" DIN TIMIŞOARA, ROMÂNIA
SERIA MECANICĂ
Tom 56 (70) ISSN 1224 - 6077 Fasc. S1, 2011

AN APPROACH TO CITY LOGISTICS TERMINAL LOCATION PROBLEM IN NOVI SAD

Marko VELICKOVIC[*], Djurdjica STOJANOVIC[**], Valentina BASARIC[***]
[*] Faculty of Technical Sciences, University of Novi Sad, Serbia, markosao@yahoo.com
[**] Faculty of Technical Sciences, University of Novi Sad, Serbia, djurdja@uns.ac.rs
[***] Faculty of Technical Sciences, University of Novi Sad, Serbia, plast@uns.ac.rs

Abstract. The usage of urban freight terminals for city deliveries represents one of the main concepts of city logistics. This concept aims to improve the urban freight transport, because it may reduce costs and congestion and reduce the impact of freight transport on pollution.
Here is presented a preliminary analysis of city logistics terminal location in Novi Sad and proposed the best one, according to freight distances. Here the results of recent research, which has been performed by public enterprise "Urbanizam", are used as a starting point. The local traffic planners analyze three locations, according to macroeconomic conditions. At the contrary, our research is focused on microeconomic flows, i.e. urban freight flows. The best location is proposed according to the minimum average distance from the terminal regarding the main city freight flows attractors. This criterion should ultimately lead toward freight transport costs minimization, less pollution and congestion in the city.

Keywords: City logistics, Freight transport terminals, Location problem

1. Introduction

Freight flows have an adverse impact on the environment and traffic in cities. A development of different planning and technical measures should reduce negative impact of heavy goods vehicles movement in urban areas. These measures certainly includes the development of city logistics terminals, which represents a linkage between the macro and micro logistics flows.

The aim of the analysis is a choice of optimal city freight terminal location in case of limited data about the characteristics of realized freight flows. More precisely, the location problem is solved regarding to location of large freight flows attractors, i.e. on the basis of minimum average distances. City logistics terminal location problem is solved for the city of Novi Sad. There are several studies in recent years dealing with these problems in Novi Sad. Public Enterprise "Urbanizam" carried out a "Conditions and feasibility study of the freight terminal in Novi Sad" [1], where several terminal locations is analyzed. The local traffic planners analyze three locations, according to macroeconomic conditions. At the contrary, our research is focused on microeconomic flows, i.e. urban freight flows. In that sense, this paper also aims to define possible problems and constraints related to the development of logistics terminal in the city of Novi Sad.

The paper is organized as follows. In the second Section, a brief theoretical background is given. In the third Section, the main demographic and traffic infrastructure characteristics of Novi Sad city are shown. In the fourth Section, the methodology and main results are presented. Discussion, final remarks and conclusion are given in fifth and sixth Sections, respectively.

2. Theoretical background

Logistics centres can be configured to provide a wide range of functions such as: storage, transport, distribution, assembly, direct shipment, shipment with milk runs, cargo consolidation, sorting, break-bulk, distribution network management / vehicle routing, delivery, package tracking, e-commerce services, etc. [2]. All these functions can provide a lot of positive effects in terms of congestion and pollution.

Taniguchi et al. define city logistics as "the process for totally optimising the logistics and transport activities by private companies in urban areas while considering the traffic environment, the traffic congestion and energy consumption within the framework of a market economy" [3, 4]. Urban logistics system structure consists of subsystems that include logistic flows, generators and attractors of urban logistics flows, transportation system, information system and logistics services organization system [5].

3. Demographic characteristics and traffic infrastructure in city of Novi Sad

Novi Sad, with more than 300,000 inhabitants, is the largest city and capital of the Autonomous Province of Vojvodina (see Figure 1). The city is located on the Danube river banks and the Little Backa canal. Today, Novi Sad represents one of the major industrial and financial centers of Serbian economy. With 16 suburban settlements, the area of Novi Sad covers an area of 702.7 km², while the core area of Novi Sad with Petrovaradin and Sremska Kamenica occupies an area of 129.4km².

Novi Sad is a significant generator – attractor (origin – destination) of freight flows and road transport have a dominant role over other modes of transport. Significant contribution to that gives high road network density and nearness of European route E-75 which belongs to series of main roads in Europe. Total road network length in city of Novi Sad is 347 km. City authorities of Novi Sad introduced appropriate regulatory measures in recent years, in order to improve traffic and living conditions in the city.

Figure 1 South Backa County with all the municipalities and their positions in Vojvodina [1]

Namely, the local traffic planners introduced zone borders in which heavy goods vehicles are not allowed is one of implemented restrictive measures, and it covers wide CBD area. Heavy goods vehicles can enter into zone only with special permission. Figure 2 shows HGV restriction zone area (area filled in black). Area hatched with black lines represents the area planned to be included into the restricted zone in near future.

Figure 2 Existing and planned HGV restriction zone [6]

Other modes of transport in Novi Sad are also developed as well as road transport. The main characteristics of rail transport sub-system in Novi Sad region are reflected in uniform spatial disposition and density of rail network, which significantly influenced the development of many settlements along the railway lines. Danube waterway provides a relatively simple and direct connections with all Danube countries ports. The fact that Novi Sad is located approximately in the middle Danube waterway (at 1255-th kilometer) goes in favor to city waterway connections. Air traffic with its high level of service meets the requirements of transport speed and efficiency what plays special role in modern economic systems.

4. The choice of an optimal city logistics terminal location in Novi Sad

4.1. The methodology

Optimized city logistics terminals can transfer the center of gravity of freight transport from city center to suburb, and alleviate traffic pressure in the center and improve the efficiency of the whole urban transport system [7]. First, we need to define terminal alternative locations in order to analyze and propose best location that meets city logistics needs. Then, the location problem is solved regarding to location of large freight flows attractors, i.e. on the basis of minimum average distances

At first, we adopted alternative locations according to [1]. This study proposes and evaluates three logistics terminal locations (I, II and IV in Figure 4). Their analysis and evaluation of each location results in selecting location I as the best solution. This location represents current cargo port of Novi Sad. However, it is clear that location IV will not be acceptable because of its notably higher distance from CBD and city facilities in comparison to other two locations, as the freight distances will be the main evaluation criterion. Therefore, we introduced new location (Location III, see Figure 4) for the analysis in this paper. Position and proximity of this location to the city center and attractors of freight flows was the main criterion to add this alternative location into the analysis.

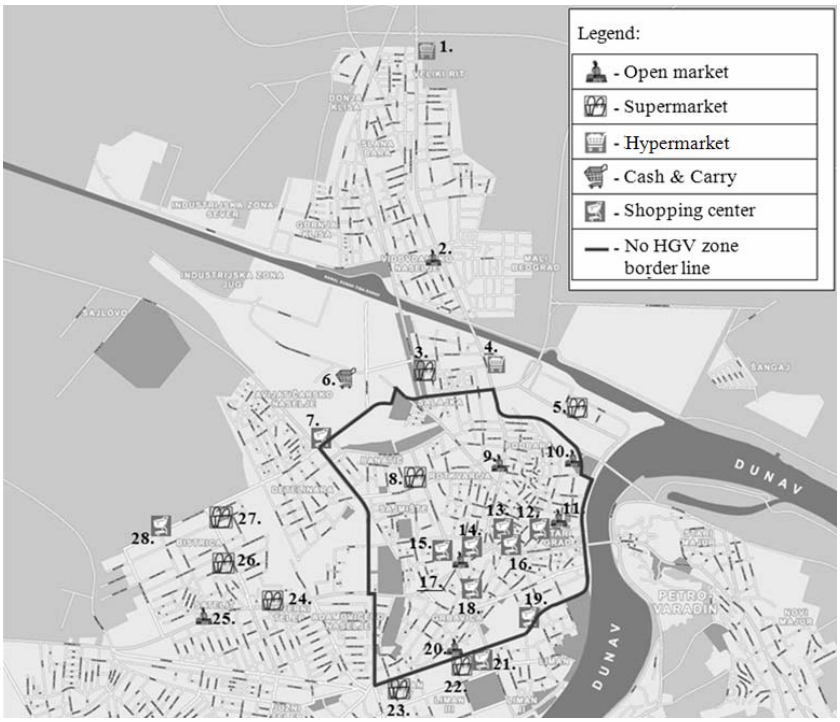

Figure 3 Position of the main attractors of freight flows in Novi Sad

Figure 4 Proposed logistics terminal locations

4.2. Characteristics and position of main freight flows attractors

Large supermarkets in city certainly have significant impact on city logistics indicators. Therefore, it is very important to identify them in order to analyze and understand their interaction. Position and size of retail stores has a significant influence on distribution, size and structure of freight flows. Hence, it is important to define their basic characteristics. For the purpose of this research, positions and sizes of the following retailers were identified: open markets, supermarkets, hypermarkets, cash & carry facilities and shopping centers. A total number of 28 objects were found and all objects are marked on the map shown in Figure 3. All recorded objects consists of:

- 7 open markets,
- 8 supermarkets,
- 2 hypermarkets,
- 1 cash and carry, and
- 10 shopping centers.

4.3. Analysis and location proposal based on attractors position

Minimum average distance from logistics terminal locations to retail outlets is certainly one of the most important factors that influence the selection of terminal location. As much as the average transport length is lower, the fuel consumption is lower; consequently, it reduces costs and emissions of freight transport. First, we need to define the actual distance from the logistics terminals to identified attractors of main freight flows in the city (see Table 1) in order to calculate the minimum average distance from the terminal to retail outlets.

Based on data presented in Table 1 we can calculate minimum average distance per location (see Table 2) using the following equation:

$$Dx = \frac{\sum_{i=1}^{n} di}{n} \quad (1)$$

Dx – average distance from terminal location x to every identified object (attractor) in city
n – total number of analyzed objects (attractors)

Different groups of attractors can show different freight flows demands. Alternative locations will be analyzed and evaluated based on groups differed by size and product range of objects (freight flows attractors).

Table 1 The distances from terminal alternative locations to identified attractors of main freight flows in Novi Sad (in kilometers)

Attr.	Locations			Attr.	Locations		
	I	II	III		I	II	III
1	5,10	7,40	6,60	15	3,60	4,45	3,35
2	2,70	4,90	4,05	16	3,10	3,60	4,15
3	2,10	4,40	2,75	17	3,40	4,25	3,50
4	1,35	3,55	4,25	18	3,60	4,45	3,70
5	0,05	2,60	4,80	19	3,50	4,00	5,15
6	3,15	5,35	2,35	20	4,55	5,00	4,85
7	3,35	6,25	1,00	21	4,15	4,60	4,50
8	3,20	5,45	2,50	22	4,55	5,00	4,85
9	2,00	3,70	3,65	23	5,25	4,75	4,10
10	1,55	2,00	5,35	24	5,55	6,45	2,20
11	2,30	3,00	4,40	25	6,45	7,30	2,40
12	2,55	3,50	4,80	26	5,55	7,30	1,25
13	2,80	3,75	4,00	27	5,05	7,80	0,75
14	3,35	4,15	3,65	28	5,45	8,35	1,15

Table 2 Min. average distances per locations

Locations	Minimum average distances [km]
I	3,55
II	4,90
III	3,57

The question is whether the Location I (which was selected as the best in the last analysis) will be optimal for different groups of attractors. The size (area) of objects will be criterion for creating groups of attractors. In other words, groups of attractors will be created depending on their type (supermarket, hypermarket, shopping center, etc.). Table 3 shows five formed groups of attractors with all objects that make a group. Numbers of attractors are shown in Figure 3.

Table 3 Groups of attractors with all objects

Group	Type	Object number	Sum
I	Shopping centers	7, 12, 13, 14, 15, 16, 18, 19, 21, 28	10
II	*Cash & Carry* objects	6	1
III	Hypermarkets	1, 4	2
IV	Supermarkets	3, 5, 8, 22, 23, 24, 26, 27	8
V	Open markets	2, 9, 10, 11, 17, 20, 25	7

As before, it is necessary to calculate minimum average transport distance for each proposed logistics terminal location, except that now it should be done by groups of attractors. The results are shown in Table 4.

Table 4 Minimum average distance (in kilometers) from proposed terminal locations to all groups of attractors

Groups	Locations		
	I	II	III
I	**3,885**	5,135	3,895
II	3,150	5,350	**2,350**
III	**3,225**	5,475	5,425
IV	3,913	5,469	**2,900**
V	**3,279**	4,307	4,029

5. Discussion

Table 2 shows that vehicles which transport goods from location II have to drive considerably longer average distance than the vehicles from other two locations. Therefore, if we consider only data on the minimum average distance, location II is not suitable for the construction of logistics terminal. Locations I and III are approximately at the same level of acceptability with respect to minimum average transport distances. However, logistics terminal at location III would have a much worse position because of the difficulty in connecting it with different modes of transport, at first with waterways, but also with other transport infrastructures. Based on these advantages we can conclude that **Location I**, if one takes into account the location of attractors, continue to be regarded as the best choice.

Modified analysis results (shown in Table 4) lead to similar conclusions as individual analysis of all attractors. Therefore, a modified analysis confirms results of previous analysis and partially mitigates it's disadventages.

The main limitation of this approach is that it considers only spatial characteristics of freight demands in the city of Novi Sad. Other important freight flows characteristics, e.g. time demand characteristics, flows intensities etc. are not included into the analysis. Therefore, the results have to be treated only as a preliminary ones.

6. Conclusion

Here is proposed an approach to choice of optimal location of city logistics terminal in case of lack of data about freight flows characteristics. The choice was made according to the minimum average transport distance from terminal location to main freight flows attractors in the city, as well as certain groups of these objects. Location in north-eastern part of Novi Sad (Location I in Figure 3) is proved to be the optimal one.

The selected location has relatively easy connectivity with various modes of transport (road, rail and water). Connecting road transport modes with waterways from this location is simple since it is located on canal bank. The presence of railway infrastructure enables connecting terminal with international rail routes without large investments. Highway M-7 (Novi Sad – Zrenjanin) near given location allows direct connection with international road E-75, while heavy goods vehicles from longer distances don't have to use city streets for distribution.

Our research show that the city logistics was an underestimated issue in Novi Sad. An optimal location for city freight terminal could be proposed mainly according to average transport distances and available infrastructure characteristics.

Further research toward development of a comprehensive city logistics database in Novi Sad is necessary. This database should be used not only for finding an optimal location for city logistics terminal. It should be also used as a necessary tool within an efficient city logistics planning and controlling.

7. References

[1] Public Enterprise "Urbanizam" – Institute for Urban Planning in Novi Sad: *Conditions and feasibility study of the freight terminal in Novi Sad*. Novi Sad, 2004.

[2] Farook R. Hamzeh, Iris D. Tommelein, Glenn Ballard, Philip M. Kaminsky: *Logistics centers to support project-based production in the construction industry*. Michigan, 2007.

[3] Taniguchi, E., R.G. Thompson and T. Yamada: *Modelling city logistics*. In: City Logistics I (E. Taniguchi and R.G. Thompson, eds.), pp.3-37, Institute of Systems Science Research, Kyoto, 1999.

[4] Taniguchi, E., R.G. Thompson, T. Yamada and R. van Duin: *City Logistics - Network Modelling and Intelligent Transport System*. Pergamon, 2001.

[5] Zecević, S.: *City logistics*. University of Belgrade, Faculty of transport and traffic engineering, Belgrade, 2006.

[6] Public Enterprise "Urbanizam" – Institute for Urban Planning in Novi Sad: *Novi Sad traffic*

study with dinamic traffic planning – NOSTRAM. Novi Sad, 2009.

[7] Yang, Z., Liu, C., Song, X.: *Optimizing the scale and spatial location of city logistics terminals*. Journal of the Eastern Asia Society for Transportation Studies, Vol. 6, pp. 2937 - 2946, 2005

Scientific reviewers: **Dragan Jovanović, Faculty of Technical Sciences, Novi Sad**
Predrag Atanasković, Faculty of Technical Sciences, Novi Sad

A SHORT HISTORY OF THE JOURNAL

The history of this journal of "Politehnica" University of Timisoara is strongly related to its creation under the name Polytechnic School of Timisoara (Ecole Polytechnique de Timisoara). Due to the changes of names and development of new areas of specialization, the university journal has been adapted several times during its long history. These adaptations are presented below in a synthetic history.

Polytechnic School of Timisoara

1925 The first number in a single series for all areas of specialization in technical, mathematical, physical and chemical sciences

1925 and Bulletin Scientifique de l'Ecole Polytechnique de Timisoara

1928-1947 (Comptes Rendus des Seances de la Societe Scientifique de Timisoara)

1948 Bulletin de Science et Technique de la Polytechnique de Timisoara, ISSN 0563-5594

1949 - Change of name to Polytechnic Institute of Timisoara

1949 Buletinul de Stiinta si Tehnica al Institutului Politehnic din Timisoara (Bulletin for Science and Technique of Polytehnic Institute of Timisoara, Naucino-tehniceskij biuleten' Politehniceskogo Instituta Timisoara, Bulletin des Science et Technique de L'Institut Polytechnique de Timisoara)

1956-1969 Buletinul stiintific si tehnic al Institutului Politehnic Timisoara (Scientific and Technical Bulletin of Polytehnic Institute of Timisoara), New series ISSN 0373-4374

1970 Editing on areas of specialization (series) specific to the main engineering fields of the Institute

- Chemical Series, ISSN 0366-3701

- Civil Engineering Series, ISSN 1220-0573

- Mechanical Engineering Series, ISSN 0373-4390

- Mathematics-Physics-Theoretical and applied mechanics Series, ISSN 0366-3779

1970-1971 Buletinul stiintific si tehnic al Institutului Politehnic Timisoara, Seria Mecanica (Scientific and Technical Bulletin of Polytechnic Institute of Timisoara, Mechanical Engineering Series), ISSN 0373-4390

1972 - Change of name to "Traian Vuia" Polytechnic Institute of Timisoara

1972 - 1974 Buletinul stiintific si tehnic al Institutului Politehnic "Traian Vuia" Timisoara, Seria Mecanica (Scientific and Technical Bulletin of "Traian Vuia" Polytechnic Institute of Timisoara, Mechanical Engineering Series), ISSN 0253-2026

1975 - 1977 Buletinul stiintific si tehnic al Institutului Politehnic "Traian Vuia" Timisoara (Scientific and Technical Bulletin of "Traian Vuia" Polytechnic Institute of Timisoara) [Single series] Mathematics, Physics, Theoretical and applied mechanics, Electrical engineering, Civil engineering, Chemistry, ISSN 1220-0581

1978-1990 Buletinul stiintific si tehnic al Institutului Politehnic "Traian Vuia" Timisoara (Scientific and Technical Bulletin of "Traian Vuia" Polytechnic Institute of Timisoara, Mechanical Engineering Series), ISSN 0253-2026

1990 - Change of name to Technical University of Timisoara

1991-1994 Buletinul stiintific si tehnic al Universitatii Tehnice din Timisoara Scientific and Technical Bulletin of Technical University of Timisoara, Mechanical Engineering Series)

1995 Buletinul stiintific si tehnic al Universitatii Tehnice din Timisoara, Seria Mecanica (Scientific and Technical Bulletin of Technical University of Timisoara, Transactions on Mechanics)

1996 - Change of name to "Politehnica" University of Timisoara

1996 - Today; Buletinul stiintific al Universitatii "Politehnica" din Timisoara. România, Seria Mecanica (Scientific Bulletin of "Politehnica" University of Timisoara, Romania, Transactions on Mechanics), ISSN 1224-6077

(Also see http://www.upt.ro/cercetare/publicatii_upt.php)

The Scientific Bulletin of the Faculty of Mechanics within POLITEHNICA University of Timişoara, as it was in 1929. This is a copy of the cower who are existing in the archives of the Faculty of Mechanics.

BULLETIN SCIENTIFIQUE

DE

L'ÉCOLE POLYTECHNIQUE

DE

TIMIŞOARA

COMPTES RENDUS DES SÉANCES DE LA
„SOCIÉTÉ SCIENTIFIQUE DE TIMIŞOARA"

TOME 2. FASC 3 — 4.

TIMIŞOARA
IMPRIMERIE „CARTEA ROMÂNEASCĂ"
1 9 2 9.

Buletinul Ştiinţific al Facultăţii de Mecanica din Universitatea POLITEHNICA din Timişoara, aşa cum se prezenta în anul 1929. Copia este a coperţii Buletinului din arhiva Facultăţii de Mecanică